University of Zurich[UZH]

Developing a machine learning model based on Earth Observation data to predict grass growth and assess the impact of drought on Swiss grasslands

ESS 511 Master's Thesis

Author
Daria Larcher
18-702-910

Supervised by
Dr. Helge Aasen (helge.aasen@agroscope.admin.ch)
Dr. Andreas Hüni

Faculty representative
Prof. Dr. Meredith Schuman

30.09.2024
Department of Geography, University of Zurich

Abstract

Grasslands cover 70% of the global agricultural area, securing the livelihood of millions of people and providing a wide range of ecosystem services. The changing climate puts increasing pressure on these ecosystems, and extreme events such as droughts can significantly affect the state and productivity of grasslands. It is, therefore, essential to monitor and understand the ongoing processes. Remote sensing has proven to be a valuable tool to monitor land surfaces on a larger scale. To our knowledge, using Earth Observation (EO) data to train a grass growth model has not yet been explored. Thus, this study established a robust Machine Learning (ML) grass growth model based on EO data and environmental variables to analyse the impact of drought on grassland growth in Switzerland.

The ML grass growth model was developed by training a Random Forest (RF) algorithm with Sentinel-2 derived grass growth from the first growing period from 2018 to 2023 on 37 field parcels and the respective meteorological data. Leaf Area Index (LAI) derived from Sentinel-2 data showed to be a good proxy for biomass when comparing it to in-situ measured LAI observed with comparable light absorption methods. Comparisons to biomass measurements based on swath height densification have achieved R^2 values of 0.12 for LAI and 0.22 for Enhanced Vegetation Index (EVI). Sentinel-2's ability to capture changes in grassland biomass over time was confirmed by R^2 scores of up to 0.92 when comparing Sentinel-2 derived LAI to in-situ measured LAI. This was emphasised by an 87% agreement of mowing events in a time series when comparing the time series data to high-resolution satellite imagery and a grassland use-intensity map. The assessment of the growth prediction on an independent field has resulted in R^2 values of up to 0.93, underlining the predictive power of the ML grass growth model, with growth overestimations in the later season. The model's ability to capture the impact of drought conditions on grass growth proved difficult. Different precipitation scenarios and the quantification of potential decrease in growth during a dry period in spring 2020 have shown to be minimal (2-12%). Improved growth predictions and drought sensitivity of the grass growth model are expected when the RF algorithm is trained on data from the full growing season, including growth characteristics of the whole growing period, and more diverse meteorological conditions, including drought periods.

The ML grass growth model has shown that grass growth can be learned from EO and environmental data, and based on that, reliably predict grass growth under varying weather conditions. Such models have the potential to be valuable tools for complementing missing data at times when direct satellite measurements are not available.

Acknowledgments

I would like to express my sincere gratitude to my supervisor Dr. Helge Aasen from Agroscope for his insights, expertise and constructive feedback. His invaluable guidance and encouragement have supported me throughout this research. I am grateful for his patience and mentorship and for always fully including me in his team. I would also like to thank the whole EOA team for the positive and supportive environment, I was fortunate to have had the opportunity to join you to complete my thesis. Special thanks go out to Sélène Ledain and Fabio Oriani for their inputs and always being available to support me through content-related and technical difficulties.

A big thanks to Kevin Kramer from Agroscope, for continuously providing me with the outputs of ModVege and taking the time for discussions.

Also thanks to Thomas Steinsberger, Nadine Engbersen and Serafin Martig from VSLU for kindly sharing their valuable in-situ biomass data, the constructive exchange in Sursee and the continuous support during the process of preparing the data.

I would like to thank Lorenz Allemann from the Grassland Science group at ETH for sharing the in-situ measured LAI data from the FluxNet field, which was crucial for testing my model on independent data.

Also thanks to my co-supervisor Dr. Andreas Hueni and faculty representative Dr. Meredith Schuman for their support and constructive feedback.

Finally, I would like thank my friends for their mental support throughout this journey, and my parents, who made my studies possible.

Contents

Acronyms

AVHRR Advanced Very High Resolution Radiometer.

CV Cross-Validation.

DOY Day Of the Year.

EO Earth Observation.

EODAL Earth Observation Data Access Library.

ET_{rel} relative Evaporation.

ETP Evapotranspiration.

EVI Enhanced Vegetation Index.

GPP Gross Primary Production.

LAI Leaf Area Index.

LUT Look-up table.

ML Machine Learning.

MODIS Moderate Resolution Imaging Spectroradiometer.

NDVI Normalized Difference Vegetation Index.

NIR Near-infrared.

NN Neural Network.

NPP Net Primary Production.

PAR Photosynthetically Active Radiation.

RF Random Forest.

RGB Red-Green-Blue.

RMSE Root Mean Square Error.

RTM Radiative Transfer Model.

SAVI Soil-Adjusted Vegetation Index.

SCL Scene Classification Layer.

SPEI Standardised Precipitation Evapotranspiration Index.

SPI Standardized Precipitation Index.

UAV Unmanned Aerial Vehicle.

VHI Vegetation Health Index.

VI Vegetation Index.

VSLU Versuchsstation "Nährstoffflüsse" Luzern.

List of Figures

List of Tables

Chapter 1

Introduction

Grasslands cover about one-third of the Earth's terrestrial surface and play a crucial role in global ecosystems due to their extensive coverage and influence on climate regulation (Reynolds, 2005). 70% of the world's agricultural land are grasslands (Reynolds, 2005) and primarily used for livestock production through fodder cultivation and grazing. For centuries, they have secured the livelihood of millions of people globally (FAO, 2009). Besides their economic importance, grasslands also offer numerous essential ecosystem services. They provide habitats for bird species and insects, preserve biodiversity, sequester carbon, purify water, and mitigate soil erosion (Gibon, 2005; Gibson, 2009; Li et al., 2022). However, many grassland ecosystems are increasingly under pressure due to various factors, from intensified management to abandonment or climatic changes (Habel et al., 2013; Veen et al., 2014). In northern and central Europe in the last 30 year alone, 50-70% of the species-rich grassland have been lost (Habel et al., 2013). Despite their great occurrence globally and their invaluable ecosystem services, grasslands have not received much attention from the public, scientific community or policy makers in the past (Temperton et al., 2019). Considering the ecological importance of grassland, scientists are calling for more research in that field (Temperton et al., 2019; Török et al., 2021).

In Switzerland, about 36% of the total area is covered by agriculture, of which 70% is covered by grasslands (33% alpine pastures, 25% meadows and alpine meadows, and 12% farm pastures) (Figure 1.1). This equals a total area of 10'000 km2, which corresponds to a quarter of the country's total area covered by permanent grassland (Federal Statistical Office, 2023).

Different parameters influence the state and productivity of grasslands. Anthropogenic activities such as the frequency and quantity of mowing, the use of fertilizers and the intensity of grazing affect the quality of these lands (Di Giulio et al., 2001; Schils et al., 2022; Y. Zhang et al., 2018). Intensive management practices have shown to have negative impacts on grasslands, such as a decrease in biodiversity (Di Giulio et al., 2001), decrease in groundwater recharge (Rose et al., 2011) and loss of soil carbon and nitrogen (Guo & Gifford, 2002; G. Zhou et al., 2016). Management practices usually include mowing, grazing, fertilization and irrigation of a field. In the context of this work, management events refer exclusively to the mowing or cutting of grassland unless otherwise stated.

But also environmental factors, including temperature, precipitation, soil composition, and the availability of water and nutrients, play a crucial role in shaping the condition of grasslands. Additionally, extreme climate events like heavy rainfall and droughts can significantly affect the functioning of grassland

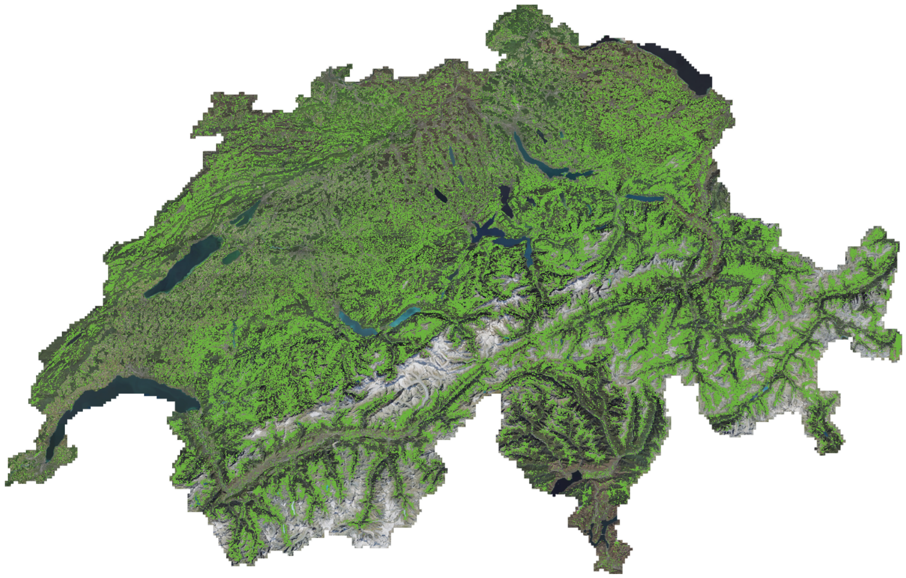

Figure 1.1: The area in green is the total area of grassland covering Switzerland (Weber et al., 2023).

ecosystems. Such extreme events have shown to induce shifts in plant interactions, to reduce above- and belowground Net Primary Production (NPP) (Carroll, 2021) and to intensify negative drought effects on fertilized grasslands (Van Sundert et al., 2021).

In the context of climate change, the frequency and intensity of these extreme weather events are expected to increase (Calanca, 2007; IPCC, 2023). Climate predictions for Switzerland suggest that the near-surface temperature will increase by 2.5 - 4.5 degrees in the summer months, heatwaves will become more frequent and severe, and dry periods will last up to 3 weeks (NCCS (Hrsg.), 2018). Especially droughts will increasingly have an impact on grassland productivity (Gibson & Newman, 2019). Calanca et al. (2022) found that drought conditions can reduce forage production up to 25%. It is thus essential to monitor and evaluate the state and growth of grasslands to help policies to optimize grassland management and conservation. However, tracking their status is challenging: fodder produced by the farms is usually not sold but used directly on the farms and, therefore, often not quantified. The losses due to changing climates and extreme events such as droughts are consequently not easily quantifiable (Reinermann et al., 2020).

Another approach to monitoring grassland production and management involves collecting in-situ data, though this process is both time-consuming and costly. Nevertheless, a reliable methodology is essential to study the impact of increasingly severe weather conditions effectively. Remote sensing offers a promising alternative, providing a cost-effective and scalable solution for analyzing grassland dynamics and assessing the effects of changing environmental factors (Ali et al., 2016; Reinermann et al., 2020; Stumpf et al., 2020). Various methods and parameters enable the monitoring of vegetation from their data. The use of Vegetation Indices (VIs) based on optical sensors is one of the most widely applied methods. VIs measure properties like grassland productivity, management type, or use-intensity (Reinermann et al., 2020). The limitations of the available data are its spatial and temporal resolution, and the degree to which biological processes are simplified. These constraints underline the potential of modelling approaches that can compensate for gaps in observational data. Models can simulate missing or incomplete data and thus gain insights when satellite data is insufficient. The integration of meteorological data, which include some of the main drivers for vegetation growth, combined with satellite imagery can facilitate the creation of comprehensive datasets. With these datasets, machine learning algorithms can be trained to learn the relationships between environmental parameters and plant traits (Verrelst et al., 2019), to model vegetation properties such as Leaf Area Index (LAI). LAI is defined as the total leaf area per unit of ground area (Watson, 1947) and is an important vegetation measure as it can be interpreted in its physical means, helping to understand structural characteristics of a plant canopy (Parker, 2020). It is retrieved from satellite imagery using plant canopy Radiative Transfer Model (RTM)s. RTMs are computational tools used to simulate the propagation of light through the atmosphere and its interaction with various surfaces along its path to derive vegetation properties from remotely sensed data (Jacquemoud et al., 2009). Recently, it has been argued that such trait retrieval methods should be further connected to crop growth models (Kooistra et al., 2024). Based on mathematical equations, mechanistic growth models replicate the underlying physical processes that drive vegetation growth, like photosynthesis, respiration, and evapotranspiration (Gaso et al., 2021). Plant growth is mainly controlled by temperature, light, water, humidity, and nutrient availability (Ryu et al., 2019). Most of these factors can be derived from meteorological variables and used as model input to predict plant growth under different environmental conditions (Nagamani & Nethaji Mariappan, 2017). However, the calibration of mechanistic models is complex, and the computation of each iteration limits the application of mechanistic growth models at the landscape level at high resolution (Dlamini et al., 2023). In their review, Dlamini et al. (2023) conclude that further research is needed on integrating external observations of crop parameters from Remote Sensing (RS) into crop models to improve model calibration and the accuracy of estimates from high-resolution datasets such as Sentinel-2.

In this study, we take a different approach and investigate whether grass growth can directly be learned from Earth Observation (EO) data: The objective of the thesis is to establish a robust Machine Learning (ML) grass growth model based on EO data, process-based modelling (RTM) and environmental variables. To the best of our knowledge, the proposed methodology for modelling vegetation growth is novel and promising. Grassland growth in Switzerland is investigated over the period from 2018 - 2023. In-situ measurements and LAI derived from Sentinel-2 images are used in combination with meteorological data to train a model to predict grass growth under different weather conditions. The ML based grass growth model is then used to analyze the impact of drought conditions on grass growth.

1.1 Research questions

The following research questions are formulated:

1. Is the LAI showing a better correlation with biomass compared to the EVI?
2. Can Sentinel-2 capture changes in grassland biomass, expressed as changes in LAI, over space time?
3. Can a grass growth model be learned from Earth Observation data?
4. Is the grass growth model trained on Earth Observation data capable of capturing the impact of drought on grassland growth?

Chapter 2

Background

This section summarizes existing research on satellite-based biomass estimations and methods, grass growth modelling, and drought assessment. Various modelling techniques are evaluated, the integration of satellite imagery and meteorological data is examined, and the impact of drought on grassland and how it is analysed is discussed.

The first section introduces the basic principles of remote sensing of grasslands and the optical satellites used most frequently. Studies estimating biomass and monitoring grassland dynamics using satellite imagery will be discussed (Section 2.1). The second section gives an overview of the approaches developed for grassland modelling, discussing empirical, mechanistic and ML models with their respective advantages and limitations (Section 2.2). In the final section, the effects of drought on grassland are addressed. Different drought indices and their application in assessing the effects of drought on grassland growth are discussed (Section 2.3).

2.1 Remote sensing of grasslands

Conventional monitoring of grasslands includes field measurements of biomass provided by farmers. Eddy covariance towers, phenocams or measurements from field spectrometers are other data sources often used to analyse grasslands (Reinermann et al., 2020). However, these methods are either time-consuming and expensive or spatially limited. Remote optical multi-spectral sensors provide continuous and large-scale data. This is especially valuable when analysing large or remote areas (Reinermann et al., 2020). From the spectral reflectance properties of this data, several vegetation characteristics like greenness, vitality, or density can be derived (Xue & Su, 2017).

2.1.1 Optical satellites for vegetation monitoring

The most commonly used multi-spectral optical sensors for vegetation monitoring are Moderate Resolution Imaging Spectroradiometer (MODIS), Landsat, the Advanced Very High Resolution Radiometer (AVHRR), SPOT-VGT and Sentinel-2 (Reinermann et al., 2020). Each of them having its own advantages and limitations, as each sensor represents a compromise between spectral, temporal and spatial resolution. Table 2.1 presents an overview of the period of operation and resolution of these sensors.

Sensor	active	Spectral res.	Temporal res.	Spatial res.
MODIS	1999 - today	36 bands	1 - 2 days	1 km
Landsat	1972 - today	4 - 11 bands	16 - 18 days	80 - 30 m
AVHRR	1978 - today	4 - 6 bands	1 day	1.1 km
SPOT-VGT	1998 - 2014	4 bands	1 day	1 km
Sentinel-2 (A / B)	2015 / 2017 - today	13 bands	5 days	10, 20, 60 m
PlanetScope	2014 - today	4 or 8 bands[1]	1 day	3 - 4 m

Table 2.1: List of optical satellites most often used for vegetation monitoring including their spectral, temporal and spatial resolutions.

For vegetation studies, Sentinel-2, the second satellite series in the Copernicus Sentinel fleet, is of particular interest for several reasons: The constellation, consisting of two satellites (Sentinel-2 A and Sentinel-2 B) in the same orbit, reduces the temporal resolution from 10 days to 5 days at the equator; with an even higher resolution at higher latitudes. The sensor offers 13 bands between 490 and 2190 nm at different spatial resolutions (10, 20 and 60 m) (European Space Agency, 2024) and currently provides the best combination of temporal and spatial resolution among non-commercial sensors. The Red-Green-Blue (RGB) and Near-infrared (NIR) bands with a resolution of 10 metres, which are needed for VI, are particularly valuable for vegetation analysis.

Due to its relatively high temporal resolution, Sentinel-2 provides a valuable data source for monitoring and analysing changes in vegetation and land cover over time, although the effectiveness of this advantage can be diminished by cloud cover.

2.1.2 Derivation of grassland parameters

The most commonly studied grassland parameters derived from satellite imagery are total biomass, productivity and management practices (such as mowing, grazing, irrigation, and fertilization) (Reinermann et al., 2020). To assess these parameters, indices like the Normalized Difference Vegetation Index (NDVI), Enhanced Vegetation Index (EVI), Soil-Adjusted Vegetation Index (SAVI), and LAI are frequently utilized (Reinermann et al., 2020; Xue & Su, 2017). RTMs are often used to quantitatively estimate biophysical parameters such as LAI (Reinermann et al., 2020).

2.1.2.1 Spectral indices

Multi-spectral optical sensors like Sentinel-2 measure the reflection of light at different wavelengths. In remote sensing, a spectral index refers to a mathematical combination of different spectral bands. By combining reflectance values from different wavelengths, these indices are intended to enhance the signal for specific properties such as the state of vegetation, soil characteristics or water bodies (Xue & Su, 2017). While VI are widely used due to their simplicity and ease of computation, they have certain disadvantages. The main limitation of VIs is the assumption of homogeneous surface cover. They only partially account for uncertainties related to atmospheric conditions and soil background effects and do not account for specific physical properties of the vegetation type. VIs assess the vitality of vegetation by measuring

[1] depending on the cubesat. Dove-C has 4 bands, Dove-R has 8 bands.

"greenness", which is not directly interpretable but used as a proxy for productivity, chlorophyll content or vegetation fraction (Huete et al., 2006).

2.1.2.2 NDVI and EVI

To investigate grasslands, the NDVI is the most widely used index, primarily due to its simplicity, requiring only the red and NIR bands for its calculation (Gao et al., 2016; Reinermann et al., 2020; Xue & Su, 2017). However, NDVI is known to exhibit saturation effects in areas of high biomass (Wu et al., 2010). Red reflectance values decrease as biomass increases, which reduces the sensitivity of the index to dense vegetation and causes saturation problems. The EVI addresses these limitations by incorporating a blue band in addition to the red and NIR bands to correct for atmospheric effects (Huete et al., 2002; Xue & Su, 2017). Additionally, EVI contains a gain factor to reduce sensitivity to saturation and a soil adjustment factor, making it less sensitive to canopy background effects. The additional coefficients make the calculation of the EVI more complex, but it outperforms NDVI, making it a more reliable index for biomass estimations (Huete et al., 2002).

Guerini Filho et al. (2020) demonstrated in a study that VIs based on Sentinel-2 are promising indicators for biomass estimations of grasslands. Y. Zhou et al. (2014) have used different VIs to estimate Gross Primary Production (GPP) in China with a simple linear model using MODIS data. They found that EVI performed best at approximating GPP due to its background adjustment factor and remaining sensitive to vegetation changes. Another study investigating the effectiveness of VIs to estimate GPP in Australia has found that the red-edge chlorophyll index CIr performs best in estimating GPP. Looking only at non red-edge indices, they found all models using EVI performing better than the models using NDVI (Lin et al., 2019).
However, Danner et al. (2021) argue that most VIs do not capture the complex, non-linear relationship between photons and biophysical and -chemical plant properties. They are more sensitive to noise, since they only take into account a few bands. In addition, parametric regressions (especially VIs) usually provide only one variable at a time. RTMs on the other hand, account for some of these limitations.

2.1.2.3 Plant Canopy RTMs

A review by Ali et al. (2016) has found that retrieving biophysical parameters from traditional regression analyses with VIs progresses to more sophisticated, efficient, and robust modelling approaches. Among these advanced methods is the use of RTMs, which enables the estimation of productivity by deriving biophysical parameters directly from remote sensing imagery.

An RTM is a computational tool commonly used in remote sensing to simulate light propagation through the atmosphere and its interaction with various surfaces along its path. RTMs are based on principles derived from radiative transfer theory, which quantifies the interaction of radiation with matter that affects the radiance observed by sensors on satellites or ground-based instruments. This includes interactions with atmospheric gasses and aerosols, and the way radiation is absorbed and scattered by different surface types. Inverted RTMs can be used to retrieve various surface properties from remotely sensed data (Jacquemoud et al., 2009).
Based on these principles, the canopy's spectral and structural properties can be related to the radiation leaving a canopy. The PROSAIL RTM, which is widely used in vegetation studies to derive LAI, integrates the PROSPECT model of leaf optical properties (Jacquemoud & Baret, 1990) with the SAIL (Kuusk, 1991; Verhoef, 1984) canopy reflectance model. PROSPECT calculates the directional-hemispherical

reflectance and transmittance of leaves based on chemical constituents such as leaf chlorophyll a + b concentration, brown pigment and dry matter content, equivalent water thickness and a leaf structural parameter (Jacquemoud et al., 2009). SAIL is one of the first canopy reflectance models (Verhoef, 1984). By solving the scattering and absorption of four upward and downward radiative fluxes, it simulates a one-dimensional bidirectional reflectance factor of horizontally homogenous and semi-infinite layers (Jacquemoud et al., 2009). SAIL assumes each layer to consist of many small vegetation elements of varying geometry and density that absorb and scatter incoming radiation (Darvishzadeh et al., 2008). The model requires parameters such as sun and sensor angle, fraction of diffuse solar radiation, LAI and Average Leaf inclination Angle (ALA) to describe the interaction of radiation with the canopy. A parameter for soil brightness takes into account the effects of soil moisture and roughness on reflectance (Jacquemoud et al., 2009). Finally, a hot spot parameter accounts for the maximum backward scattering of radiation when the sun and the sensor are aligned (Kuusk, 1991). By combining PROSPECT and SAIL into PROSAIL, the model leverages a physically-based approach to simulate the entire chain of radiation interactions within vegetation canopies. PROSAIL starts with detailed leaf-level properties (PROSPECT) and uses them as inputs to compute canopy-level reflectance (SAIL) (Jacquemoud et al., 2009).

To retrieve a biophysical parameter, PROSAIL is first run in forward mode to generate a Look-up table (LUT). By giving the model a range of input parameters of different properties like chlorophyll, dry matter or leaf orientation, it generates a given number of random combinations of input parameter values and relates each combination with a reflectance spectrum (Jacquemoud & Baret, 1990). The simplest way of solving the inversion of an RTM is by using a LUT (Darvishzadeh et al., 2008). To retrieve a biophysical parameter from the satellite images, a cost function is used to match each spectrum measured by the satellite with a modelled spectrum in the LUT. The corresponding biophysical parameters of the modelled spectrum with the smallest deviation from the measured and modelled spectrum are assigned to the pixel (Combal et al., 2003).

RTMs, while more complex to retrieve, offer several advantages over VIs. Compared to VIs, RTMs physically model the canopy structure and can account for factors like leaf orientation and density, providing a more mechanistic understanding of vegetation dynamics (Danner et al., 2021). RTMs rely on a predefined set of parameters adapted to realistic value ranges based on prior knowledge about the prevailing vegetation type. They are equipped with a more detailed and exhaustive characterization of site-specific properties, providing them with a distinct advantage in vegetation and biomass estimation. The main limitation of RTMs is that they are computationally expensive (Verrelst et al., 2019).

2.1.2.4 LAI

LAI is considered to be a state-of-the-art parameter, derived with RTMs such as PROSPECT and often integrated in vegetation studies (Alexandridis et al., 2020; Ali et al., 2016; Asam et al., 2015; Atzberger & Richter, 2012). It is physiologically interpretable and is a direct indicator of the amount of leaf area on a given ground area, measured in m^2/m^2 (Watson, 1947). LAI is one of the most fundamental parameters in ecosystem modelling (Wang et al., 2022), providing insights into plant photosynthesis and the growth status of vegetation. LAI can have both, positive and negative impacts on growth. Higher LAI can increase growth due to a higher photosynthetic capacity. However, the shadowing of the lower leaves found to decrease growth rates (Street et al., 2007).
LAI derivations have shown to be more sensitive in regions with dense vegetation, making it a more reliable proxy for biomass compared to the EVI, which tends to saturate earlier (Alexandridis et al., 2020). This

makes the analysis of physiological processes like plant growth or absolute biomass more straightforward and allows for direct comparison with the outputs of mechanistic models, which frequently provide LAI as a key parameter (Calanca et al., 2016).

Quan et al. (2017) have used different methods, among others the PROSAIL RTM to derive LAI as a proxy for grassland above ground biomass from Landsat-8 data. They have found the highest accuracy of estimating biomass is the RTM-based method and argue that it offers great robustness at a large scale, especially when no field measurements are available. Punalekar et al. (2018) have also investigated the potential of LAI estimations from PROSAIL. They have found that the retrieved LAI from Sentinel-2 images compared well with in-situ measured LAI and outperformed biomass estimates based on the NDVI. However, they found that LAI was overestimated for pasture mixtures with high LAI.

2.1.3 Monitoring grassland dynamics and use-intensity

While spectral indices as well as LAI derived from single satellite images represent individual points in time, it is essential to also capture the temporal dynamics of grassland ecosystems. This is particularly important for the effective monitoring of ecological and anthropogenic influences such as droughts or use-intensity of grassland. Vegetation dynamics can be investigated using satellite time series data. Monitoring these dynamics involves assessing changes in biomass over time, which provides insights into how grasslands respond to different conditions and management practices. For example, mowing frequency is often used as an indicator of management intensity, which serves as a proxy for monitoring grassland conservation and is of direct relevance to policy making (Griffiths et al., 2020).

A variety of methods were used to monitor the dynamics of grassland. In their study Andreatta et al. (2022) investigated mowing frequency on grasslands in the Italian Alps. For their algorithms, they used Sentinel-2 time series data and several VIs. They achieved an 89% accuracy of detecting mowings. Similarly, Griffiths et al. (2020) have developed an NDVI-based algorithm to detect and quantify the number and timing of mowing events from Sentinel-2 and Landsat-8 imagery for grasslands in all of Germany. Lange et al. (2022) have explored the possibility of land-use intensity mapping for grazing, mowing and fertilisation by combining ML algorithms with Sentinel-2 time series across Germany. With their approach, they achieved a 68% classification accuracy for mowing events. Weber et al. (2023) have developed a rule-based algorithm to produce annual grassland-management maps capturing the number and date of cutting events for all of Switzerland based on Sentinel-2 data. Most of the detected management events corresponded to actual events (78%), but they also found that grazing events at higher elevations were more challenging to detect, missing up to 57% of events.

2.2 Grassland growth modelling

The main limitations of satellite-based monitoring are its temporal resolution, and the inherent simplification of complex biological processes. These constraints highlight the potential of modelling approaches, which can generate predictions across varying temporal scales and incorporate multiple levels of complexity to better represent plant dynamics. Furthermore, models are not constrained by cloud cover, enabling them to fill gaps in satellite data and provide continuous insights into ecosystem functioning.
To simulate vegetation growth, different types of models can be used. This section outlines mechanistic, empirical and ML models in more detail. Their principles and applications as well as their advantages and limitations are described.

2.2.1 Mechanistic or process-based models

Mechanistic or process-based models are based on explicit assumption about how a system works (Cuddington et al., 2013). These models are rooted in understanding the fundamental mechanisms of plant growth, such as photosynthesis, respiration, nutrient uptake, and water use. On the basis of these principles, they are designed to simulate the physiological and biochemical processes that control vegetation growth, enabling them to predict grass growth under a variety of environmental conditions. These models typically incorporate parameters such as soil moisture, temperature, and nutrient availability, which are essential for accurately simulating growth processes. However, they can be complex and computationally intensive, requiring detailed input data that may not always be available (Cuddington et al., 2013). Additionally, the accuracy of these models heavily depends on the quality of the input data and the precision of the parameterization.
The previously discussed RTM is an example of a mechanistic model that simulates radiation based on the propagation and interaction of light along its path.

2.2.1.1 ModVege

ModVege is a mechanistic, dynamic model that simulates seasonal patterns of above-ground herbage growth at the field scale (Jouven et al., 2006). It is designed as a bucket model with four main compartments: green leaves and sheath, dead leaves and sheath, green stems and flowers, and dead stems and flowers. The compartments are characterized by its biomass, age and digestibility. It models mass flux as a function of the proportion of functional groups, weather data (temperature, Photosynthetically Active Radiation (PAR), precipitation, potential Evapotranspiration (ETP)) and site specific characteristics like a nitrogen nutrition index and soil water-holding capacity. Age affects the three main processes: growth, senescence and abscission. The ageing of the plant parts is determined by the cumulative thermal time from the 1st of January and by the biomass flows (Calanca et al., 2016; Jouven et al., 2006). The greatest impact on the modelled growth comes from the functional groups, which define the frequency of defoliation and the fertility of a site and could be considered as an approximation for the use intensity.

2.2.2 Empirical models

Empirical models rely on statistical relationships (Cuddington et al., 2013) between observed grass growth and environmental variables such as temperature, precipitation, and soil properties. These models are often based on regression analysis or other statistical techniques that establish correlations between input variables and biomass or productivity. They are particularly useful in scenarios where historical data is available, allowing for the derivation of reliable statistical models. An example is the use of NDVI-based regression models to estimate grassland biomass. The primary advantage of empirical models is their simplicity and ease of use. However, they are limited by their reliance on historical data and their inability to account for complex, non-linear interactions between variables. They may also struggle to predict growth accurately under novel conditions not represented in the data from which the model learned the statistical relationship (Cuddington et al., 2013).

2.2.3 Machine learning models

ML models represent a more recent approach to predicting grass growth, utilizing advanced algorithms that can learn patterns and relationships from large datasets (Lary et al., 2016; Olden et al., 2008). These models can handle a wide range of input variables, including both traditional environmental factors and remotely sensed data, to predict grass growth with high accuracy. ML models can automatically adjust and improve their predictions as more data becomes available. Techniques such as Neural Network (NN), Random Forest (RF), and support vector machines (SVM) are commonly used in this category (Olden et al., 2008). These models can capture complex, non-linear relationships between variables that traditional statistical methods might miss (Lary et al., 2016). A NN model might be trained on historical weather and growth data to predict future biomass under varying conditions. The major advantage of ML models is their ability to process and learn from large, complex datasets, making them highly flexible and adaptive. However, these models require substantial amounts of data for training and can be prone to overfitting if not carefully managed (Olden et al., 2008).

Kenny et al. (2024) have investigated the potential of ML and mechanistic models for grass growth predictions. They argue that mechanistic models are more robust in modelling disruptive climate events compared to ML models. However, overall ML models are performing better in grass growth predictions than mechanistic models, given the data they are trained on is clean and precise. Although ML models have already been applied for modelling crops, their use for predicting grass growth is still quite uncommon. Kenny et al. (2024) reason that this is due to the lack of quality data, the need for a full-year model as grass grows all year around and generally lower investments in the sector. A study by De Rosa et al. (2021) uses data from an Unmanned Aerial Vehicle (UAV) and a ML model to predict grassland biomass. Using a RF model, they achieved an R^2 of 0.68 in predicting pasture biomass. Muro et al. (2022) stated that machine and deep learning models achieved biomass predictions with accuracies of R^2 values between 0.2 and 0.7.

2.2.3.1 Random Forest model

The following passages provide more detailed technical information on the RF model. RF is an ensemble learning method developed by Breiman (2001) that is often used for regression (RF Regressor) and classification (RF Classifier) tasks. RF employs several decision trees, where each tree is built on a random subset of the data and features that are created during training. The final prediction of the model is the average prediction of all individual trees, improving prediction accuracy and controlling overfitting compared to single decision trees (Pedregosa et al., 2011).

To establish a RF model, three main factors have an influence on how well a model can describe the target variable. Firstly, the amount of data and its quality and quantity, secondly the variables (features) chosen to explain the target variable, and thirdly the hyperparameters that define the structure of the RF regressor. The features and hyperparameters are described in more detail below.

K-fold cross validation

To prevent a model from overfitting the k-fold Cross-Validation (CV) can be applied. This method prevents the RF model from using the same data for learning and testing, which would result in an overfitted model. The k-fold CV randomly splits the full dataset into k folds and then trains a model using k-1 folds as training data. The remaining fold represents the test data with which the resulting model is then evaluated (Pedregosa et al., 2023).

Features

Features are the explanatory variables of a RF model. The quality and the combination of the features is crucial for the accuracy of the model predictions. Evaluating the importance of features in a model can help to find the best set of features to predict the response variable. Based on the Gini importance, the feature importance property measures how effectively each feature reduces model uncertainty. The higher the feature importance, the more uncertainty it reduces (Pedregosa et al., 2011).

Hyperparameters

Hyperparameters are configuration settings that are defined before model training begins. Their purpose is to guide the learning process of ML algorithms. Unlike model parameters, which are learned during training, hyperparameters are set manually and can significantly affect the performance and efficiency of a model. In a RF model, the hyperparameters play a crucial role in determining the complexity and accuracy of the model (Bergstra & Bengio, 2012).

The hyperparameters often used for modelling are:

- number of trees ('n_estimator'): this defines the number of trees in the forest. More trees usually lead to better performance of the model, but increase computational costs.
- maximum depth of trees ('max_depth'): this limits the maximum depth of each decision tree. Smaller depths usually prevent overfitting.
- minimum sample number for a split ('min_sample_split'): this specifies the minimum number of samples required to split the samples again at a node. Higher values can prevent overfitting.
- minimum samples per leaf ('min_samples_leaf'): this defines the minimum number of samples that a leaf node must have.
- bootstrapping samples ('bootstrap'): this determines whether to bootstrap samples or not when building the trees. If this parameter is set to False, all data is used to build each tree in the model.

For optimising hyperparameters, grid search and manual search are the most commonly used strategies, whereas random search shows to be more efficient (Bergstra & Bengio, 2012). The open source library for ML scikit-learn Python (Pedregosa et al., 2011) offers a package for both, the Random Search CV as well as the Grid Search CV.

To initialize a Random Search CV, a RF Regressor model with its features and a predefined search space for hyperparameters is required. This search space usually covers a wide range of possible values for each hyperparameter. The Random Search CV method then generates n models with random combinations within this search space and trains the model for each combination. After training, the performance of each combination is evaluated using an evaluation metric, which measures how well the model explains the variance in the data. The method then ranks these combinations based on their scores and identifies the best performing hyperparameters. This process is repeated N times. From this initial analysis, a list of the best performing hyperparameters is created. This list helps refining the search space by narrowing down the ranges or values of the hyperparameters for more targeted tuning. The refined search space is then provided to the Grid Search CV method, which systematically examines an exhaustive set of hyperparameter combinations within the narrowed range. This Grid Search CV method aims to find the best possible set of hyperparameters, again based on the R^2 score, and provides a more precise tuning of the model for improved performance.

2.3 Impact of drought on grassland

2.3.1 Drought effects on grasslands

Drought is typically defined as a deficit in rainfall relative to normal levels, known as meteorological drought (Mishra & Singh, 2010). As the NCCS (Hrsg.) (2018) states, dry periods will last up to 3 weeks in Switzerland in the future. As a consequence of a changing climate, grasslands will be subject to change too. Especially precipitation, or lack thereof, has shown to be a major determining factor for grassland productivity (Reinermann et al., 2020). The effect of climate on the productivity of grassland is increasingly becoming a subject of interest (Lei et al., 2015; Reinermann et al., 2019; Vogel et al., 2012a).
Studies have found that above and below ground grassland productivity is reduced by drought conditions (Carroll, 2021; Hoover et al., 2014). Lei (2020) has investigated grasslands in Mongolia and found that different grassland types react differently to droughts, and increasing drought levels significantly increased NPP loss. Reinermann et al. (2019) have found strong negative anomalies in EVI when analysing grasslands during drought years in Germany. Vogel et al. (2012a) have found that increased species richness can increase the resilience of grasslands to droughts, reducing the loss of above ground productivity. A study conducted in Switzerland has found that there is no general drought response of Swiss grasslands, but they conclude that sites with lower annual precipitation are more vulnerable to summer droughts compared to sites with higher annual precipitation (Gilgen & Buchmann, 2009). In another study by Finger et al. (2013), who have investigated the economic impact of droughts on grassland productivity in Switzerland, the relative yield losses were estimated to be up to 37% on sub-alpine fields.

2.3.2 Drought indices

Drought indices are useful tools for monitoring and quantifying the effects of drought on grasslands. These indices translate complex environmental data into simplified, interpretable values that can be used to assess the severity, duration, and spatial extent of drought conditions. The Standardized Precipitation Index (SPI) is is a widely used measure for assessing drought events (Almeida-Ñauñay et al., 2022). This index quantifies wetness by comparing precipitation levels over a specific time frame against the entire time series. The Standardised Precipitation Evapotranspiration Index (SPEI) is an improved version of the SPI, additionally incorporating ETP (Vicente-Serrano et al., 2010), and has shown to be a better drought indicator due to the consideration of the effect of temperature. Drought indices used in agriculture are the Vegetation Condition Index (VCI), which bases on the NDVI and compares current NDVI to a reference period, the Vegetation Health Index (VHI) which is a combination of the VCI and the Thermal Condition Index (TCI), which itself is derived from land surface temperature (Bento et al., 2018).
Studies have used drought indices such as the SPI and the SPEI to investigate at what time scale a meteorological drought index is able to detect agricultural drought indicated by the agricultural drought index VHI (Almeida-Ñauñay et al., 2022), or have evaluated the success of a meteorological drought index (SPEI) and an agricultural drought index (VHI) in recognizing drought in agriculture (Pogačar et al., 2022). Calanca et al. (2022) have analysed if summer droughts can be observed in meadow and pasture yields in Switzerland. They used relative Evaporation (ET_{rel}), defined as the ratio of actual to potential evaporation, as a proxy for drought. This metric is advantageous because it can be calculated for each location independently while still allowing for comparison between different locations as it is not, like other indices, calculated relative to a reference period. They have found that drought can reduce forage production from grasslands up to 25%.

Chapter 3

Data

3.1 Study area

The main study area of this thesis is a set of field plots located in the canton of Lucerne in central Switzerland. Lucerne is one of the most important agricultural cantons in Switzerland, it has the highest density of pig farms, and is also one of the top producers of cattle. To feed their livestock, many farms cultivate grasslands. 20 % of the canton's area is open arable land, of which almost 70 % is used for grazing and animal feed production (Schläpfer, 2021).
Lucerne's elevation ranges from 419 to 1'123 meters above sea level. In the summer months, the average maximum temperature is around 24 °C, and the minimum is around 14 °C. In winter, temperatures reach an average maximum of around five and minimum of around -2 °C. Average precipitation in the summer is around 165 mm and around 65 mm in winter. With climate change, mean precipitation amounts will tend to decrease in summer and increase in winter. The longest dry periods in summer of 10 days will increase by 1.4 days (-0.4, +8.6 days) (NCCS (Hrsg.), 2021).

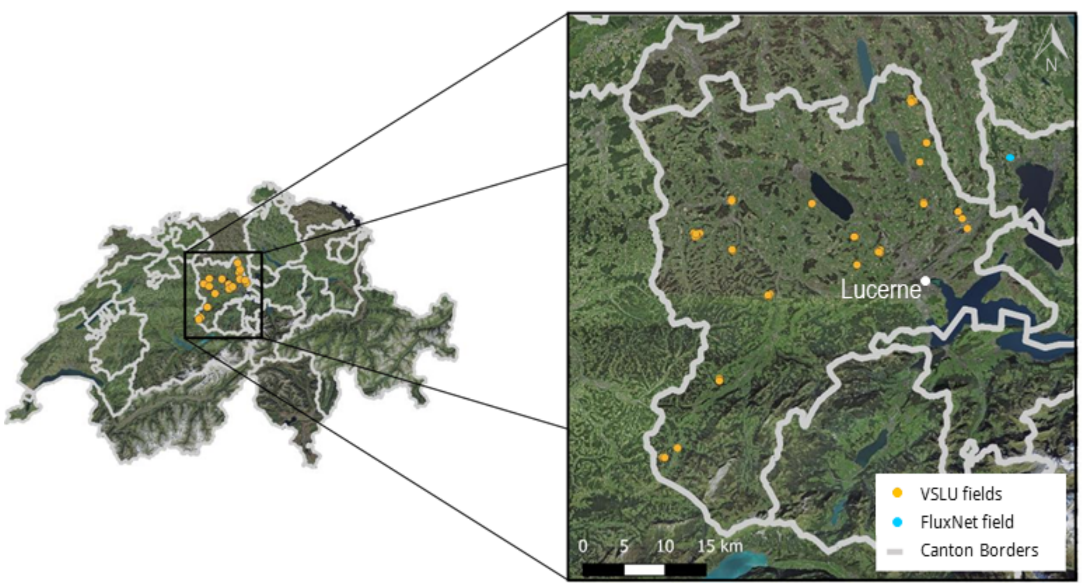

Figure 3.1: Map showing the locations of the 37 VSLU fields in canton Lucerne from which grassland growth was derived to train the grass growth model.

3.1.1 VSLU fields

Grassland biomass measurements from 13 farms on 37 different fields were used for the study (Figure 3.1, Versuchsstation "Nährstoffflüsse" Luzern (VSLU) fields). The field sizes vary between 0.5 and 1 hectare. The grassland parcels are used for hay production and grazing, and are managed 4 to 7 times per year (Weber et al., 2023). Precise management practices and use-intensities of the fields are not known. The farms from which the data were collected are located in the midlands and on the northern flanks of the Alps. They are part of a farm network that collaborates with Agroscope's experimental research station for nutrient flow (VSLU) located in Sursee. The network of farms they collaborate with is distributed across the whole canton.

3.1.2 FluxNet field

The field on which the in-situ LAI measurements were acquired is located in Chamau in the canton of Zug (Figure 3.1, FluxNet field) at 393 m above sea level and part of the Swiss FluxNet sites (Swiss FluxNet, 2024). The predominant vegetation on the field is a mixture of Italian ryegrass and white clover. The parcel is used for fodder production and occasional winter grazing by sheep. The field is an intensively managed grassland parcel with six cuts per year (Swiss FluxNet, 2024).

3.2 In-situ data sets

3.2.1 VSLU biomass field data

The biomass data provided by VSLU, was collected during the growing period of 2022 from March to October and the beginning of 2023. Each year, the 13 farms were visited multiple times, to measure grass biomass on a field that was soon to be grazed by cows. At each visit, biomass was measured on another field. The measurement locations were localized with a cell phone GPS. The exact extents of the fields on which measurements were taken were not recorded. With a rising plate meter (EC20 Bluetooth Electronic Platemeter (Jenquip, New Zealand)), the grass height was recorded approximately every meter across the field parcel. Around 60 readings were taken for each field, on smaller fields a bit less. These measurements showed a large variation in grass heights. To estimate the biomass on the whole field, a reference area of $7\,\mathrm{m}^2$ was mowed and weighed and used to generate a field-specific calibration equation for the plate meter measurements to determine the average biomass on the whole field. An average biomass estimation in fresh and dry $\mathrm{kg/m}^2$ was determined for each field.
The dataset received from VSLU contained 82 unique fields. Biomass was not measured at some locations because the grass was too low to cut or fields were no longer grazed, so that only 61 biomass measurements were available. Out of these 61 biomass measurements, 24 measurements were discarded due to an unclear location of the field, tree coverage, fields that were too small or narrow shapes, or too close to roads, buildings, or forests that caused significant radiometric impacts or shadows. The final data set consisted of 37 biomass measurements, each measured on a separate field.

3.2.2 FluxNet in-situ LAI

The in-situ measured LAI data from the FluxNet field was provided by ETH's Grassland Sciences Group. LAI data is acquired at the site with the LAI-2000 Plant Canopy Analyzer (LI-COR Biosciences, USA) since 2015. For this study, data from 2019, 2020, 2022 and 2023 was used. Data from 2018 was not included as there were too little data points available. 2021 was not considered in the analysis because the field was in very poor conditions and showed patches of bare soil in 2019 and 2020, such that it was ploughed and reseeded in 2021. The final data set comprised a total of 46 LAI measurements over the four years. Besides the LAI measurements, the timing and type of management (fertilization, mowing, grazing) occurring on the field was also provided.

3.3 Satellite data

3.3.1 Sentinel-2

All Sentinel-2 data used for the study was acquired using Earth Observation Data Access Library (EODAL) (Graf et al., 2022). EODAL is a platform for accessing and retrieving satellite data. The platform allows the download of specified areas within a Sentinel-2 image tile, such that not the full tile has to be downloaded and processed. For the study, the atmospherically corrected surface reflectance data (Level 2A) from 2018 to 2023 was downloaded and pre-processed. The pre-processing consisted of filtering out scenes that were covered with snow, clouds or shadows. To identify these unsuitable images, the Scene Classification Layer (SCL) was consulted, a standardized product which is included in the Level 2A deliverables. The SCL is a 20 m resolved band, that contains a label with a surface type for each pixel (Copernicus Open Access Hub, n.d.). Two filters were applied, one scene and one pixel-based. The scene-based filter discarded the images with an overall cloud coverage higher than 70%. The pixel-based filtering evaluated the pixels on the field parcels and discarded the scenes with more than 10% of all pixels classified as non-vegetated. Due to the limited detection of cloud and shadow edges in the SCL, a buffer of 50 m was implemented around the field plots for the pixel-based filtering. The enlargement of the fields ensured the removal of images containing clouds or shadows in proximity to the plots, reducing possible influences on the radiometry of the scene. For the 37 field measurements and the period of the 6 years, a total of 6'133 snow and cloud-free Sentinel-2 images were collected and used for further analysis. Each of the scenes was saved as a TIFF file, including all 10 and 20 m resolved bands (B2, B3, B4, B5, B6, B7, B8, B8A, B11, B12).

3.3.2 PlanetScope

Planet is a private earth imaging company that operates a fleet of small satellites named "Doves". These satellites provide global coverage with daily RGB-images and a spatial resolution of 3-4 m. For this study, single images were consulted as a reference for qualitative comparison. The scenes were accessed through the Planet Explorer (Planet Labs PBC, 2024).

3.4 MeteoSwiss weather data

MeteoSwiss, the Swiss Federal Office of Meteorology and Climatology, provides a range of weather and climate data for Switzerland. An extensive monitoring network across the whole country collects the data. To reach full spatial coverage of Switzerland, the data from the monitoring network is combined with radar and satellite imagery that is integrated into a gridded data product with a spatial resolution of 1'000 m covering the whole country (MeteoSwiss, 2024). The data set contains different variables at daily, monthly and yearly resolutions. For the thesis, three variables were used in daily resolution from

2018 to 2023: daily average temperature ("TabsD") in degrees Celsius, daily precipitation ("RhiresD") in mm and daily relative sunshine duration ("SrelD"). These three variables were obtained for the locations of the 13 VSLU farms as well as for the FluxNet field. Since relative sunshine duration is not directly correlated with plant growth, PAR was estimated from that measurement (see Section 4.4.1.2). Figure 3.2 gives an overview of the daily values of precipitation, temperature and PAR at the FluxNet field in 2020.

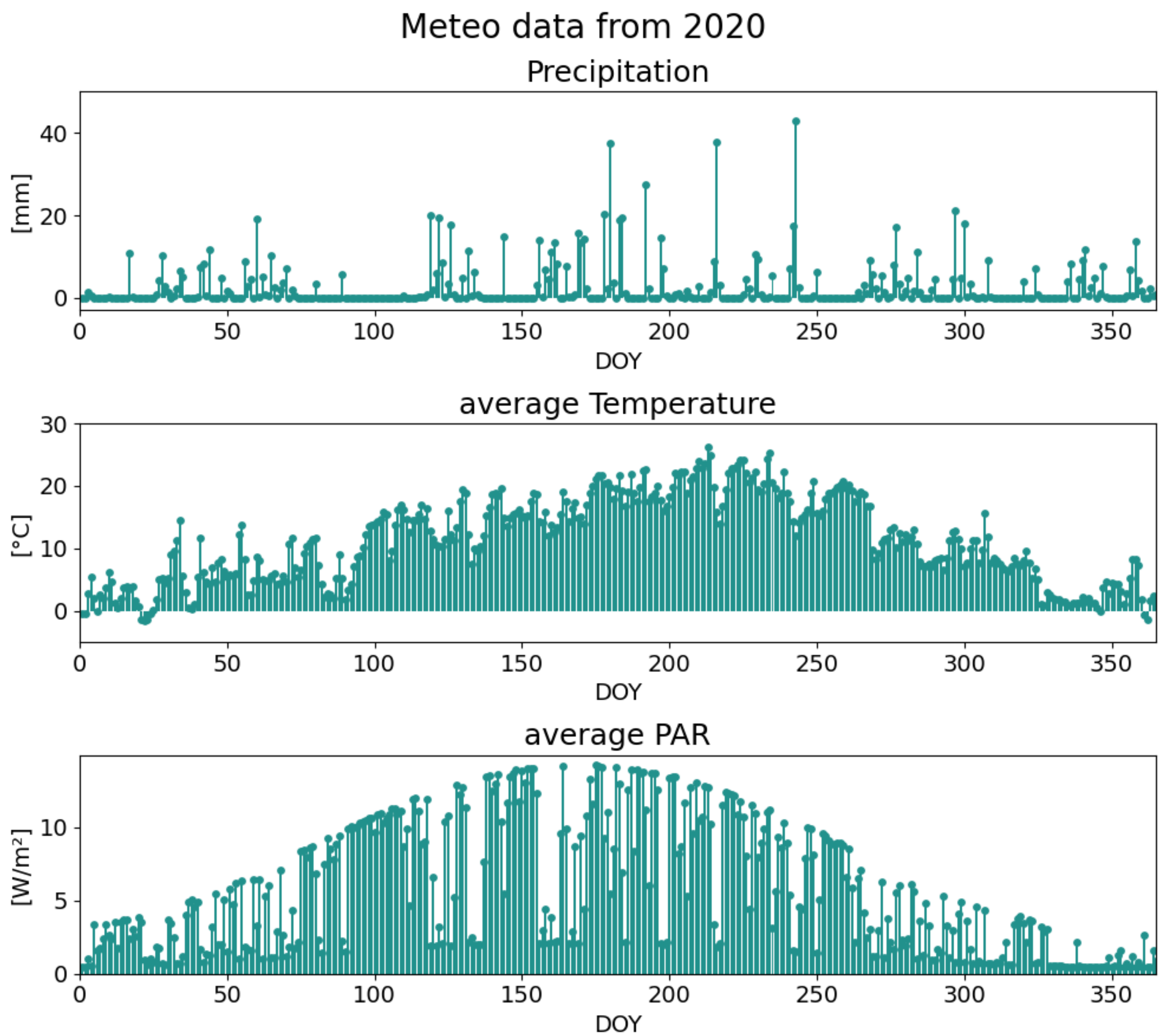

Figure 3.2: Daily meteorological data at the FluxNet site in 2020.

Figure 3.3 provides a comprehensive overview of the weather conditions in the examined years. The figures on the left show the 7-day average cumulative sums of precipitation, temperature and PAR at the FluxNet site for all years from 2018 to 2023. The right column shows the difference of the years relative to the average of the six years. The cumulative data shows how the individual variables have accumulated over time, highlighting years with excessive rain as well as droughts. The relative difference between the years provides an overview of the conditions between the studied years.

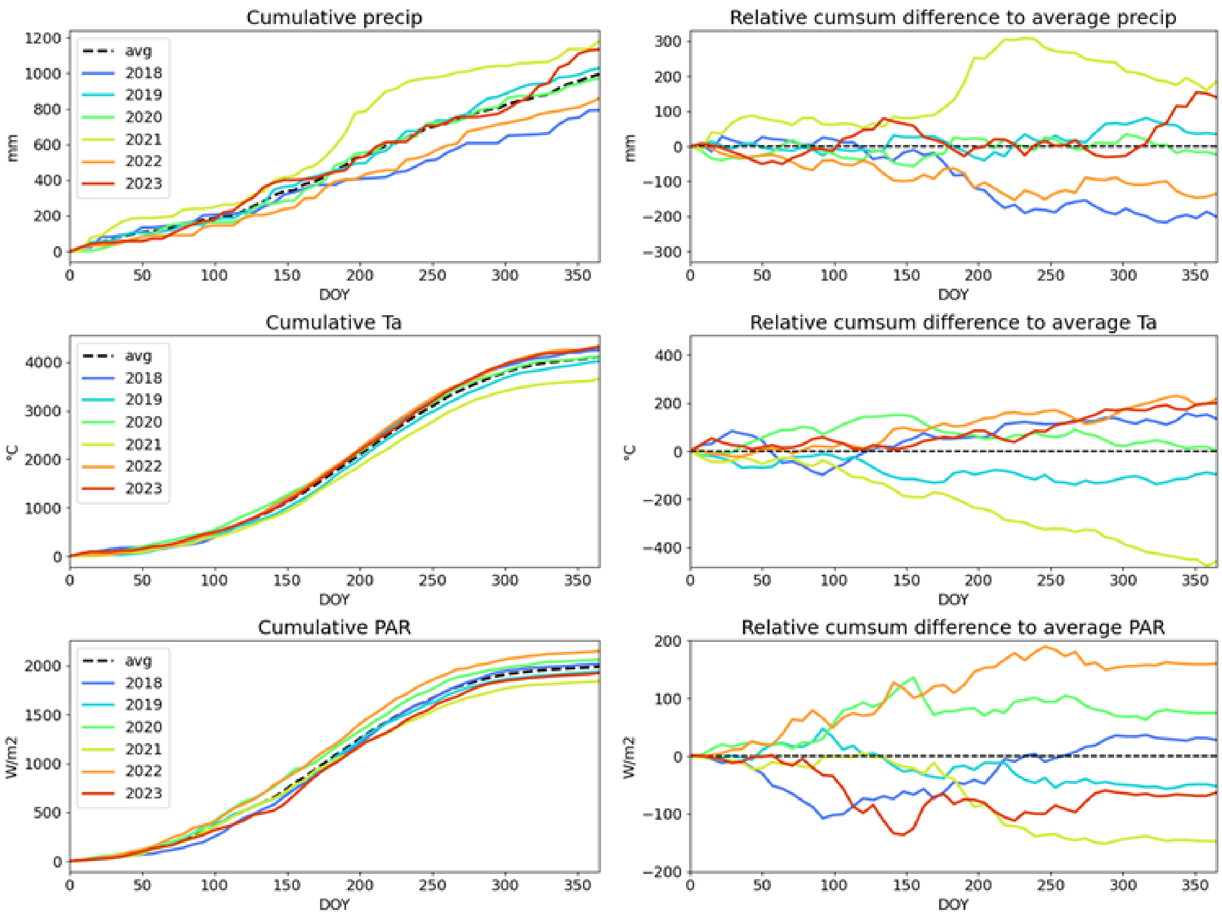

Figure 3.3: Cumulative sum of precipitation, temperature and sunshine at one of the locations for all years from 2018 to 2023.

3.5 Grassland use-intensity maps

Using Sentinel-2 and Landsat data, Weber et al. (2023) have developed a rule-based algorithm to create annual maps that indicate the number and timing of management events (mowing and grazing) on grasslands throughout a year in Switzerland. The detection of management events was validated by using independent reference data obtained from daily time series of publicly available webcams distributed across Switzerland. The grassland use-intensity maps are rasters at a 10 m resolution provided for each year between 2018 and 2021, covering all Swiss grasslands (Weber et al., 2023). In this study, the cutting dates indicated by these maps were used for a comparative analysis.

Chapter 4

Methods

4.1 Overview

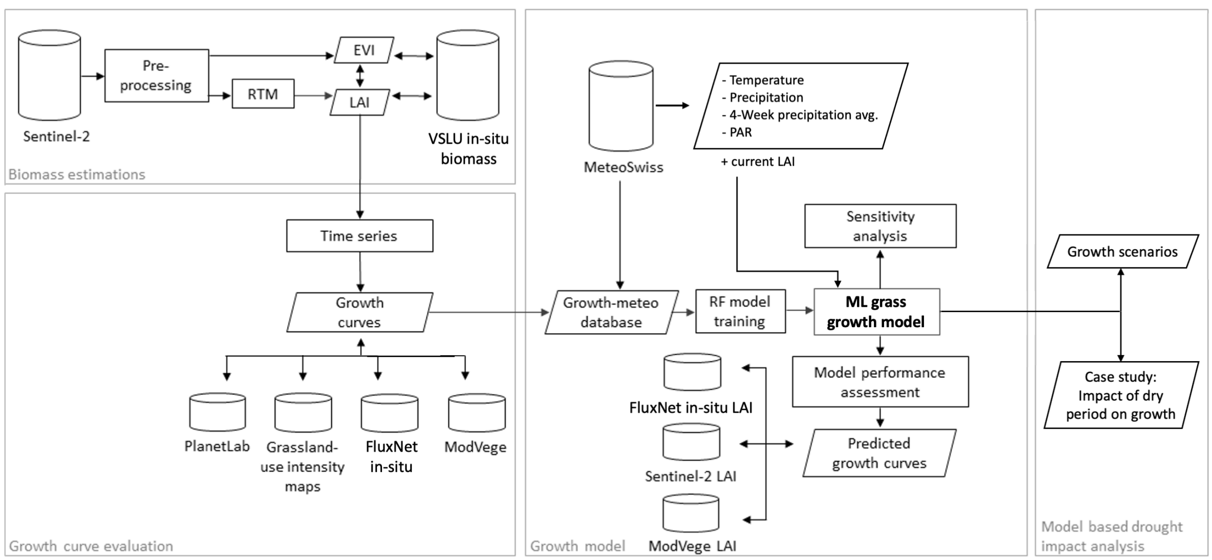

Figure 4.1: Flow chart showing the four main parts including the processing steps.

The methods of the thesis are divided into four main parts, as illustrated in the flow chart (Figure 4.1). The first part examined whether LAI is a better proxy for biomass than EVI. This was done by deriving the EVI and the LAI from Sentinel-2 data acquired from the VSLU fields and comparing it to the VSLU biomass data (Section 4.2).
In the second part time series were evaluated, and it was investigated whether Sentinel-2 can capture changes in grassland biomass, expressed as changes in LAI over time. For this, time series data was extracted from the Sentinel-2 images from 2018 to 2023 from each VSLU field. These were then compared with the highly resolved PlanetScope data (Planet Labs PBC, 2024) and a Grassland use-intensity map (Weber et al., 2023) to cross-check the timing of management events. To investigate the time series dynamic, the curves were compared with in-situ measured LAI time series as well as to the predicted growth of the mechanistic model ModVege (Kramer & Calanca, 2024) (Section 4.3).
The third part included the development of the ML grass growth model. This was established by creating

a database containing the grass growth derived from the LAI time series and meteorological data of the corresponding time period and location. A RF model was then trained to predict grass growth and investigate how different weather conditions influence growth. To assess the performance of the model, grass growth was predicted for a FluxNet field and the predicted growing curve was compared with in-situ, Sentinel-2 and ModVege time series data. A sensitivity analysis was conducted to test how sensitive the model is to each input variable (Section 4.4).
In the last part, growth for different precipitation scenarios was simulated to investigate the model's capability of assessing the impact of reduced and increased precipitation on grass growth. Finally, a case study investigated how grass growth was impacted during an elongated dry period on the FluxNet field in spring 2020 (Section 4.5).

4.2 Biomass estimations: EVI and LAI as proxies for grassland biomass

This section describes how the EVI was calculated and the LAI was derived from the Sentinel-2 data from the VSLU fields. It further outlines how the two biomass proxies were compared with the VSLU biomass field data to investigate whether LAI shows a better correlation with biomass than EVI.

4.2.1 EVI calculation

In the literature, EVI is stated as a proxy for biomass (Lin et al., 2019; Reinermann et al., 2020; Tanaka et al., 2015). Consequently, EVI was calculated for every pixel in each image according to the following formula (Huete et al., 2002):

$$\mathrm{EVI} = G \times \frac{\mathrm{NIR} - \mathrm{RED}}{\mathrm{NIR} + C_1 \times \mathrm{RED} - C_2 \times \mathrm{BLUE} + L}$$

where:

$$\begin{aligned}
&\mathrm{NIR} = \text{Near Infrared (Band 8, 833 nm)},\\
&\mathrm{RED} = \text{Red (Band 4, 665 nm)},\\
&\mathrm{BLUE} = \text{Blue (Band 2, 560 nm)},\\
&G = 2.5 \text{ (gain factor)},\\
&C_1 = 6 \text{ (coefficient)},\\
&C_2 = 7.5 \text{ (coefficient)},\\
&L = 1 \text{ (canopy background adjustment)}.
\end{aligned}$$

The median EVI was calculated as the representative metric of above ground biomass per field for each satellite image. The median was chosen to reduce the impact of outliers. From all available median EVIs, a time series was created for each field and year (Figure A.1).

4.2.2 LAI trait retrieval

To retrieve the LAI from the Sentinel-2 images the PROSAIL RTM as described in Section 2.1.2.3 was used. For this a LUT with 50'000 spectra corresponding to a suitable range of LAI values was generated. The parametrization of the PROSAIL model was defined based on values from literature (Asam et al., 2015; Atzberger et al., 2015; Imran et al., 2020; Punalekar et al., 2018) (see table 4.1). The value ranges were constrained to values that corresponded to study sites similar to Swiss grasslands. The solar and sensor viewing angles were determined based on the visiting times of Sentinel-2 over Switzerland (approx. 10:30 in the morning).

Table 4.1: Distribution of the PROSAIL initialization parameters for the generation of the LUT using forward calculation.

Parameter	Min	Max	Mode	Std	Distribution
N - Structure coefficient	1.5	1.9		0.2	Gaussian
Cab - Chlorophyll a+b	15	80	50	30	Gaussian
Car - Carotenoid	4	12			Gaussian
Ant - Anthocyanin	0	0			Uniform
Cbrown - Brown pigments	0	0.3			Uniform
Cw - Equivalent water thickness	0.01	0.02			Gaussian
Cm - Dry matter	0.004	0.01		0.0045	Uniform
LAI - Leave Area Index	0.1	8			Uniform
LIDFa - Average Leaf Angle	30	70	45	15	Uniform
LIDFb - Bimodality of Leaf Distribution	0	0			Constant
hspot - Hot Spot	0.05	0.1			Uniform
rsoil - Soil Brightness Factor	0	1			Uniform
psoil - Dry/Wet Soil Factor	0.1	1	0.7		Uniform
tts - Solar Zenith Angle	25	25			Constant
tto - Sensor Viewing Angle	10.3	10.3			Constant
psi - Relative Azimuth Angle	110	110			Constant
TypeLidf - Ellipsoidal distribution	2	2			Constant

A more detailed analysis was conducted to define the value range for LAI. Literature proposes a minimum LAI of 0.1 and a maximum of 8. To see whether this maximum is also accurate for grasslands in Switzerland, a preliminary analysis was carried out by setting the max LAI to 5, 8 and 12. The Sentinel-2 derived LAI time series were then compared with the FluxNet LAI data that were acquired during 2022 (Figure A.2). The maximum LAI of 12 overestimated field LAI, while a maximum of 5 underestimated LAI. The proposed maximum of 8 seemed to fit the in-situ LAI measurements best. Consequently, the LUT with 50'000 spectra was generated with LAI max 8.

To retrieve the LAI from the satellite images, the spectral signature of each pixel was extracted and compared with each spectrum of the LUT. The Root Mean Square Error (RMSE), was used as the cost function in this study. The LAI of the LUT spectrum with the minimum RMSE compared to the observed spectrum was assigned to the respective pixel. The median LAI of all pixels on a field was then chosen to represent the LAI of that field for that point in time. This approach was again chosen to reduce the impact of outliers and the influence of adjacent pixels. From all available LAI medians, a time series was created for each field and year.

4.2.3 Comparison to VSLU biomass field data

To assess the correlation between EVI, LAI and biomass, the corresponding EVI and LAI values from the day on which an in-situ biomass measurement was taken was extracted from the time series. Each extracted proxy was then plotted against the respective VSLU biomass measurement.

4.3 Sentinel-2 LAI time series evaluation

Compared to the first part where LAI was related to individual biomass measurements, the second part investigated LAI change over time on the VSLU fields by evaluating its variation over the six growing periods from 2018 to 2023. To assess the extracted time series data and the dynamics of the LAI, four comparisons were made. Two to check the plausibility of the indicated cuts in the time series (Section 4.3.1). And two to further investigate the dynamics of the LAI (Section 4.3.2).

4.3.1 Plausibility check of mowing events

4.3.1.1 PlanetScope imagery

The first comparison consisted of a cross-check with the PlanetScope data. The temporally highly resolved data provide continuous observations of the fields at daily resolution. The high spatial resolution of 3 - 4 m enables an easy detection of mowing events, as the fields appear much brighter after mowing. To verify whether the observed decreases in the Sentinel-2 derived LAI time series are actually due to management events, the PlanetScope data from the days immediately before and after the proposed cuts were consulted. For this comparison single images of random mowing events in some of the Sentinel-2 time series were consulted (Figure 5.3).

4.3.1.2 Grassland use-intensity maps

To obtain a more comprehensive overview and a quantitative estimate of how well the Sentinel-2 LAI time series captured mowing events, grassland use-intensity maps were used for a second comparison. To determine whether the retrieved management days from the use-intensity maps corresponded to the dips in the Sentinel-2 LAI time series, the slopes from the time series were extracted on the days on which a management event was recorded on the use-intensity maps. Figure 4.2 shows a field parcel covered by the grassland use-intensity map. The map is at a 10 m pixel resolution and each field covers multiple pixels. Each pixel indicates how many times and on which Day Of the Year (DOY) the grass was cut. Due to the heterogeneous surface characteristics of grassland, at times each pixel covering a field captured a different day for the first management event. However, for the analysis one single DOY for each management event per field was required. To extract this single DOY, all DOYs of a cut within the field parcel were extracted. If the most frequently occurring DOY appeared in more than 50% of the pixels, then this DOY was designated as a cutting day (example Figure 4.2). However, some fields were more heterogeneous and the most frequently occurring DOY for a cut did not appear on more than 50% of the pixels. In that case the minimum value was chosen as DOY for cutting day. This was done for each management event. The slope on the DOY of each management event was then extracted from the Sentinel-2 time series. The extracted slopes were then further analysed. A negative slope signified a cutting event, while a positive slope indicated growth. The percentage of negative slopes was calculated from all slopes in order to evaluate the agreement of management events between the Sentinel-2 time series and the grassland use-intensity maps.

Figure 4.2: Field parcel with underlying grassland use-intensity map at a 10 m pixel resolution. Each pixel indicates the timing and number of management events that have been detected within one year.

4.3.2 Comparison with other LAI time series

4.3.2.1 FluxNet in-situ LAI time series

Next, the LAI time series were compared with in-situ measured LAI time series data. Due to the lack of in-situ measured time series data from the VSLU fields, this analysis was conducted with the in-situ measurements from the FluxNet fields. The comparison was only conducted for the years 2019, 2020, 2022 and 2023 from which 5-19 measurements were available per year. To quantify the correlation between the two curves R^2 and RMSE were calculated.

4.3.2.2 Mechanistically modelled LAI time series

As a last step, the LAI time series from the VSLU fields were compared with the modelled growth of the mechanistic model ModVege. The ModVege growth curves were generated with growR. growR is an implementation of the original ModVege model code in R (Calanca et al., 2016; Kramer & Calanca, 2024), and requires the same inputs as ModVege. growR required the management timing, weather data, functional group proportions (approximation for use intensity) as well as the nitrogen nutrition index and soil-water holding capacity. The comparison was done for the year 2022. In that year, the biomass measurements on the VSLU fields were recorded in spring, the first management event of the year was therefore precisely known and could be implemented in the model. Since this was the only known timing of a management event, the growth dynamic was only compared up to the first cut. As an input to Modvege weather data was downloaded from MeteoSwiss. Use intensity was not known but assumed to be intense, such that the functional groups were set to A (frequent and fertile) and B (infrequent an fertile) (consult Jouven et al. (2006) for more information on the functional groups). Nitrogen nutrition index and soil-water holding capacity were adjusted manually. The precise initialization parameters for the modelling of the VSLU sites can be found in Appendix A.3.

4.4 Developing a machine learning grass growth model based on Earth Observation data

In the third part, the ML grass growth model based on EO data was developed. The LAI time series generated from the Sentinel-2 images of the VSLU fields in the last part were used to derive grass growth by means of changes in LAI. The growth data combined with a set of weather variables from MeteoSwiss were used to build a growth-meteo database (Section 4.4.1) which was then used to train the ML grass growth model, to learn the relationship between meteorological conditions and increase in LAI (Section 4.4.2) to ultimately predict grass growth under various weather conditions (Section 4.4.3). To investigate the model's sensitivity to every explanatory variable, a sensitivity analysis was conducted (Section 4.4.4). To assess the overall performance of the model, the modelled grass growth prediction for the independent FluxNet field was compared with other time series data (Sentinel-2, in-situ and ModVege) acquired on that field (Section 4.4.5).

4.4.1 Growth-meteo database

To train the ML grass growth model, a database called the growth-meteo database, was established. In this database, the grass growth and meteorological data from the VSLU fields were matched over the same time periods, such that the model could correlate growth to the respective meteorological conditions during the growing period. To provide the ML algorithm a wide range of possible explanatory variables, several additional variables were derived from the three directly measured weather parameters temperature, precipitation and sunshine.

4.4.1.1 Growth data

To derive LAI growth from the growth curves established in the first part, the absolute difference of LAI between two acquisitions was calculated:

$$LAI_{acq2} - LAI_{acq1} = LAI_{abs\ growth} \tag{4.1}$$

The absolute difference between two acquisitions was the total growth that was recorded between two consecutive dates, given the difference was positive. To reach daily growth rates, the absolute LAI growth between the two consecutive dates was divided by the number of days between the two acquisitions:

$$\frac{LAI_{abs\ growth}}{DOY_{acq2} - DOY_{acq1}} = LAI_{daily\ avg\ growth} \tag{4.2}$$

The current LAI present on a field was also added to the growth-meteo database.

4.4.1.2 Meteo data

To extend the growth-meteo database with the weather data, the variables measured by MeteoSwiss were added. This included the three variables temperature, precipitation and sunshine as well as the additionally derived parameters.

Estimation of PAR from relative sunshine duration

Relative sunshine duration is not the most accurate measure of the light spectrum available for plant growth. A more precise indicator is PAR, which represents the portion of the light spectrum between 400 and 700 nm (McCree, 1971), corresponding to the wavelengths plants use most effectively for photosynthesis. Thus, PAR was estimated from the measured relative sunshine. PAR is measured in W/m^2 and was estimated from daily relative solar radiation, DOY and latitude (see Appendix A.4 for more details on the calculation).

Data matching

To match the meteo data to the growth data, the three MeteoSwiss variables temperature, precipitation and PAR were summed over the same periods the absolute LAI growth was calculated:

$$sum(var_{acq1,\ acq2}) = var_{sum\ between\ acquisitions} \tag{4.3}$$

To match the daily average growth data, the meteo sums were divided by the number of days between two consecutive image acquisitions:

$$\frac{var_{sum\ between\ acquisitions}}{DOY_{acq2} - DOY_{acq1}} = var_{daily\ avg} \tag{4.4}$$

To provide the model a wide variety of parameters that could explain growth, several additional variables e.g. the cumulative sum of each of the three meteo variables temperature, precipitation and PAR, the 1-, 2- and 4-week average precipitation before an image acquisition and the number of dry days within the last 1, 2 and 4 weeks before an image acquisition were calculated and added to the growth-meteo database. The full list of variables included in the growth-meteo database can be found in the Appendix (see Appendix A.5).

4.4.2 Machine learning grass growth model development

Establishing the ML model required the selection of input data (Section 4.4.2.2), a model feature selection (Section 4.4.2.3), hyperparameter tuning (Section 4.4.2.4) and a final model selection (Section 4.4.2.5). For this, the RF Regressor from the open source machine learning library scikit-learn Python (Pedregosa et al., 2011) was used.

4.4.2.1 Random Forest

To train the ML grass growth model the RF algorithm was used. RF is a popular form of decision tree ensembles and has great potential to predict LAI growth for several reasons. (1) The prediction of LAI growth involves multiple input variables. RF can efficiently handle high dimensional data (Belgiu & Drăguţ, 2016). (2) The relationship between LAI growth and its predicting meteorological data is often non-linear. Due to its tree-based structure, the method is capable of capturing these non-linear relationships (Breiman, 2001). (3) Environmental data is noisy and variable, averaging the results of multiple trees reduces the impact of outliers, prevents overfitting and produces overall more robust results (Belgiu & Drăguţ, 2016).

4.4.2.2 Model input data selection

To clean the input data and optimise the training of the ML model in predicting LAI growth, the growth-meteo database was filtered. The following filters have been applied to create the best possible growth-meteo training data set:

- Growth only: the ML grass growth model is, as the name says, a growth model, which means that the training set must only include positive absolute changes in LAI. Negative changes indicate management events (mowing, grazing), and were removed from the training set.
- First growth period: in order to filter out noise that appeared based on cuts in the later season, only the growth period until the first cut was used to train the model. For each field, the first cut was extracted from the grassland use-intensity maps (Weber et al., 2023). If no data was available for the field, the median DOY for the first cut on all fields of the respective year was assumed. Only the data before the detected first cut was included in the training data.
- Time between two acquisitions: only LAI changes of Sentinel-2 acquisitions that occurred no longer than 10 days apart from each other were considered. Longer periods of time between two acquisitions lead to increasing uncertainties. After filtering, the median number of days between two acquisitions was three days.
- Max increase in LAI: absolute changes in LAI that were larger than three were excluded. Such large increases within only 10 days are unlikely, and probably outliers.
- Increase in LAI relative to time between acquisitions: if the absolute increase in LAI was larger than two but the time period between the two acquisitions was less than five days, the data was discarded for the same reasoning as above; unlikely large increase for a short period of time.
- Outliers: Some curves still showed individual data points that did not look plausible but were not removed from the time series, such as single low LAI measurements within continuously high values. These outliers falsely indicated strong growth. To remove such values, points with a very strong decrease followed by a large increase of LAI (2<) were removed from the time series.

After the filtering of the growth-meteo database, the growth-meteo training data set included 956 data points. Figure A.6 in the Appendix shows the growing periods that were included in the training of the grass growth model.

4.4.2.3 Feature selection

To find the best set of features (explanatory variables) to train the grass growth model, the k-fold CV from the open source machine learning library scikit-learn Python (Pedregosa et al., 2011) was used. The k-fold CV method is described in more detail in Section 2.2.3.1. To identify the most valuable features that explain grass growth (target variable) best, the features were systematically included or excluded during the model training and testing. The features tested were the variables in the growth-meteo database, which included daily temperature, precipitation and PAR, the 1-, 2- and 4-week average precipitation before an image acquisition, the number of dry days 1, 2 and 4 weeks before an image acquisition as well as current LAI (see Appendix for the full list A.5). For the training and testing, the growth-meteo database was split into 30 folds. For each combination, the model was evaluated with an evaluation metric (R^2) and the feature importance was examined. The feature importance measures how effectively each feature reduces model uncertainty (see Section 2.2.3.1), and can be used to identify the most relevant explanatory variables of a model. The feature combination from the model with the highest R^2 was then chosen as the final feature set. This included: daily average temperature, daily average PAR, daily average precipitation, 4-week precipitation average and the current LAI.

4.4.2.4 Hyperparameter tuning

For the ML grass growth model the following hyperparameters were included: number of trees ('n_estimator'), maximum depth of trees ('max_depth'), minimum sample number for a split ('min_sample_split'), minimum samples per leaf ('min_samples_leaf'), and bootstrapping samples ('bootstrap').

To tune the hyperparameters and find their best configuration, the Random Search CV and Grid Search CV methods provided by the open source machine learning library scikit-learn Python were used (Pedregosa et al., 2011) (described in more detail in Section 2.2.3.1). The first search space of the Random Search CV was defined as:

Hyperparameter	**Values**
n_estimator	100, 300, 500, 700
max_depth	2, 14, 26, 50, 76
min_samples_split	2, 5, 8, 11
min_samples_leaf	1, 4, 10, 18
bootstrap	true, false

Table 4.2: Search space for the Random Search CV.

From this search space (Table 4.2), 30 times 100 models were trained with random combinations of values for the hyperparameters, with 80% of the data in the training and 20% of the data in the testing set. Each model was evaluated by means of R^2. From the best performing models, the value ranges for each hyperparameter were recorded. Based on the best performing hyperparameter values a more refined search space was created for the Grid Search CV.

To fine-tune the hyperparameters 100 models were trained with random hyperparameter combinations from the Grid Search. The final hyperparameters were chosen from the model with the best performance based on R^2:

Model	**Hyperparameter**	**Value**
RF	n_estimator	300
	max_depth	12
	min_samples_split	4
	min_samples_leaf	3
	bootstrap	true

Table 4.3: Final set of tuned hyperparameters to train the final grass growth model.

4.4.2.5 Final model selection

To obtain the final model, 100 RF models were generated with the best set of features and the tuned hyperparameters. Each time with a different random split of the data into training (80 %) and testing sets (20 %). Each tree was evaluated by means of R^2. To select the final model, the R^2 and test-training data splits were recorded for every tree. The model with the highest R^2 was then selected as the final ML grass growth model.

4.4.3 Machine learning grass growth model predictions

To test the ML grass growth model, growth was predicted for the FluxNet field, as the most accurate in-situ and management data was available from this field and consequently the models evaluation and comparison to results from the ModVege model and in-situ data could be facilitated in the best possible way. To run the model the meteorological data from MeteoSwiss was extracted for the location of the FluxNet field. Given the selection of features, which included the current LAI (see Section 4.4.2.3), and considering that this value was unknown in the first iteration, current LAI was set to zero to initialize the model. Subsequently, it was iteratively updated with each successive growth prediction, representing the cumulative effect of previous predictions and reflecting the progressive nature of plant growth over time. Grass growth was modelled twice, once without management (i.e. cuts) and once including management events. The updating of $LAI_{current}$ to $LAI_{current\ of\ the\ next\ prediction}$ was performed in two different ways, depending on whether management was included in the modelling or not. In case of no management, daily growth was simply added cumulatively and the following equation applied:

$$LAI_{current\ of\ the\ next\ prediction} = LAI_{current} + LAI_{modelled\ growth} \tag{4.5}$$

When including management events, current LAI was reset when the currently modelled day reached a mowing date. The residual LAI after a cut varies on the density of the grass as well as the height at which the grass was cut. For this study, a residual LAI of 0.1 was assumed:

$$LAI_{current\ of\ the\ next\ prediction} = 0.1 + LAI_{modelled\ growth} \tag{4.6}$$

For the FluxNet field, both cases were modelled for the year 2022 (Figure 5.9). To quantitatively evaluate the impact of management on the total productivity of the field, the cumulative sum was calculated for both years.

4.4.4 Sensitivity analysis

To assess the sensitivity of the ML grass growth model, a one-at-a-time sensitivity analysis was conducted on the predictions for the FluxNet field. In this approach each feature was systematically varied while the others were held constant at their average values. This analysis provided insights into the sensitivity of the model, identifying those features with the greatest influence on the model's output.
A synthetic input data set was created with the five final features, setting each feature to the mean value from the available data, establishing a baseline that represents an average scenario. To isolate the effect of each variable on the predicted daily LAI growth, one variable at a time was varied over a range defined by the 10th to the 90th percentile of its original distribution (see x-axis of the respective variable in Figure 5.11), while the others remained at their average values.
Based on the findings from this first sensitivity analysis, it became apparent that further investigation into the value of the current LAI was required. To further assess the effect of current LAI on growth, the sensitivity analysis was repeated with three different average LAI values (3, 4.5 and 5.5) set as the mean in the average scenario. This additional analysis aimed to better understand how variations in the

baseline LAI value affect the model's sensitivity and growth predictions.

4.4.5 Model performance assessment: Comparison with other LAI time series

To assess the performance of the ML grass growth model, its cumulative growth prediction including management events for the independent FluxNet field was tested against i) Sentinel-2 LAI estimations, ii) the FluxNet in-situ LAI data, and iii) the predicted growth of the mechanistic model ModVege. Different modifications were applied to the ML grass growth model predictions to directly compare the cumulative LAI to the three datasets. To evaluate the correlation between the different data sets the R^2 and RMSE were calculated for each time series comparison.

4.4.5.1 Sentinel-2 derived LAI estimates

As a first comparison, the ML grass growth prediction for the FluxNet field was compared with the RTM derived LAI time series from the Sentinel-2 images (as described in Section 4.2.2). To compare the Sentinel-2 derived LAI with the ML grass growth model predicted LAI, adjustments were required for the Sentinel-2 time series. Since the model only predicts growth, the periods in which LAI declined in the Sentinel-2 time series were set to zero growth. These periods had to be accounted for in the model's predictions to prevent it from continuing to model growth during those times, which would have led to a significant overestimation of the total LAI. By adjusting the model to halt growth during the data gaps, a more accurate comparison with the Sentinel-2 derived LAI was ensured.

4.4.5.2 FluxNet in-situ LAI observations and scale factor estimation

Depending on the year, between 5 and 19 in-situ LAI measurements were available from the FluxNet fields. Based on a time series comparison of the in-situ data with the Sentinel-2 derived LAI it has been expected, that the model will overestimate LAI. To therefore directly compare the dynamics of the two LAIs, a scale factor was introduced. The factor was calculated by plotting the predicted sum of LAI growth between two in-situ measurements vs. the in-situ measured absolute LAI (Figure 4.3). The slope of the trend line (0.31) that describes this relationship was used to scale down the overestimated Sentinel-2 LAI measurements. The same scale factor was used for all years. To compare the in-situ measured LAI with the ML grass growth model prediction, the recorded management events were included in the modelling. This was done by resetting the current LAI to a residual LAI of 0.1, when the model reached a day on which a mowing event occurred (see Equation 4.6).

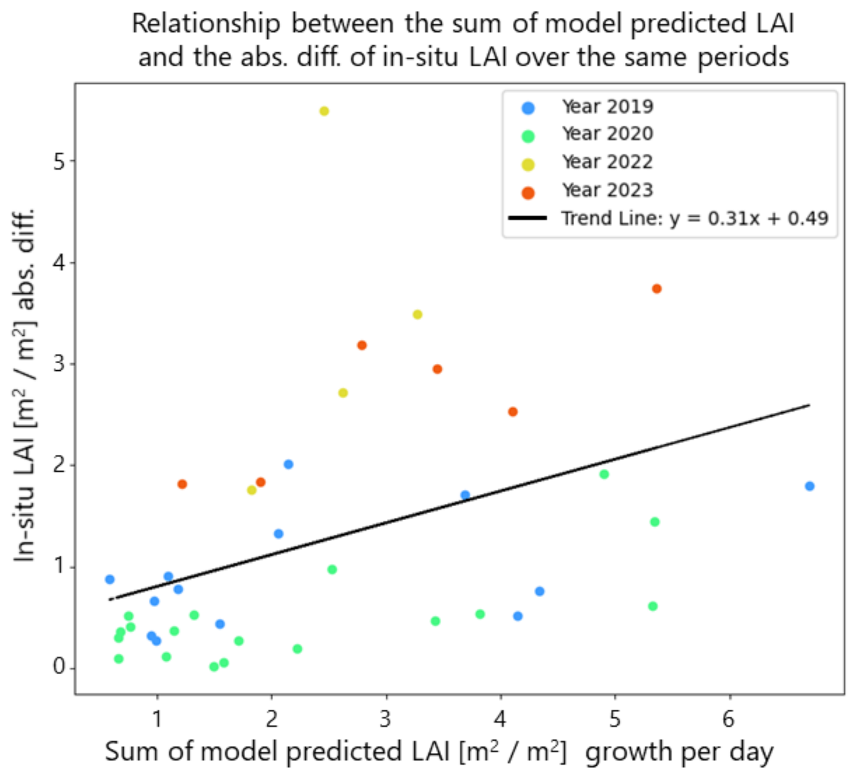

Figure 4.3: Scatter plot showing the sum of predicted LAI in the period between two in-situ measurements vs. the absolute in-situ measured LAI. The slope from the trend line was used as a scale factor to fit the time series from the two datasets.

4.4.5.3 Mechanistically modelled LAI

The last comparison was between the ML grass growth model predicted LAI and the ModVege model outputs for the FluxNet field. The ModVege outputs were generated with growR (Calanca et al., 2016; Kramer & Calanca, 2024). The following inputs were used to predict growth with the ModVege model. The weather data (temperature, PAR, precipitation, potential evapotranspiration) was derived from the data provided by MeteoSwiss. Use-intensity was assumed to be relatively intense, defined by the functional group A (frequent and fertile) (Jouven et al., 2006). The site specific nitrogen nutrition index and the soil water-holding capacity were manually fine-tuned for each year. The precise initialization parameters for the model can be found in appendix A.3. Growth was modelled twice, once without management and once including management (mowing). Management events consisted of an immediate reset of the biomass to a small value. For direct comparison of the growth dynamics between the ML grass growth model and ModVege, growth was initiated and stopped on the same days ModVege modelled growth. To evaluate the performance of the grass grwoth model compared with ModVege, R^2 and RMSE was calculated for the ML grass growth model prediction and the ModVege prediction including management events.

4.5 Model based drought impact analysis

In this last part, an analysis was conducted to assess the ML grass growth model's capability of capturing the effects of drought on growth. This was done by synthetically reducing precipitation to calculate growth scenarios under drought conditions as well as a case study, which investigated the impact of a prolonged dry period in Chamau in spring 2020, by a counterfactual analysis.

4.5.1 Future water availability: Scenarios

Different scenarios were modelled to investigate the model's capability of capturing the impact of drought on grass growth under more extreme conditions. To simulate future weather conditions, precipitation and the 4-week precipitation average, the two features related to water availability included in the ML grass growth model were adjusted. To investigate the effect of more or less available water on grass growth, scenarios were created with a 20% and 50% reduction and increase in each variable individually, as well as in combination. Prior to feeding the actual measured meteorological variables into the model, the values of precipitation and soil moisture were adjusted accordingly.

4.5.2 Case study: impact of a dry period on grass growth in Chamau in spring 2020

To evaluate the models capability of capturing an effect of the dry period, the FluxNet field was investigated during a 3-week period with little to no precipitation in April 2020. This period was chosen because the ML grass growth model was trained on growth data acquired in spring. The top plot in Figure 3.2 indicated a period with little precipitation between DOY 90 and 120. Thus, ET_{rel}, was calculated (see Appendix A.8 for details on calculation) to confirm the dry period.

For the analysis, growth was first modelled with the actual weather data measured during that period. To isolate the effect of limited precipitation on growth, two scenarios were modelled in which rainfall was synthetically increased. In Lucerne it rains an average of 100 mm in April (MeteoSwiss, 2024), which corresponds to an average daily precipitation of 3.33 mm. In the analysis precipitation was increased by 2 and 5 mm per day, on days that originally recorded less than 0.1 mm of precipitation. Increasing precipitation by 2 and 5 mm on these days simulated the effects of small to moderate rainfall events that can help alleviate drought conditions. This comparative approach allowed for quantifying how much the dry period reduced growth by contrasting actual and synthetic precipitation-driven growth predictions.

Chapter 5

Results

This chapter presents the results of all four parts of this study. In the first section the results of the correlation of in-situ measured biomass with the Sentinel-2 derived EVI and LAI, and the relationship between these two proxies are presented (Section 5.1). The second section shows the results of the comparison between Sentinel-2 derived LAI with the PlanetScope data and the grassland use-intensity map, as well as the ModVege modelled LAI, while focusing on the growth dynamics up to the first cut (Section 5.2). The third section presents the ML grass growth model predicted daily LAI growth (with and without management) and the model performance assessment including the comparison of the predicted LAI with the in-situ measured, Sentinel-2 derived and ModVege modelled LAI (Section 5.3). In the last section, modelled growth under various drought scenarios and the results of the case study are outlined (Section 5.4).

5.1 Biomass estimations: EVI and LAI as proxies for grassland biomass

To evaluate the EVI and LAI as biomass proxies, both measures were compared to the in-situ measured grassland biomass acquired on the VSLU fields (see Section 4.2). Figure 5.1 illustrates the correlation between EVI and LAI and the in-situ measured fresh and dry biomass respectively. The upper plots represent EVI, while the lower plots depict LAI. The R^2 for the correlation between EVI and fresh biomass reached 0.22, for EVI and dry biomass 0.18 with an RMSE of 0.11 and 0.12 respectively. The correlation between LAI and fresh and dry biomass reached an R^2 of 0.12 with an RMSE of 1.01.

To directly compare the two biomass proxies with each other, a scatter plot was generated (Figure 5.2). At lower values EVI showed an increased sensitivity compared to LAI, while LAI showed an increased sensitivity at LAI values larger than three.

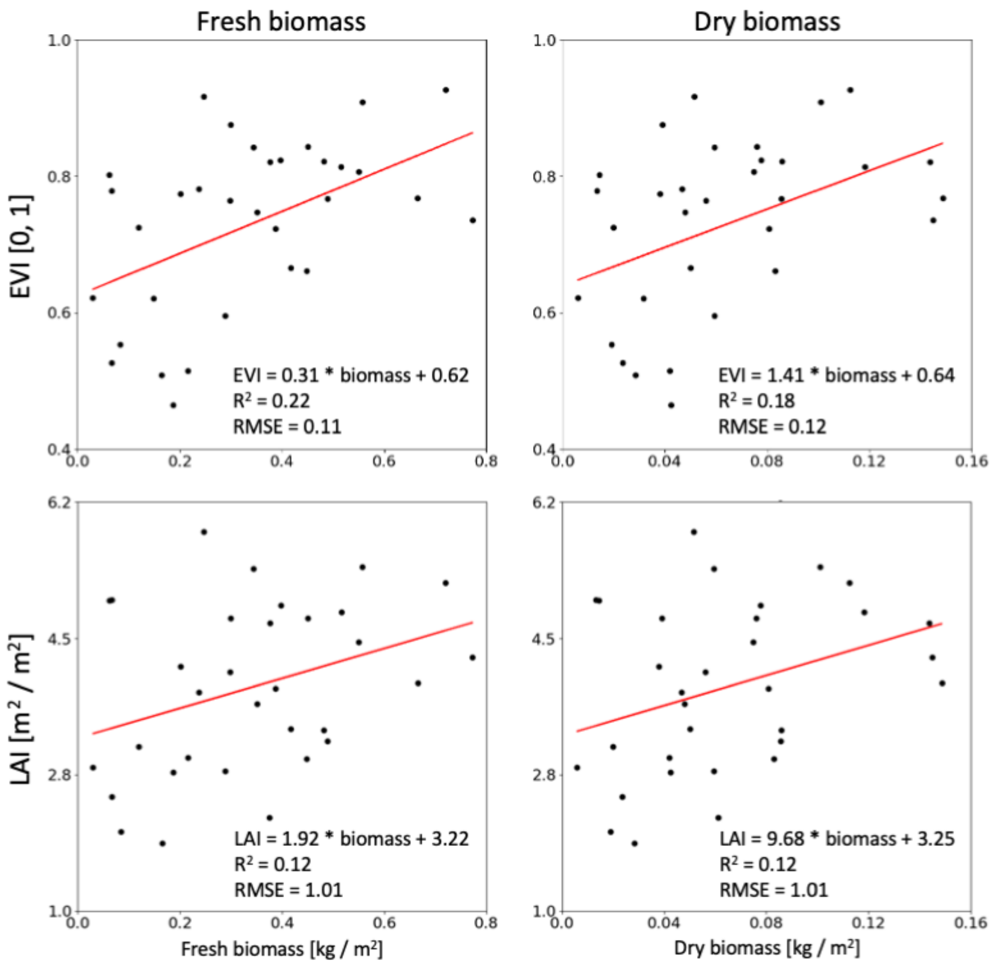

Figure 5.1: Correlation between EVI and LAI and fresh and dry biomass.

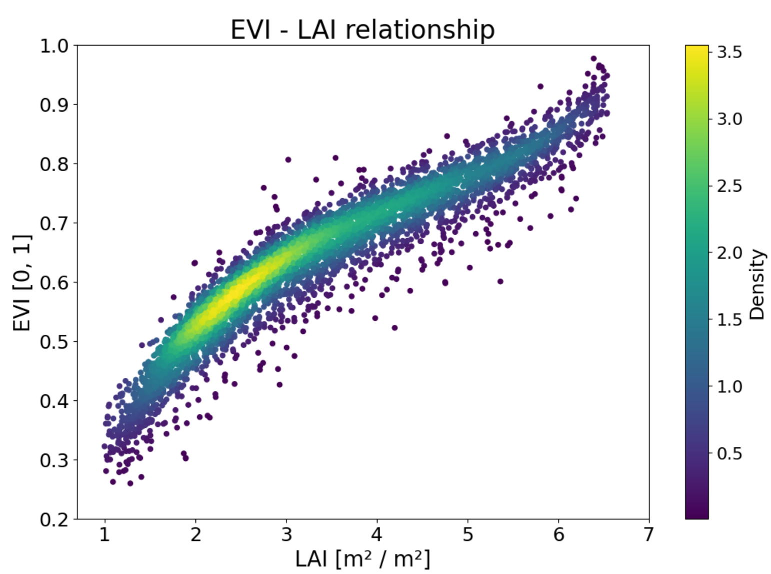

Figure 5.2: Relationship between EVI and LAI data on all VSLU fields and years (2018-2023).

5.2 Sentinel-2 LAI time series evaluation

For the evaluation of the extracted time series data and the dynamics of the LAI, four comparisons were made. Two to check the plausibility of the indicated cuts in the time series, and two to validate the LAI growth dynamics.

5.2.1 Plausibility check of mowing events

In order to assess the plausibility of the LAI time series derived from the Sentinel-2 data, two comparisons were conducted. The results of the first comparison which comprised the cross-check of single cuts within the time series with PlanetScope imagery is shown in Section 5.2.1.1. The results of the second comparison which included the comparison of the cutting dates to the timing of the managements specified by the grassland use-intensity maps is provided in Section 5.2.1.2.

5.2.1.1 PlanetScope imagery

To verify whether the observed decreases in the Sentinel-2 derived LAI time series are actually due to management events, the PlanetScope data from the days immediately before and after the proposed cuts were consulted (see Section 4.3.1.1). Figure 5.3 shows a LAI time series from one of the VSLU fields used for the training of the grass growth model, with a distinct dip in the curve around DOY 150. The PlanetScope images on the right show the field right before and after DOY 150. The distinctively brighter color on the lower image indicates that a mowing event has taken place since the last image was recorded.

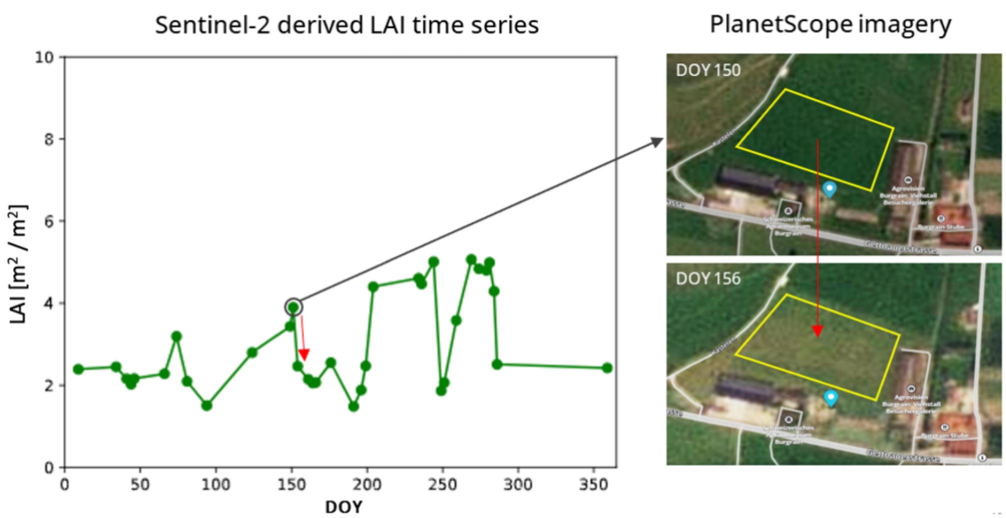

Figure 5.3: LAI time series curve with a distinct dip in the curve around DOY 150, and visible changes on the field in the PlanetScope images, indicating that a mowing event took place between the two image acquisitions.

5.2.1.2 Grassland use-intensity maps

To quantitatively evaluate the timing of the management events on all VSLU fields, the DOY of the dips in the time series curves derived from the Sentinel-2 images were compared to the DOY indicated on the grassland use-intensity maps (see Section 4.3.1.2). In 87% of all extracted DOYs on which a management event was recorded on the grassland use-intensity map by Weber et al. (2023), the slopes in the Sentinel-2 LAI time series were negative, also indicating a mowing.

5.2.2 Comparison with other LAI time series

Two additional comparisons were conducted to evaluate the LAI dynamic over time and the ability of the RTM to derive LAI from Sentinel-2 imagery. One to the in-situ measured LAI on the FluxNet field, and a second one to the mechanistically modelled LAI time series by ModVege.

5.2.2.1 FluxNet in-situ LAI time series

As an evaluation of the ability of the RTM to derive LAI from Sentinel-2 imagery, the time series were compared with the in-situ measured LAI data from the FluxNet field. Figure 5.4 shows how the Sentinel-2 derived LAI time series correlate to the in-situ measured LAI. 2019 shows the best results with an R^2 of 0.92. 2023 also shows a relatively good agreement of the curves with an R^2 of 0.84, while Sentinel-2 slightly underestimates the in-situ measured LAI. In 2020 and 2022 Sentinel-2 overestimates in-situ measured LAI and R^2 achieved -0.15 and 0.35 respectively.

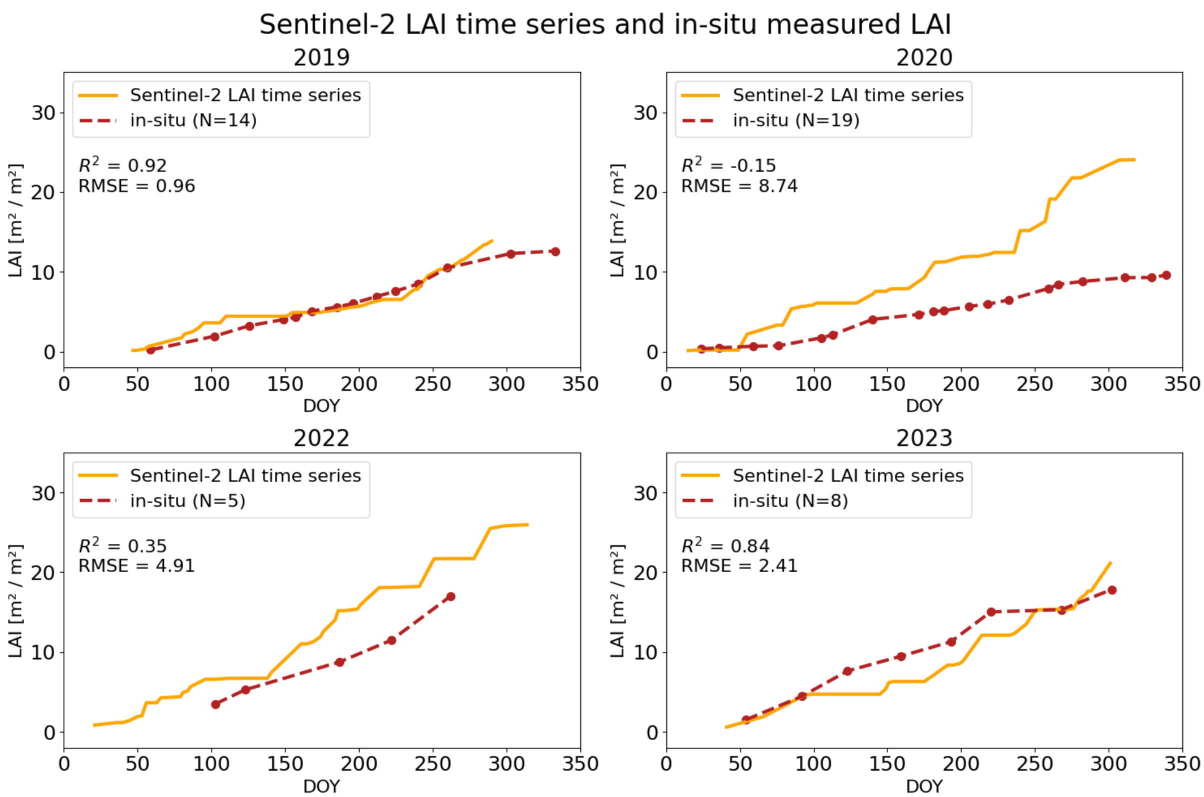

Figure 5.4: Sentinel-2 derived vs. in-situ cumulative sum of LAI including R^2 and RMSE.

5.2.2.2 Mechanistically modelled LAI time series

The Sentinel-2 derived LAI time series from 2022, were also compared with the growth curves predicted by the mechanistic model ModVege (see Section 4.3.2.2). Figure 5.5 shows the comparison of the Sentinel-2 derived LAI time series to the mechanistically modelled LAI time series by ModVege of four different fields. Figure 5.6 shows the meteo data for the year 2022, the year in which the VSLU biomass measurements were acquired and based on which ModVege modelled LAI growth.

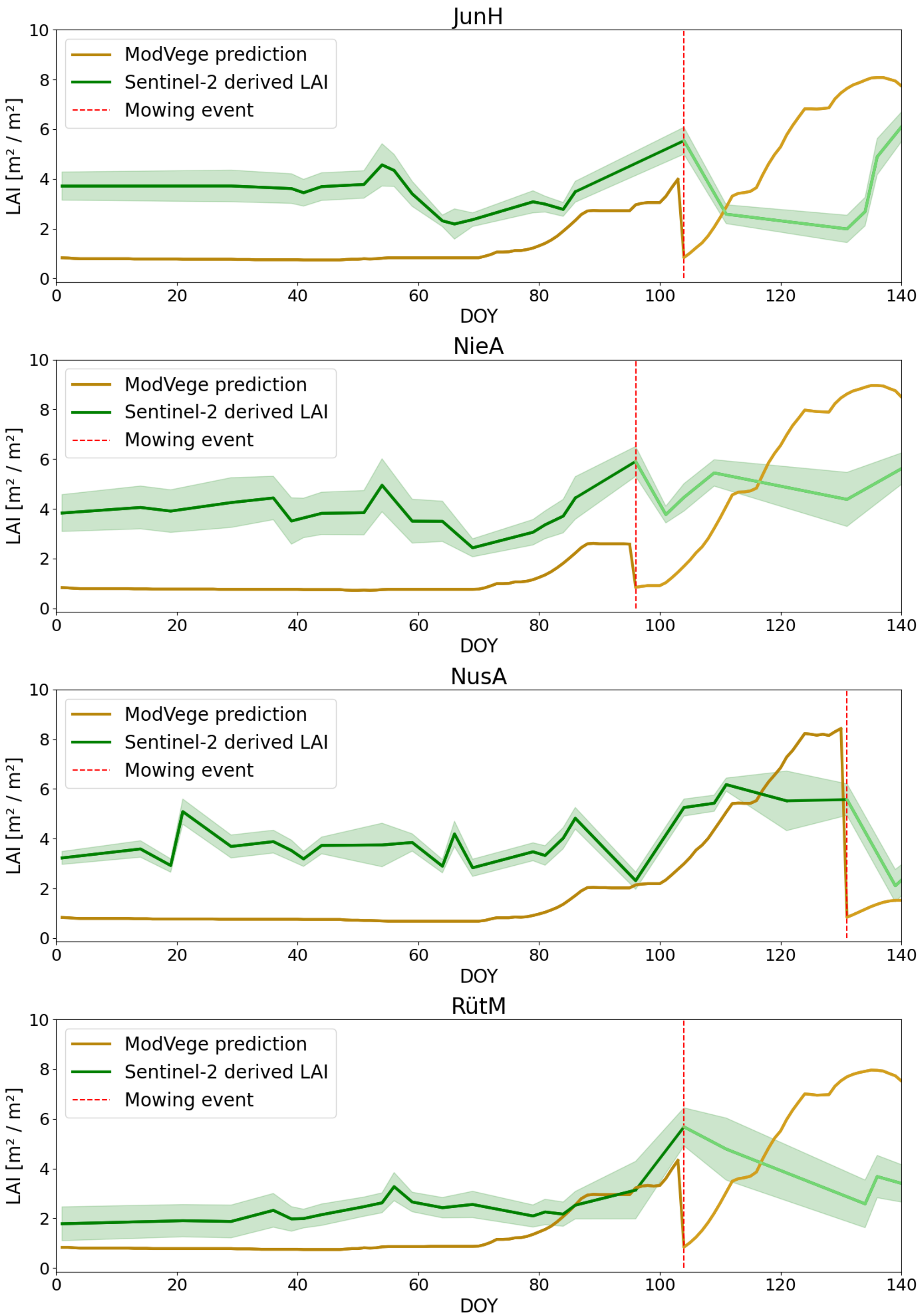

Figure 5.5: LAI time series comparison between Sentinel-2 derived LAI and ModVege modelled LAI. Only the time until the first cut can be compared.

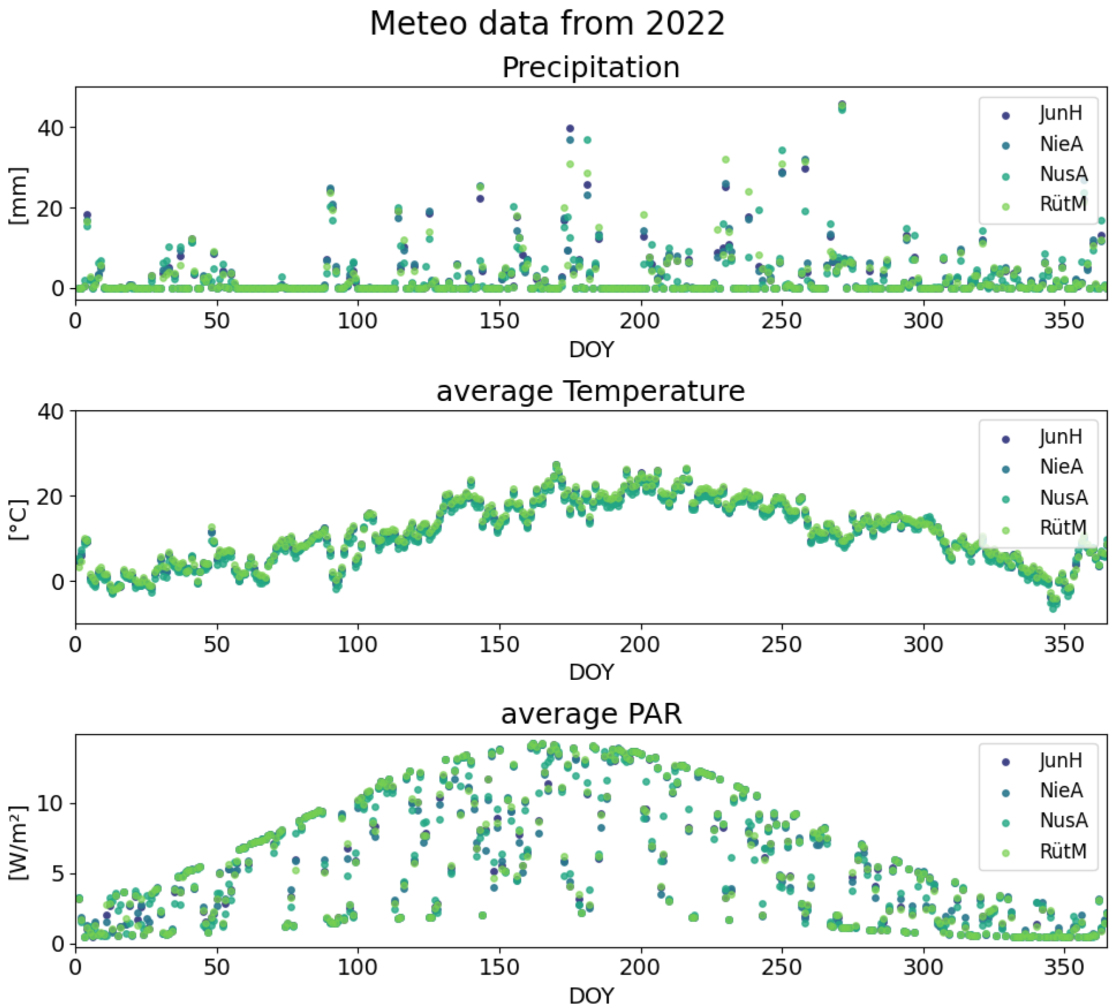

Figure 5.6: Precipitation, temperature and PAR data from 2022 at the four different fields.

The Sentinel-2 derived LAI values show generally higher values than those modelled by ModVege. Once growth picks up around DOY 70, the two curves show relatively similar increases in LAI at JunH and NieA. For a short period between DOY 80 and 95, ModVege does not show any growth, while the Sentinel-2 does not have any image acquisitions. After the cut, ModVege growth resumes quickly. At JunH the Sentinel-2 LAI remains low for about one month, but only three images available for this period. At NusA and RütM, the pattern is less clear. There is significant noise before the first growth at NusA, making it difficult to determine the exact start of the growth period. Around DOY 100, both curves show a steep increase in LAI. Right after this increase, Sentinel-2 LAI stagnates around LAI 6 while ModVege continues to grow until it reaches 8 right before the cut. After the cut, Sentinel-2 LAI increases again, while ModVege remains low. At RütM the two curves appear to be shifted. ModVege shows growth starting around DOY 70, while the Sentinel-2 LAI remains low until around DOY 80, when a slight increase is recorded. About 10 days before the first cut, both curves show a steep increase in LAI.

5.3 Machine learning grass growth model based on Earth Observation

The ML grass growth model developed in this thesis and its growth predictions were evaluated in multiple ways. Section 5.3.1 provides a statistical overview of the final model by providing the feature importance of the final set of features included in the model as well as a visualization of the performance of the model on the training and testing data split. Section 5.3.2 shows how the ML grass growth model predicts daily growth with and without management practices. In Section 5.3.3 the results of the sensitivity analysis are displayed. To finally put the growth predictions into perspective, the results of the modelled growth compared with other time series is shown in Section 5.3.4.

5.3.1 Model evaluation

100 models were generated and evaluated by means of R^2 to select the final ML grass growth model. Figure A.4 in the Appendix shows the histogram of the distribution of each of the resulting R^2 values of the 100 generated models with random training-testing splits (see Section 4.4.2.5). The models were trained with best performing set of features and the tuned hyperparameters (see Sections 4.4.2.3 and 4.4.2.4), and 80% of the growth-meteo dataset and tested on the remaining 20%. The median R^2 value of all models was 0.44 with an RMSE of 0.12. The best model achieved an R^2 of 0.61 and was selected as the final ML grass growth model used in the subsequent steps.

For each variable in the model, feature importance was assessed. Figure 5.7 shows the feature importance of all five variables included in the ML grass growth model. Daily PAR shows to reduce most uncertainty with 40%, followed by current LAI at 25% and the average daily temperature at 17%. 4-week precipitation average and precipitation seem to reduce model uncertainty the least with about 12% and 8%.

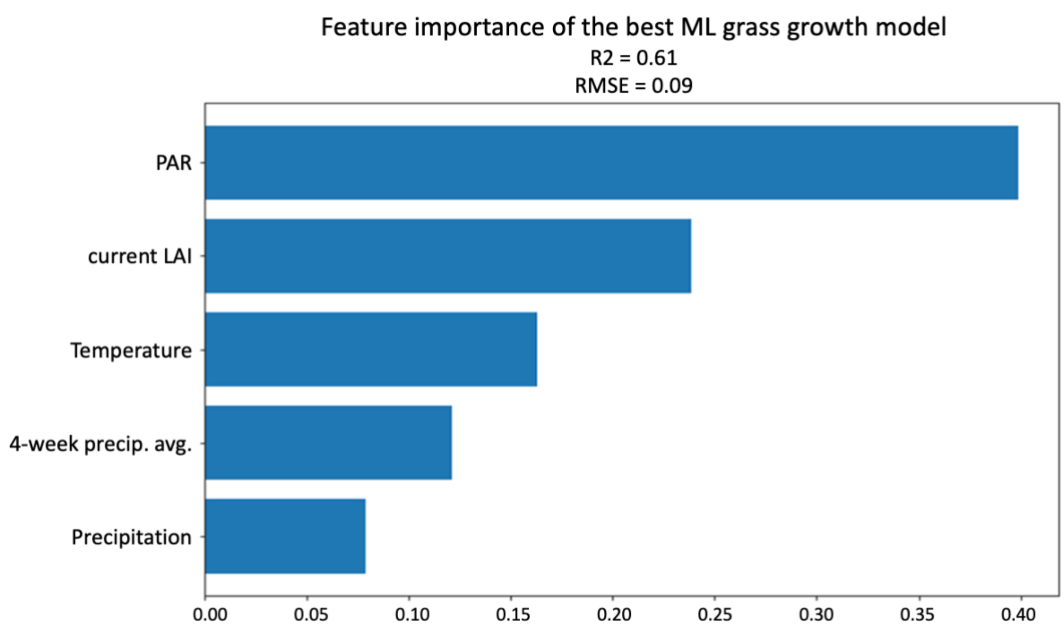

Figure 5.7: Feature importance of the final ML grass growth model. The higher the importance of a feature, the more it reduces the model's uncertainty.

The performance of the model was evaluated by determining the correlation between the ML grass growth modelled growth and the the Sentinel-2 measured growth. Figure 5.8 shows the scatter plots of the model predicted and the Sentinel-2 derived LAI for the training (left, 80% of the data) and the testing (right, 20% of the data) dataset. While an R^2 of 0.76 was achieved on the training data, an R^2 of 0.61 was obtained on the testing data. The general trend of the scatters shows a positive correlation between the two measures. The density of the scatter shows that most daily LAI growth values are around 0.1. It also shows, that the model tends to overestimate smaller LAI values while larger LAI values are underestimated.

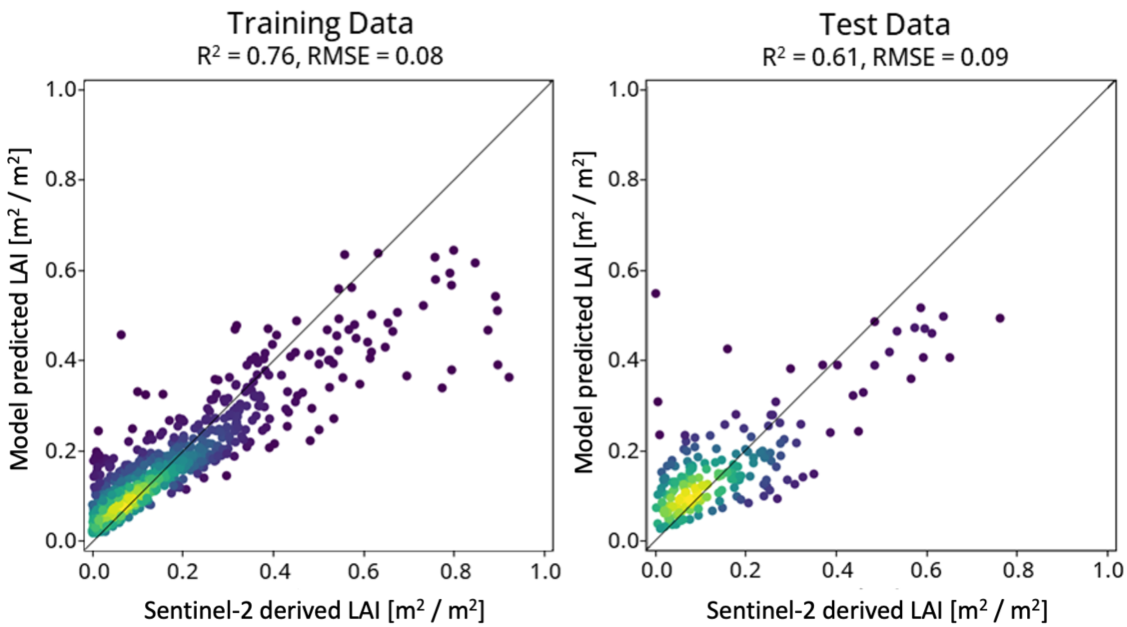

Figure 5.8: One-to-one density plot of Sentinel-2 derived LAI vs. LAI predicted with the final grass growth model. The scatter plots show the results for the training- and testing-split of the growth-meteo dataset. The black line represents the 1:1 line, the color indicates the density of data points.

5.3.2 Model predicted growth

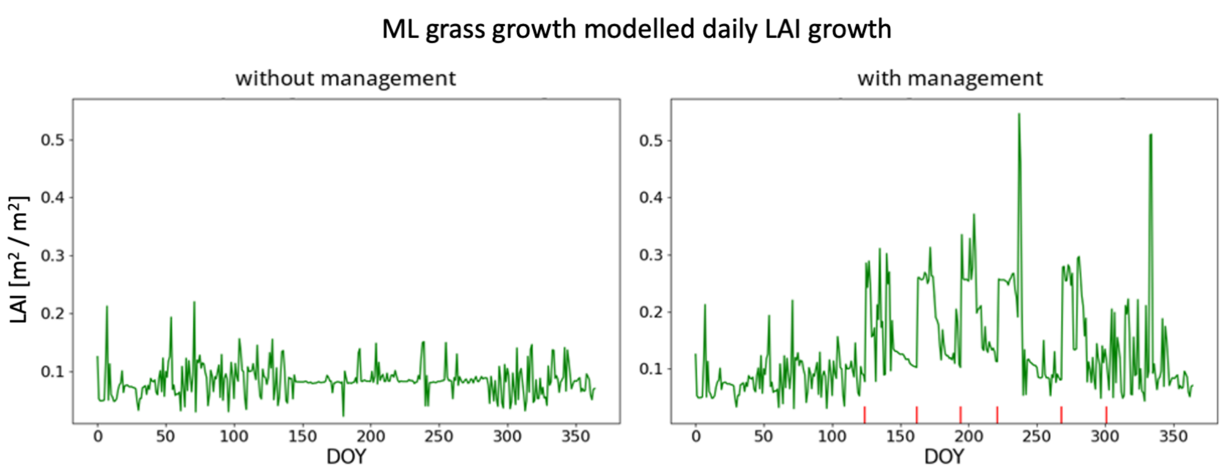

Figure 5.9: Daily LAI growth without (left) and with (right) management events. The red lines indicate mowing events.

As an assessement of the ML grass growth model performance, it was run for the FluxNet field (see Section 4.4.3). Figure 5.9 on the left shows the predicted daily LAI growth without any management. Daily LAI growth shows values around 0.1 with larger fluctuations in spring and fall compared to the summer months. The right figure shows the predicted daily LAI growth including management practices

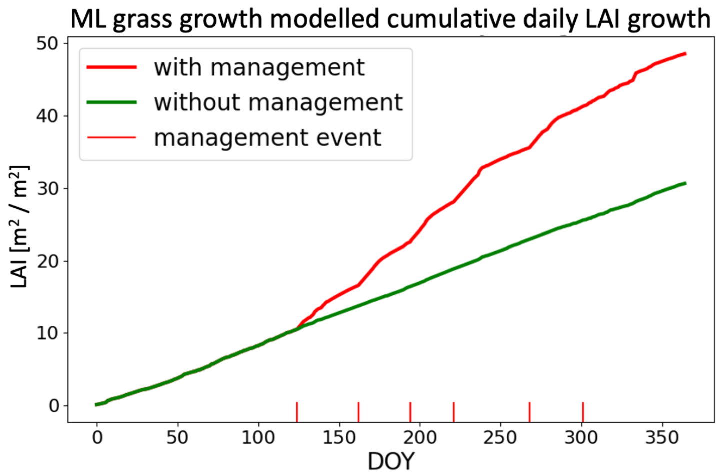

Figure 5.10: Cumulative daily LAI growth with and without management events. The red lines indicate mowing events.

(mowing events in red). In this case, daily growth shows larger fluctuations, with values ranging between 0.05 and 0.5, especially during the period in which management events took place. The curves including the management, show a distinct pattern of an immediate increase and later decrease in growth with a continuously increasing LAI. Average daily growth and consequently total productivity is higher when the grassland is managed. Figure 5.10 shows the cumulative sum of the daily LAI growth with and without management. The absolute total difference between the managed and the unmanaged cumulative sum is 18 LAI at the end of the year.

5.3.3 Sensitivity-analysis

For the assessment of the sensitivity of the ML grass growth model, a one-at-a-time sensitivity analysis was conducted on the predictions for the FluxNet field (see Section 4.4.4). Figure 5.11 displays the results of the sensitivity analysis of each input variable of the model.
The amount of precipitation influences growth with a difference of 0.05 between a lot of rain and little rain. The influence of the four week average precipitation is at around 0.025. Compared to the other variables, these two show the smallest sensitivity. Temperature shows a greater range with 0.11 LAI growth at lower temperatures and 0.23 increase of LAI at 20 °C. PAR again shows a smaller influence with 0.15 LAI growth at low PAR and an increase of 0.05 in growth at higher PAR. Current LAI shows the largest impact. At low LAI growth reaches up to 0.33 and decreases to 0.17 at high LAI, almost doubling at low LAI compared to higher LAI. To further investigate the effect of the current LAI, an additional analysis was conducted. Figure 5.12 shows how the current LAI influences the growth prediction in more detail.

The plots in figure 5.12 indicate that each variable predicts more growth at lower average LAI compared to higher LAI. Except for temperature, the change in LAI resulted in a upwards shift of the whole curve, indicating more growth at lower LAI and a downward shift of the curve, indicating less growth at higher LAI. For temperature the effect of the LAI seems to be temperature dependent and only show at higher temperatures. Between 2 and 8 °C, LAI does not have an impact on growth. From 8 °C on, the smaller LAI shows an increasingly larger growth compared to the higher LAI. At 20 °C, the model predicts 0.3 more growth at lower LAI values compared to higher LAI.

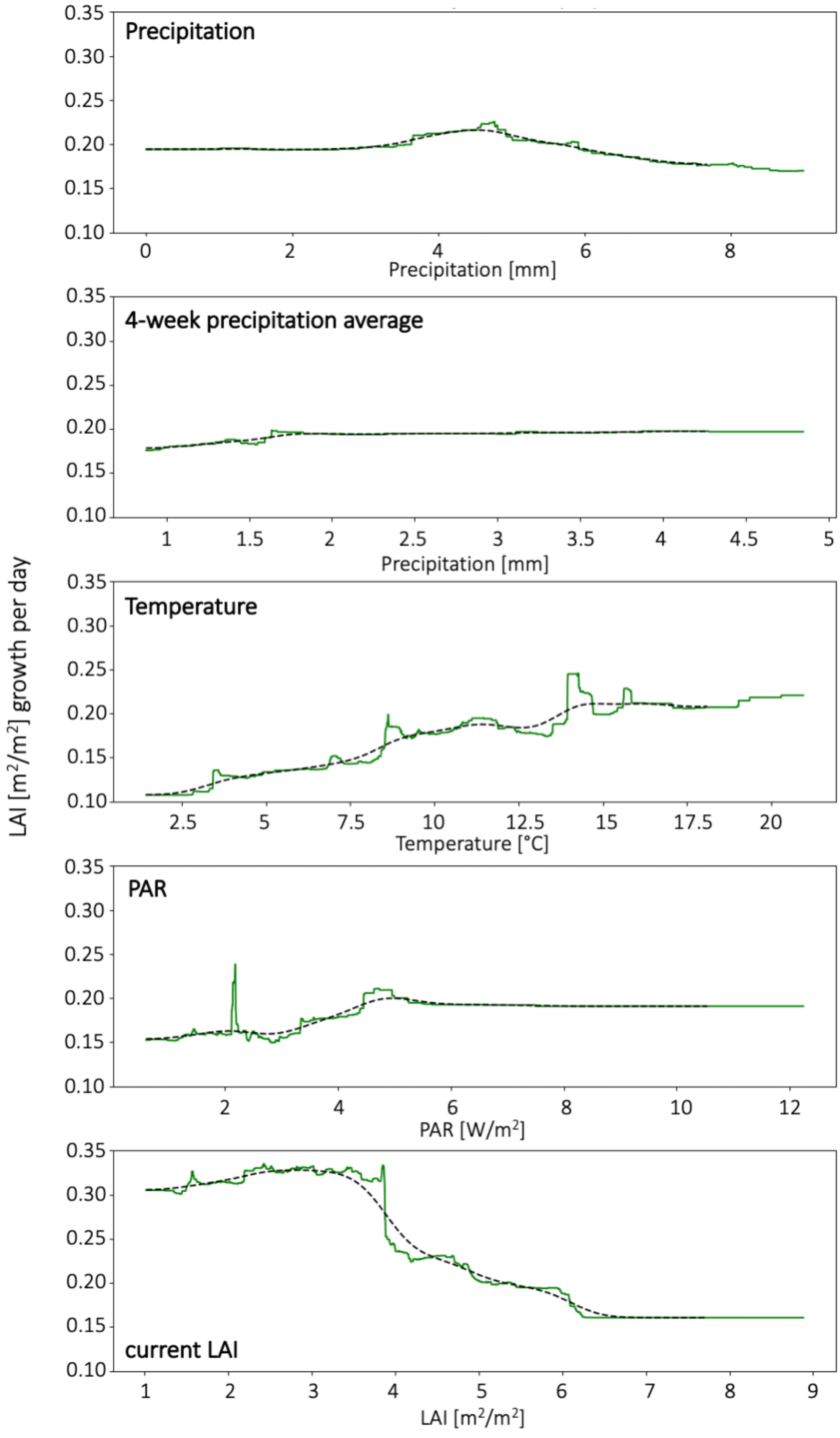

Figure 5.11: Model sensitivity analysis. To see the effect of the variables in the growth model, each variable was set to a value range while all others were kept constant. The dashed line shows the results with an applied Gaussian smoothing to eliminate the noise. The y-axis represents predicted LAI growth per day, on the x-axis are all input variables to the growth model, from the 10th to the 90th percentile of their distribution.

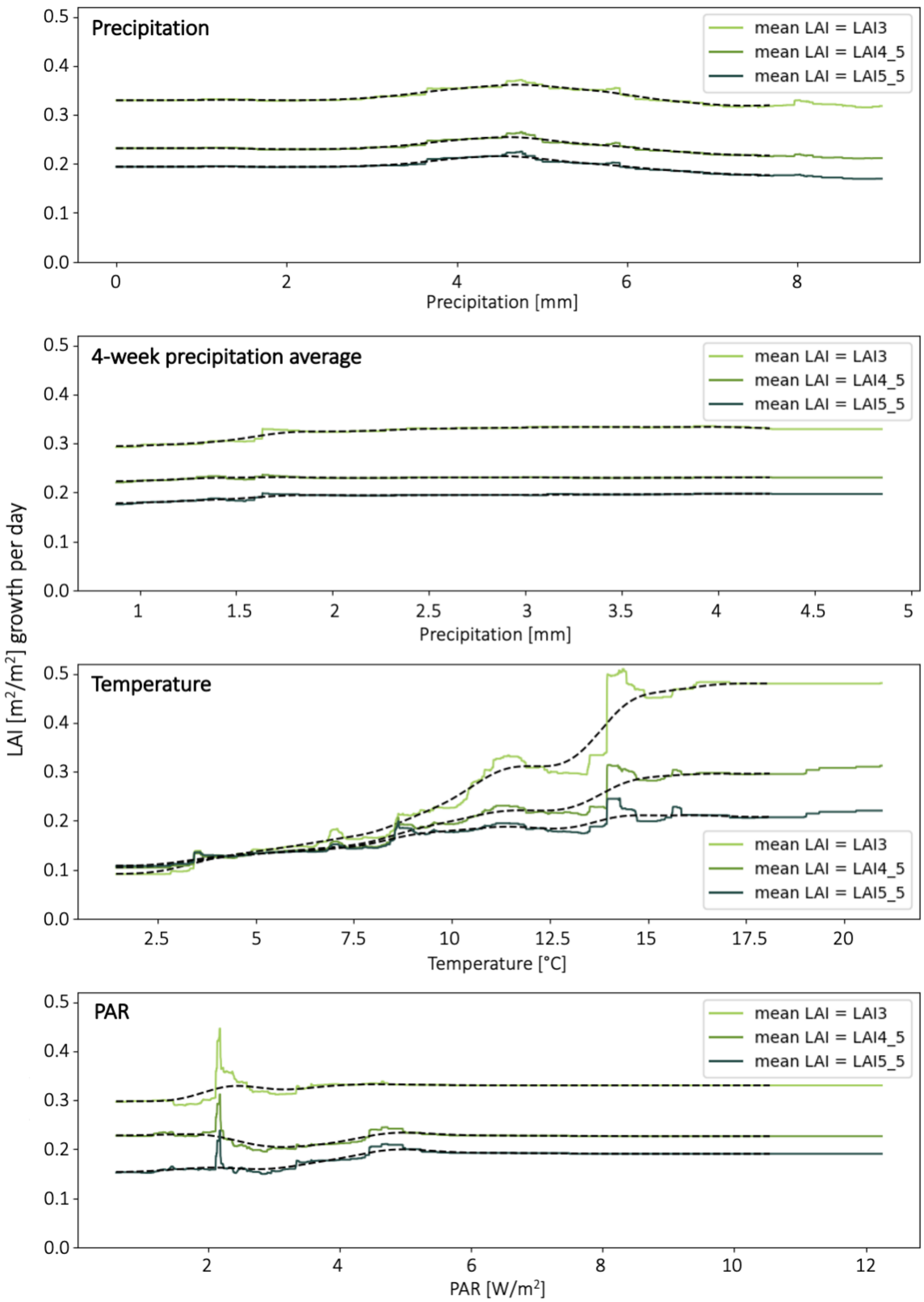

Figure 5.12: Repeated sensitivity analysis with different averages of the current LAI in the average scenario.

5.3.4 Model performance assessment: Comparison with other LAI time series

The performance of the ML grass growth model was assessed by testing its cumulative growth prediction, including management events for the independent FluxNet field, against i) Sentinel-2 LAI estimations (Section 5.3.4.1), ii) the FluxNet in-situ LAI data (Section 5.3.4.2), and iii) the predicted growth of the mechanistic model ModVege (Section 5.3.4.3).

5.3.4.1 Sentinel-2 derived LAI estimates

To directly compare the modelled growth with the Sentinel-2 derived LAI, the gaps in the Sentinel-2 data were compensated for by halting the growth model during the periods of missing data (see Section 4.4.5.1). Figure 5.13 shows the comparison of the Sentinel-2 derived LAI and the gap compensated ML grass growth model predicted LAI. In 2019 the two curves correspond well until DOY 180, after that the ML grass growth model is overestimating growth for a period of about 50 days. From DOY 230 on, the two curves are parallel again, indicating similar growth until DOY 300. The R^2 was calculated for the grass growth predicted and Sentinel-2 curves and reached 0.62 with a RMSE of 3.55 the lowest correlation of all. In 2020, the two curves show a very similar pattern with some exceptions in spring, where Sentinel-2 LAI overestimates the ML grass growth model and in late summer where the ML grass growth model overestimates the satellite derived LAI. The R^2 of 0.93 with a RMSE of 1.71 support this observation. In 2022 a very similar growth pattern can be observed until DOY 190, after that the ML grass growth model overestimates growth. R^2 reaches 0.94 and RMSE 2.4. In 2023 the two growth curves correspond significantly, after DOY 200 the model slightly overestimates the Sentinel-2 derived LAI. The R^2 of 0.96 and RMSE of 1.08 provide statistical confirmation of this observation.

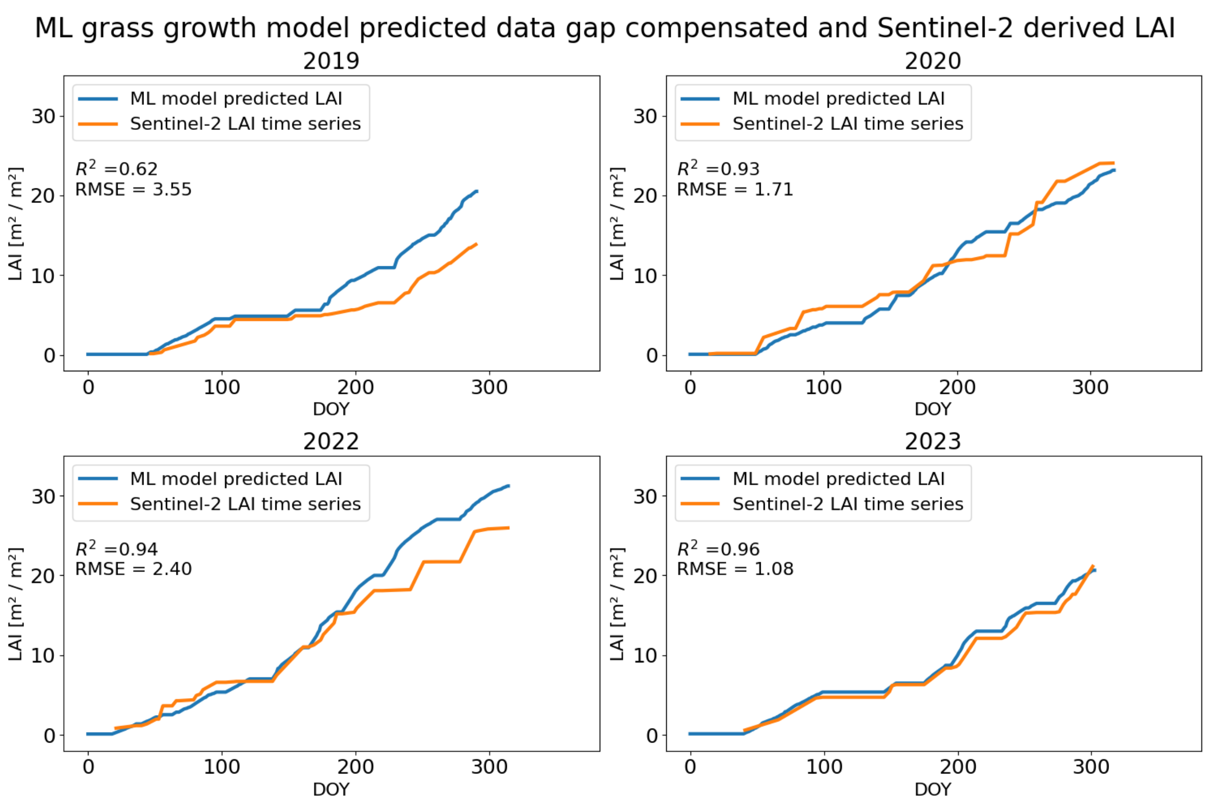

Figure 5.13: Grass growth model predicted cumulative sum vs. Sentinel-2 derived LAI including R^2 and RMSE.

5.3.4.2 FluxNet in-situ LAI observations

A scale factor was applied to directly compare the model predictions to the in-situ observations (see Section 4.4.5.2). Figure 5.14 shows the scaled cumulative sum of the predicted LAI compared with the in-situ measured LAI. The ML grass growth model predicts the daily LAI for the entire year. In the initial period from DOY 0 to 130, the predicted growth remains low. Between the 130th and 280th DOY, a significant increase in growth is observed, after which the daily growth rate decreases again. This pattern is more or less valid for all four years.

The in-situ measured LAI time series is shorter and covers, depending on the year, different periods of time. The DOY of the first measurement varies between DOY 25 (2020) - 100 (2022). The last measurement is taken between DOY 300 - 350 except in 2022, in that year the last measurement was acquired around DOY 250.

In 2019 the time series correspond quite well. At the beginning and in the middle of the season the ML grass growth model overestimates LAI. Towards the end of the season, the two curves show a very similar pattern. The R^2 reaches 0.93 with an RMSE of 0.97. In 2020 the model overestimates LAI growth throughout the whole year. R^2 reaches 0.37 with an RMSE of 2.53. In 2022 and 2023 the model underestimates the in-situ LAI measurements. For 2022 R^2 reaches 0.61 with an RMSE of 2.98, for 2023 R^2 is 0.38 with an RMSE 4.19.

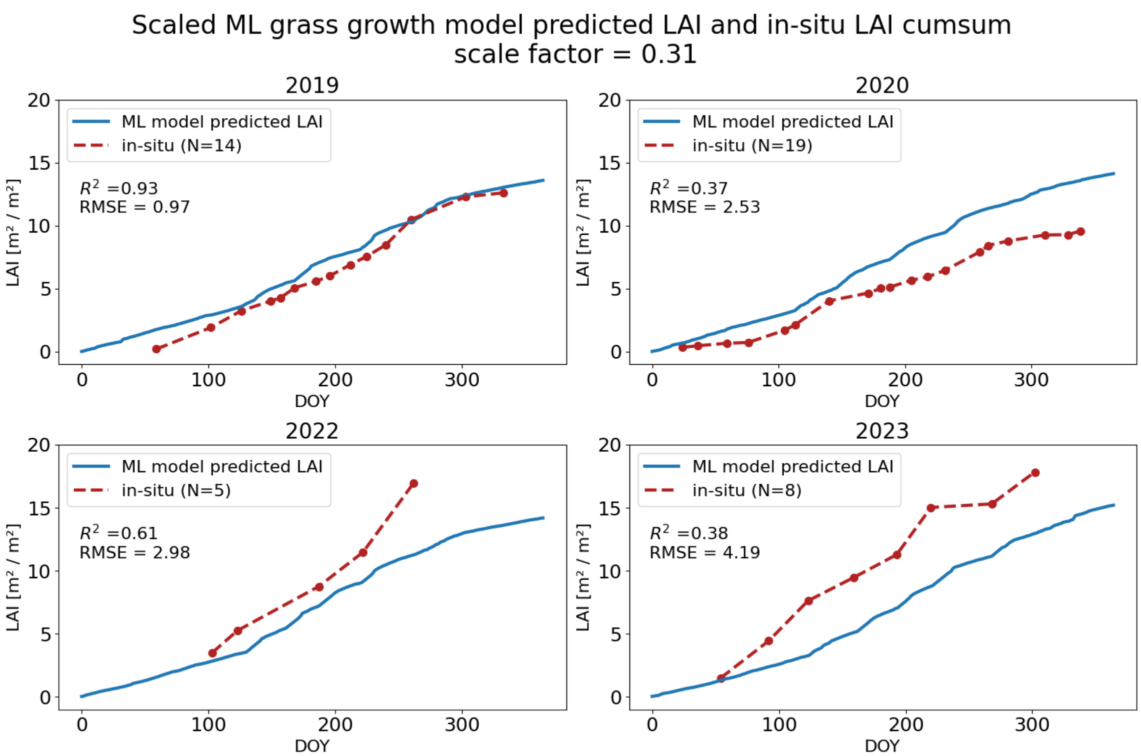

Figure 5.14: Scaled cumulative sum of grass growth model predicted vs. in-situ measured LAI.

5.3.4.3 Mechanistically modelled LAI

Figure 5.15 shows the results of the last comparison between the cumulative sum of the ML grass growth model predicted LAI and the ModVege modelled LAI growth. To directly compare these two predictions, the two models were run for exactly the same time period. The ML grass growth model was run including management events, ModVege was run twice, once with and once without management events (see Section 4.4.5.3). In the beginning of 2019 and 2020 ModVege predicts higher LAI than the grass growth model, after DOY 175 ModVege predicts lower growth compared to the grass growth model. At the end of the growing period, the cumulative sum of the ML grass growth model prediction is about 10 LAI higher than ModVege. The dynamics of the grass growth and the ModVege prediction including management agree with an R^2 of 0.86 (RMSE = 3.58) in 2019 and 0.92 (RMSE = 2.99) in 2020, which is also the highest agreement of all years. In 2022 and 2023, the ML grass growth model underestimates growth until around DOY 170, in 2022 the difference between the models was larger than in 2023. After DOY 170, the ML grass growth model continuously overestimates growth. For 2020 an R^2 of 0.76 (RMSE = 5.31) was achieved, for 2023 an R^2 of 0.82 (RMSE = 4.78). The ModVege simulation with management shows higher cumulative LAI at the end of the year compared to the simulation without management. Depending on the year, this difference is between 8 and 14 LAI.

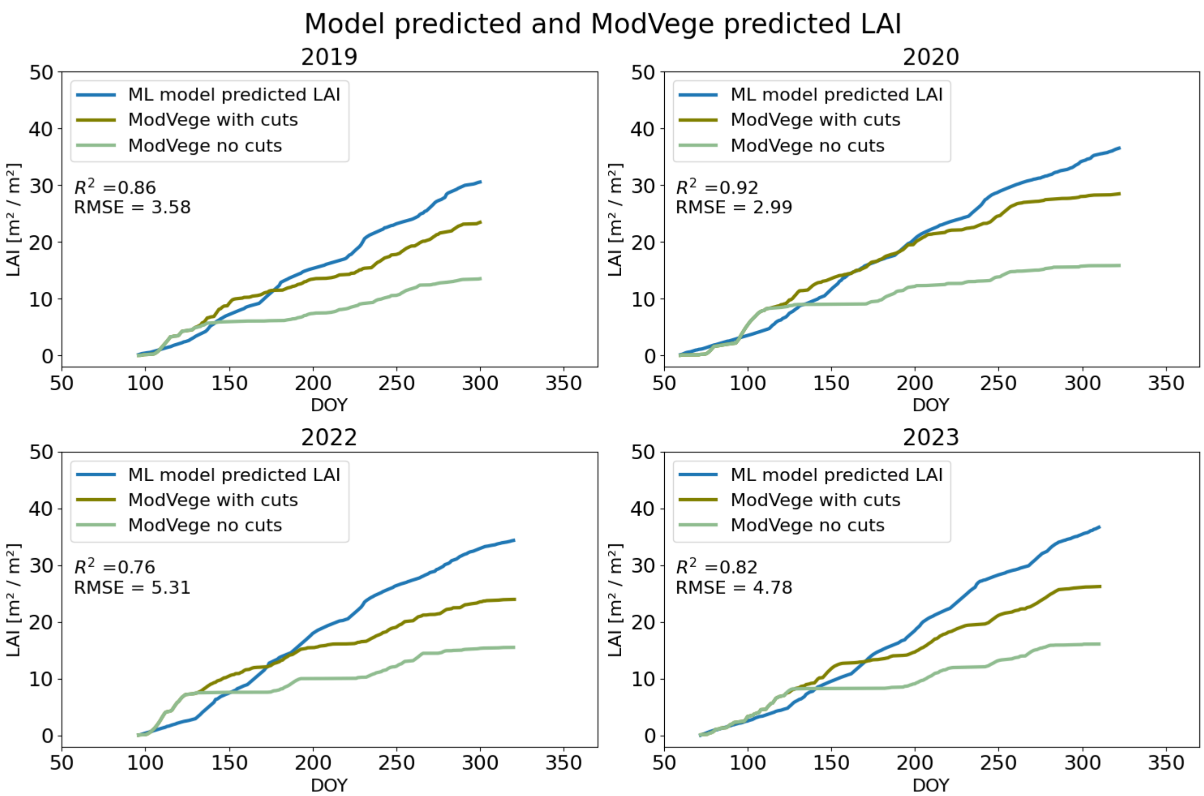

Figure 5.15: Grass growth model predicted cumulative sum vs. ModVege predicted LAI. ModVege was run twice, once with management events and once without. The grass growth model was set to start and end modelling growth on the same days as ModVege.

5.4 Model based drought impact analysis

Two analyses were conducted to assess the ML grass growth models capability of capturing the effects of drought on grass growth. Section 5.4.1 elaborates on the grass growth prediction under different precipitation scenarios. Section 5.4.2 presents the results on the case study, conducted to assess the drought impact on grass growth on the FluxNet field in spring 2020.

5.4.1 Future water availability: Scenarios

To assess the ML grass growth models capability of capturing the effects of increased and decreased rainfall, water availability was synthetically adjusted (see Section 4.5.1). The top row in Figure 5.16 shows the modelled cumulative sum of daily LAI growth over one year and the impact of adjusted water availability on daily LAI growth. The black curve represents the unaltered conditions. For all three scenarios, water shows a positive correlation with grass growth; more water leads to increased growth, less water to a decrease in total LAI.
The left graph shows how precipitation influences daily growth. From day 0 to 30, there seems to be no influence on growth. From day 40 on, more precipitation shows an increase in LAI compared to the curve with less precipitation. The curves continuously diverge over the growth period. At the end of the year, the cumulative sum reaches an LAI of about 33 for the increase precipitation scenario, while the decreased reaches a total LAI of about 27.
The middle graph shows the impact of the 4-week precipitation average on LAI growth. Until day 230 there is barely a difference visible between the different conditions, except for a small period around DOY 100. Around DOY 200 they start to diverge more strongly. The total difference between the 50% increased and decreased 4-week precipitation average scenarios is about 3 LAI at the end of the year.
The graph on the right shows the combined influence of the two variables, increased and decreased precipitation and4-week precipitation average. In this scenario, the effect becomes visible early in the year and diverges more at the end with a difference in LAI of about 7 between the scenarios with 50% more and less water.

The bottom row in Figure 5.16 shows the absolute difference between the scenarios. An increase in precipitation (left plot) of 20% results in 0.3 more total LAI at the end of the year, 50% more rain in 1.3 higher LAI. 20% less precipitation results in a decrease in total LAI of 1.1, and 2.1 at 50% less rainfall. A change in precipitation is visible from DOY 40 on. The middle plot shows the absolute difference in LAI growth when altering the 4-week precipitation average. 20% more results in 0.3 more LAI at the end of the year, an increase of 50% in 0.9 more LAI. A decrease of 20% in 0.6 less total LAI, 50% less in 1 LAI less. The plot on the right shows the absolute difference of the combination of both variables. The 20% increase results in 0.6 more LAI, the 50% in 2 LAI. A 20% decrease reduces total LAI by 1.5, 50% decrease by 3 LAI.

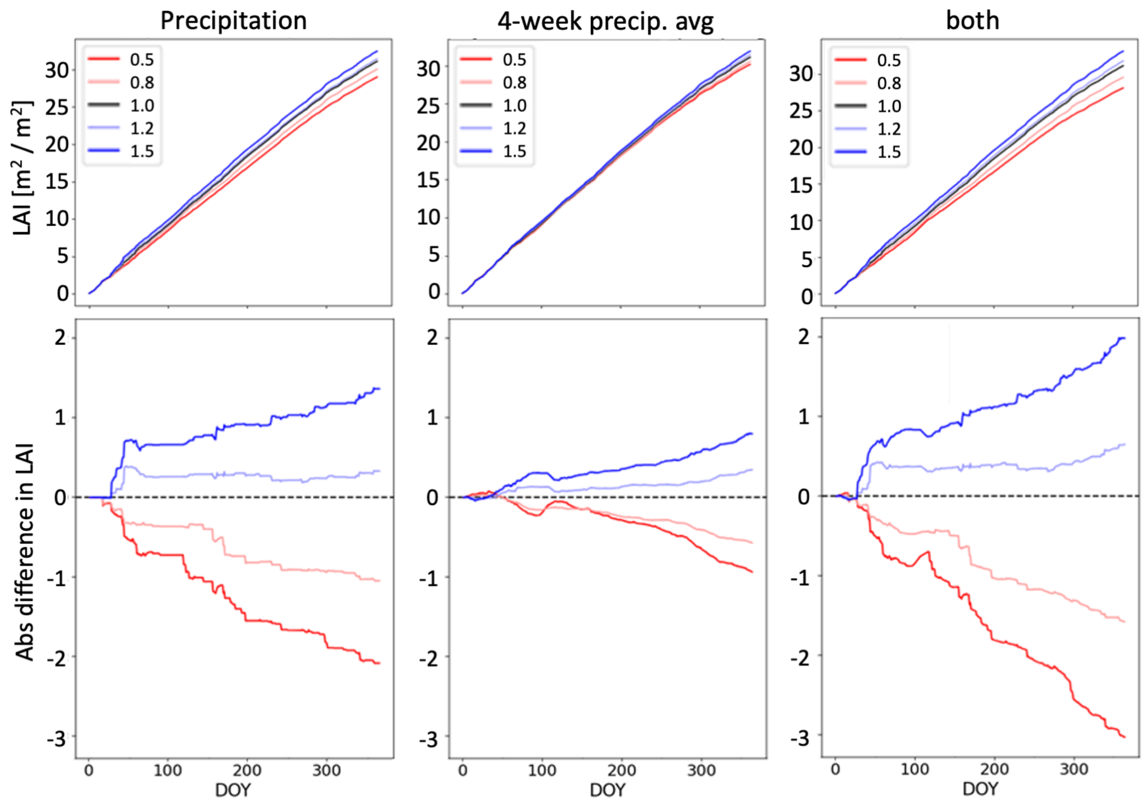

Figure 5.16: Top row: Modelled scenarios with more and less precipitation and 4-week precipitation average. Bottom row: Absolute difference between the different scenarios.

5.4.2 Case study: impact of a dry period on grass growth in Chamau in spring 2020

To evaluate the impact of a dry period between DOY 89 and 109 —characterized by notably reduced precipitation and low ET_{rel} values — on grass growth in the FluxNet field, water was artificially added to the input meteorological data of the ML grass growth model (see Section 4.5.2). This approach aimed to test the model's capability to simulate grass growth under drought conditions and quantify the reduction in growth due to the lack of precipitation during this period.

The left y-axis in Figure 5.17 represents relative evaporation ET_{rel} and LAI growth under different precipitation scenarios. The right y-axis represents the meteo variables precipitation (dark and light blue bars), PAR (yellow bars) and temperature (red bars).

During the 3-week period ET_{rel} recorded continuously low values. Precipitation was low, while PAR and temperature showed relatively high values, with an exception around DOY 105 where temperature falls for a couple of days. Around DOY 110 a small rainfall event was recorded. On this day, no precipitation was added to the input meteo data.

LAI growth was modelled with the actual precipitation (solid green line), and two synthetically generated scenarios of 2 mm (dashed green line) and 5 mm (dotted green line) increase in precipitation on dry days. With the actual precipitation, the ML grass growth model predicted an LAI growth of about 0.1 per day. When precipitation is increased 2 mm per dry day, LAI growth shows an overall increase of 2%, and 12% with an increase of 5 mm of rainfall.

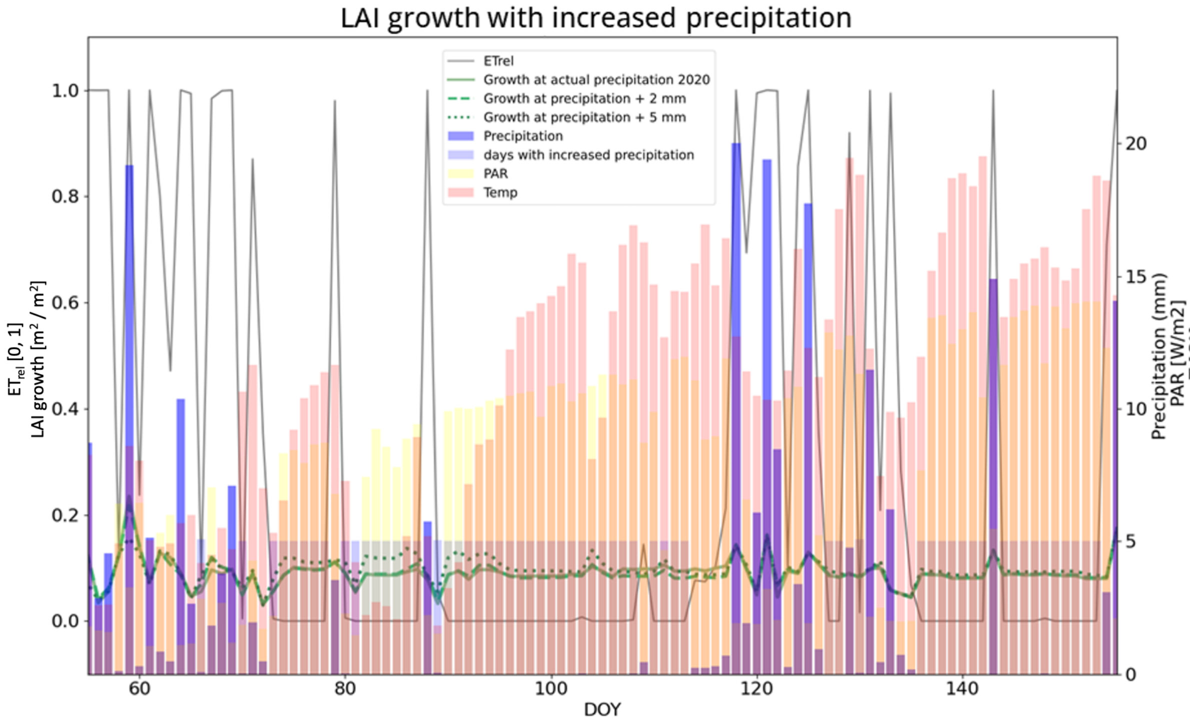

Figure 5.17: Plot showing the impact of a 3-week dry period on growth during spring 2020 at the FluxNet site in Chamau. The left axis represents ETrel, which indicates the drought level (0 = dry, 1 = wet) and LAI growth per day. Growth is modelled with the actual meteo data, a 2 mm and a 5 mm increase in precipitation on days with less than 0.1 mm of rain. The axis on the right represents the three meteo variables precipitation (dark blue bars), PAR (yellow bars) and temperature (red bars). The light blue bars going up to 5 mark the days on which precipitation was increased synthetically by 2 and 5 mm.

Chapter 6

Discussion

In this chapter, the results of this study are discussed with regard to the research questions. In the first section the EVI and LAI as biomass proxies are discussed (Section 6.1). The second section discusses the ability of Sentinel-2 to detect changes in grassland biomass, which was investigated by comparing the Sentinel-2 derived time series with PlanetScope data, the grassland use-intensity map, the FluxNet in-situ biomass and mechanistically modelled time series (Section 6.2). In the third section it is discussed whether a grass growth model can be learned from EO data by investigating the final set up, performance and limitations of the ML grass growth model in more detail (Section 6.3). In the last section it is discussed whether the ML grass growth model is able to model the impact of drought on grassland. The drought scenarios as well as the counterfactual analysis are assessed (Section 6.4).

6.1 Biomass estimations: EVI and LAI as proxies for grassland biomass

In the first research question it was investigated whether LAI is a better proxy for biomass compared to EVI. EVI was calculated from Sentinel-2 images with simple band math, while LAI was derived from the same images with an RTM. Both measures were compared to fresh and dry biomass measurements, determined using a rising plate meter, and show a positive correlation (Figure 5.1). When relating EVI with fresh biomass an R^2 of 0.22 was reached, and 0.12 with LAI. A study by Punalekar et al. (2018) has also related RTM derived LAI data with in-situ measured rising plate meter biomass measurements for three different dates and achieved an overall R^2 of 0.22. when correlating the biomass data to NDVI, they achieved an overall R^2 of 0.16. While Punalekar et al. (2018) achieved better results for the LAI, our results, contrary to our initial hypothesis, indicate that EVI, rather than LAI, shows a stronger correlation with biomass. There are several potential reasons why these results were obtained.

Based on the acquisition of the location of the fields with a cell phone and the discussions with the team at VSLU, it must be assumed that the VSLU biomass field data have not been accurately geolocated. During this thesis, a lot of work was put into locating the correct field extents in retrospect, however it is likely that the satellite images used for biomass estimation were not precisely aligned with the same field areas as the in-situ measurements. This misalignment could have led to errors in the correlation analysis, as the satellite-derived estimates do not accurately reflect the actual biomass conditions observed on the ground.

Consequently, the correlations observed in this study may be influenced by this spatial inconsistency, highlighting the need for improved geolocation accuracy in future studies.
Based on these findings, a meeting with the team from VSLU was organised to discuss the criteria the data must meet to enable better integration and use in remote sensing applications. This includes, above all, accurate geolocation and recording of the extent of the fields, no tree cover and, if possible, distance from buildings, roads and forests to minimise spectral uncertainty from adjacent surface covers. Consequently, one important outcome of this thesis is that future records of in-situ biomass data at VSLU will follow these criteria, which would ensure the data's relevance and compatibility with satellite-derived observations, ultimately facilitating more accurate and comprehensive biomass monitoring.

Additionally, two methodological constraints contributed to the uncertainty of this analysis. Despite the relatively high temporal resolution of Sentinel-2 and due to data gaps because of overcast, the satellite's acquisition dates often did not coincide with the exact dates of in-situ biomass measurements. As a result, the biomass proxies used in the correlation analysis were derived from an interpolated time series, rather than from direct observations on the day of biomass sampling. This interpolation implies that the proxies may not accurately reflect the actual in-situ biomass present on the corresponding measurement dates, potentially leading to discrepancies in the observed relationships.

Moreover, PROSPECT is designed for homogeneous surfaces (Verhoef, 1984) the efficacy of retrieving vegetation characteristics using RTMs on heterogeneous surfaces remains a topic of ongoing debate (Darvishzadeh et al., 2008). Given that the level of heterogeneity in the study fields is not well characterized, it must be assumed that the LAI retrieval using an RTM may have introduced some degree of error. Darvishzadeh et al. (2008) investigated the potential of radiative transfer modelling to predict LAI in a heterogeneous Mediterranean grassland and reported only intermediate accuracy in estimating LAI. This suggests that similar uncertainties could affect the present study's results.

Last but not least, the in-situ biomass data from VSLU were not recorded as time series from one point, but as individual measurements across several fields and with a very different measurement principle compared to retrieval based on satellite observations, i.e. estimating swath height densification versus light absorption in the canopy. This may make it difficult to establish a clear relationship between the in-situ data and the remote sensing data. When comparing the satellite observations with time series of in-situ observations based on an LAI-2000 Plant Canopy Analyzer, the relationships between the satellite-derived LAI and the in-situ LAI were better (Figure 5.4).

When EVI and LAI are directly compared to each other (Figure 5.2), the pattern shows the distinct relationship between the two proxies. At low values EVI is more sensitive to variations in biomass, but at an LAI of three EVI starts to saturate. Many studies have investigated this relationship and found the same effect (Chávez et al., 2019; Tanaka et al., 2015; Wu et al., 2010), or even more extreme saturation of EVI.

Although EVI and LAI are derived using different methods - EVI from spectral indices and LAI from radiative transfer modelling - it is useful to compare them as approximations for biomass estimation. Both are biophysically linked to vegetation productivity, with EVI reflecting canopy greenness and chlorophyll activity, while LAI measures the structural density of foliage. However, Croft et al. (2015) have investigated the relationship of leaf chlorophyll and LAI. They have found that the two measures show temporal differences at the beginning and the end of the growing season (see Figure A.9 in the Appendix). While LAI increased steeply at the beginning of the growing period, leaf chlorophyll seemed to build up more slowly. At the end of the season leaf chlorophyll started to decline earlier than LAI, as it was retracted from the plant while foliage still remained intact. The effect of this temporal difference on the relationship of Sentinel-2 derived EVI and the LAI retrieved with an RTM would have to be investigated further.

1. Research Question: *Is the LAI showing a better correlation with biomass compared to the EVI?* No, contrary to our expectations, LAI does not show a better correlation with biomass than EVI compared to in-situ biomass estimates based on rising plate meter measurements. However, this might have been caused by many confounding factors that challenged the comparison. The direct comparison of the two proxies showed that LAI has a higher sensitivity towards higher biomass compared to EVI. The effect of the temporal difference of biomass and leaf chlorophyll in the beginning of the growing period, and its impact on EVI and LAI as proxies for biomass would have to be investigated further.

6.2 Changes in grassland biomass, expressed as changes in LAI, over space and time estimated by Sentinel-2

In the second research question, it was investigated whether Sentinel-2 is able to capture changes in grassland biomass over space and time. To evaluate this, comparisons of the Sentinel-2 derived LAI time series to three other data products were made. Two comparisons evaluated the plausibility of cutting dates (Section 6.2.1). Two further analyses were conducted to assess continuous changes in LAI time series (Section 6.2.2). Finally, the advantages and disadvantages of EO and modelled data is discussed (Section 6.2.3)

6.2.1 Plausibility check of mowing events

To evaluate whether the mowings indicated in the Sentinel-2 derived LAI time series were plausible, the cutting dates were visually compared to the PlanetScope images. By consulting the highly resolved PlanetScope images just before and after randomly selected cuts in the Sentinel-2 time series, it was possible to visually confirm that a mowing event took place (Figure 5.3). This method was not suitable to confirm the indicated cuts from all time series from 2018 - 2023. So the grassland use-intensity map was consulted. The resulting 87% of coinciding management events of Sentinel-2 time series cuts with the grassland use-intensity map indicated that not only single cuts could be validated, but that the majority of cuts within all time series across all fields and years were detected when the grassland use-intensity map also suggested one. This result has confirmed that the derivation of the LAI curves from the Sentinel-2 data works and that Sentinel-2 is largely capable of detecting mowing events characterised by abrupt decreases in LAI over space and time.

6.2.2 Comparison to other LAI time series

To also evaluate the growth dynamics beside the characteristic cutting events, the LAI time series were compared to the FluxNet in-situ measured LAI time series and the mechanistically modelled LAI time series from ModVege. Figure 5.4 shows the results of the direct comparison of the Sentinel-2 RTM derived LAI and the in-situ measured LAI. Without applying a scaling factor, the two measurements correlated well in 2019 ($R^2 = 0.92$) and 2023 ($R^2 = 0.84$). Using Sentinel-2 imagery and PROSAIL with different cost functions to retrieve LAI, Verrelst et al. (2015) achieved an R^2 of 0.74 when comparing the derived LAI to in-situ measurements. In 2020 and 2022 Sentinel-2 overestimates the in-situ measured LAI. In 2020 the field was in very bad conditions showing patches of bare soil. This seems to have been captured by the in-situ measurements, while Sentinel-2, with its 10 m resolution, was not sensitive enough to capture this.

The degree of heterogeneity of the grassland was not taken into account when the LAI was retrieved using the RTM. Darvishzadeh et al. (2008) have investigated the potential of RTMs when applied to heterogeneous grasslands. They have found a significant decline of R^2 with an increasing number of species present on the field. In their study they have achieved an R^2 of 0.85 when comparing their RTM derived LAI to in-situ measured LAI on a field with a single species compared to an R^2 of 0.59 on a field with four species. The low correlation in 2022 could be due to the plowing and reseeding in 2021 which could have lead to a change in species composition and a more heterogeneous surface, but further research would be needed to be able to conclusively answer this.

Figure 5.5 shows the time series of the Sentinel-2 derived LAI and the ModVege modelled LAI at four different locations. An important note on the temporal resolution of the two time series: the Sentinel-2 LAI values are derived from individual images and then linearly interpolated to create a time series. Thus, the LAI information between two consecutive observations should be interpreted with caution. The ModVege modelled time series on the other hand consists of daily values based on the meteorological conditions.

In all time series curves Sentinel-2 reports higher LAI values from DOY 0 - 70. While ModVege models LAI around 1, Sentinel-2 detects LAI between 2 and 4 depending on the site. A possible reason for this is the fact, that many grasslands are green all year around, even in the winter months the sward does not completely lose its green color. Consequently, Sentinel-2 detects some level of LAI. Within these first weeks of the year there are also indications of growth periods, though such growth is improbable given the prevailing low temperatures. This discrepancy might be attributed to the satellite detecting swards changing its morphology after the winter or that appear to have varying LAI values due to the lighting conditions at the time of image acquisition.

Figure 5.6 shows the meteo data from 2022, the year in which the VSLU biomass measurements were taken. Looking at the time period from DOY 70 - 90, ModVege starts to model growth, showing relatively steep increases in LAI. The meteorological data indicate much sunshine and relatively warm temperatures during that period. In addition, there were several rainfalls between DOY 30 and 60, which ensured sufficient water availability. These factors collectively created optimal conditions for plant growth. Sentinel-2 also registered increases in LAI. Between DOY 90 and 100 growth seems to stagnate in ModVege. Considering the meteo data in this period this is reasonable, there are registered a couple of rainfall events at all locations, sunshine decreased and temperatures plunged considerably. Due to the rainfall and overcast, no Sentinel-2 images were usable during this period (especially well visible in the JunH and NieA time series). Right after DOY 100 sunshine and temperature increased and growth picked up again, which is visible at all locations and in both time series, the Sentinel-2 and the ModVege. Three of the four fields were also managed for the first time during this period. After the first management event, ModVege immediately shows increased growth at all locations except at NusA. Sentinel-2 implies longer periods during which LAI stayed relatively low. What is unknown to ModVege is the fact, that the management events on these fields are not mowing, but grazing events. This is ultimately visible in the Sentinel-2 time series, but not in the ModVege growth curve.

6.2.3 Advantages and disadvantages of Earth Observation and modelled data

The above comparison of the Sentinel-2 derived LAI time series and the modelled LAI curve by ModVege, discusses two very different approaches of analysing vegetation dynamics. Both of them have their advantages and limitations:
One advantage of EO data is that it provides real-time data on vegetation and its growth patterns. Satellites can cover large and remote areas at a nominal constant temporal frequency. They provide information about what is really going on in the fields and automatically present the information in a spatial context. Two main limitations of EO data are the temporal and spatial resolutions. A sensor always represents a trade off between these resolutions. The minimum spatial resolution of openly available data is 10 m, making it difficult to study small-parcelled structures. The temporal resolution is limited by the satellite's revisit time, as well as daylight, atmospheric conditions and cloud coverage. To use satellite images reliably, an accurate atmospheric correction is crucial. In particular, when using time series data, robust outlier detection is another essential prerequisite.
Mechanistic models on the other hand simulate growth based on process-based understanding. They are able to integrate multiple variables and have the predictive capability to model under varying conditions, making it possible to analyse different scenarios and forecasts. These models are often able to simulate at very high temporal resolutions, without limiting data gaps due to unfavourable environmental conditions such as cloud cover. This is visible in Figure 5.5, where the model provides daily growth rates, while data gaps lead to sudden changes in the Sentinel-2 time series. However, their output is highly dependent on the quality of the input data, such as management events. While Sentinel-2 naturally captures every change on a field, a model has to be provided with the information of cutting or grazing events in order to reflect management events in the time series. This is again visible in Figure 5.5, where the abrupt decreases in LAI represent the mowing events on the fields, which had to be given to the model as inputs. Models are defined by the equations describing the underlying processes, this forces them to simplify natural processes and make assumptions which possibly limit their accuracy. For instance, the mowing events in Figure 5.5 were all assumed to be of the same magnitude and reset to the same value, while Sentinel-2 implies different LAIs after the cut (which in this case, however, also depended on when the next image acquisition took place and how much grass had grown back since the cut).

Both satellite imagery and modelling are powerful tools for understanding and predicting vegetation growth, each with their own strengths and limitations. While satellites provide comprehensive real-time spatial information, model-based data can provide crucial information on growth patterns, for example, in times of cloud cover or limited satellite images. This data can fill in the gaps left by missing observations and ensure continuous monitoring of vegetation dynamics. Together, the two methods can be used in a complementary way to improve our understanding of vegetation dynamics.

2. Research Question*: Can Sentinel-2 capture changes in grassland biomass, expressed as changes in LAI, over space and time?*
Yes, with its relatively high temporal and spatial resolution, Sentinel-2 can detect mowing dates at high accuracy and is well suited to capture changes in grassland biomass across space and time. A key advantage of using Sentinel-2 imagery compared to models lies in its capacity to analyze vegetation dynamics without requiring input data, while inherently providing information within a spatial context. Its biggest limitations are clouds and noise induced by the atmosphere, which can introduce significant challenges when conducting time series analyses.

6.3 ML grass growth model from Earth Observation data

In the third research question the feasibility of establishing a grass growth model based on EO data was explored. The first part in this section discusses the technicalities of the final ML grass growth model (Section 6.3.1), while the second part discusses the predictive power of the established model on unseen data (Section 6.3.2). Finally, some of the limitations of the model are addressed in more detail (Section 6.3.3).

6.3.1 Final ML grass growth model setup

6.3.1.1 Model features and sensitivity

Based on the feature importance, the five variables reducing most model uncertainty were selected for the final grass growth model (Figure 5.7). The chosen features include some of the main drivers for vegetation growth:

Daily average PAR is one of the most important variables in predicting average daily growth. Short wave radiation is one of the main variables that determine photosynthesis and therefore has a major impact on plant growth (Leafe et al., 1974; Merz et al., 2022). Merz et al. (2022) have found, that on an hourly scale short wave radiation explains most of the variation in growth, demonstrating the importance of this variable. Interestingly, when considering the sensitivity analysis of the model PAR does not show to have a large influence on growth. Possible reasons for the high feature importance nevertheless could be that the feature importance reflects not only the individual effect of a variable, but also its interactions with other variables. Additionally, it needs to be considered that there is a correlation between PAR and temperature, the third most important feature, which could lead to a misleading distribution of importance between these two features. Varying one feature at a time might not show much effect in a sensitivity analysis if its contribution is already accounted for by the correlated feature, in this case temperature.

Current LAI ranked second in the feature importance. This variable is an indicator for the amount of vegetation already present on the field and has a direct impact on growth in different ways. It influences light interception positively as there is more area for photosynthesis, which leads to increasing growth (Street et al., 2007). Conversely, a larger LAI leads to a reduction of the amount of light penetrating the canopy (Lantinga et al., 1999; Street et al., 2007), potentially reducing growth. This is in line with the results of the sensitivity analysis, where the model predicts significantly higher daily growth when LAI is low compared to when it is high (Figure 5.11). The more detailed sensitivity analysis on the effects of starting LAI also showed that each variable predicted increased daily growth when the average LAI was low, compared to when it was high (Figure 5.12). The specific underlying mechanisms driving the response of each individual variable would require further investigations. The direct effect of the amount of current LAI can be seen in Figure 5.9, which shows modelled daily growth with and without management. Whenever a cut results in a reduction of current LAI, daily growth immediately increases.

Daily average temperature was the third most important feature. Temperature is one of the main factors influencing plant growth (Hatfield & Prueger, 2015). Merz et al. (2022) have found that daily average temperature showed a strong relationship with vegetation growth ($R^2 = 0.79$). Each plant species thrives in a specific temperature range that includes a minimum, maximum and optimum temperature for growth. Changes in the average and maximum temperature will also have an effect on plant growth in the future (Hatfield & Prueger, 2015), making it one of the most important inputs for predicting plant growth. The sensitivity analysis indicated continuously increased growth with increasing temperatures.

The **4-week precipitation average** was included in the model as a rough proxy for soil moisture. Soil moisture represents one of the main drivers for vegetation growth (Hopkins, 2000). It is not only influenced by recent precipitation, but rather the cumulative effects over a longer period of time, which is captured by the 4-week-average, as well as temperature and soil conditions (Hopkins, 2000).
Daily average precipitation showed the smallest impact on the model. Water plays a crucial role in photosynthesis, nutrient transport and various cellular processes, making it one of the most important factors for plant growth. Of all meteorological variables, plant-available water is most closely linked to precipitation, but it is important to be aware that this relationship is influenced by other factors such as soil type, temperature and ETP rate. The model did not show a great sensitivity to neither precipitation nor the 4-week precipitation average. This could be due to the lack of training data during water-limited periods (see Section 6.3.3.3).

6.3.1.2 Model performance on training and testing dataset

The density plots in Figure 5.8 show how the final ML grass growth model performs well on the training and testing data split. On the training data (left plot) the model achieves an R^2 of 0.76 and an R^2 of 0.61 on the testing data (right plot). This indicates that the model is able to accounts for 61% of the variance in the unseen data. However, the higher performance on the training data compared to the testing data is a possible indication that the model is potentially overfitted. This would mean that it learned the training data too well, capturing noise from the input data, and ultimately leading to a reduced generalizability on unseen data.

6.3.2 Assessing the ML grass growth model's predictive power: Comparison with other LAI time series

To assess the predictive power of the ML grass growth model on unseen data, its growth predictions for the independent FluxNet field were compared with i) the Sentinel-2 LAI observations, ii) the in-situ measured LAI data, iii) and the predicted growth of the mechanistic model ModVege.

6.3.2.1 Sentinel-2 derived LAI estimations

Figure 5.13 shows how the Sentinel-2 derived LAI time series correspond to the ML grass growth model predicted growth. With the exception of the prediction for 2019, an R^2 higher than 0.9 was achieved for all years (2020, 2022 and 2023). This strong correlation indicates that the ML grass growth model captured the inter-annual variability of grass growth from Sentinel-2 images and was able to generalise across different years despite variations in weather and management. The ML grass growth model demonstrated a reliable ability to predict LAI consistent with Sentinel-2 observations, using only site-specific meteorological data as input. The lower R^2 value in 2019 can be attributed to the poor condition of the FluxNet field, leading to overestimated growth predictions by the grass growth model. However, despite the continued poor condition of the field in 2020, the model managed to predict LAI with greater accuracy. The plowing and reseeding in 2021 has probably contributed to the improved predictions for 2022 and 2023.

6.3.2.2 FluxNet in-situ LAI observations

After applying the scaling factor to the ML grass growth model predicted LAI and comparing it to the FluxNet in-situ measured LAI, the R^2 values exhibited considerable variation between the years (Figure 5.14). Notably, the highest R^2 (0.93) was achieved in 2019, which contrasts the low correlation between model prediction and Sentinel-2 derived LAI during the same period (see Figure 5.13). This discrepancy highlights the complex relationship between field conditions and model accuracy, particularly when growth estimation is trained on satellite data and conducted for heterogeneous grasslands.

6.3.2.3 Mechanistically modelled LAI

Figure 5.15 shows the cumulative ML grass growth model predicted LAI and the ModVege predictions with and without management. The R^2 of the ML grass growth model comparison to the ModVege modelled LAI achieved relatively high values (0.86, 0.92, 0.76, 0.82 with an average RMSE of 4.17), indicating that the ML grass growth model is able to reproduce the prediction of the mechanistic model with relatively high accuracy. The ML grass growth model underestimated LAI in the beginning of the year and overestimated the ModVege prediction after DOY 170. This is consistent with the four grass growth phases from Figure 6.1. By compensating for seasonal patterns, the growth predicted by ModVege is slowed down after the growth peak (Jouven et al., 2006), whereas the ML grass growth model was only trained on the initial, fast-growing growth period and thus overestimated growth during the period when growth is in fact inhibited (see Section 6.3.3.2).

So far, no literature exists that uses EO data to train a grass growth model. When it comes to predicting grassland biomass from Sentinel-2 data with a RF model trained on Sentinel-2 data, Muro et al. (2022) achieved an R^2 0.42. The ML grass growth model predicting Sentinel-2 LAI with R^2 of up to 0.93 therefore shows promising results, particularly in an area such as environmental modelling where the data often has significant noise and complexity. This level of predictive power indicates that the model generalises well beyond the training data and is robust enough to provide reliable predictions. While the model shows solid performance, it also has certain limitations that leave room for further optimisation.

6.3.3 ML grass growth model limitations

6.3.3.1 Above average satellite imagery with high temperature and PAR

Due to an inherent property of optical satellite images, the growth-meteo database only contains data from cloud-free days. The model was therefore only trained on data that disproportionately reflect periods of high PAR and temperature and was unable to learn how growth is affected under cloudy conditions. Additionally, this bias could have distorted the perception of the model in terms of importance of the individual features for plant growth.

6.3.3.2 Overestimation of growth due to selective growth periods for model training

To simplify the methodology in this study and avoid the complexity of implementing a cutting detection algorithm to monitor growth across the entire growing season, only the initial growth periods up to the first cut were used to train the ML grass growth model. The first growth period mostly comprises data acquired in the spring months. This approach potentially lead to a bias in the training data, as grass growth dynamics change over the vegetative period. Grass growth can be divided into four growth phases

(Figure 6.1) (Vuffray et al., 2017). Reserves are mobilized to stimulate growth and stored to reduce it. Mobilization starts in early spring, reaches its peak during vegetative growth, and declines as the plant enters the reproductive phase (Bausenwein et al., 2001). As the model was trained on data from the first growth period, it has only captured patterns associated with peak growth conditions that are not representative of the slower growth rates observed in summer or autum.

6.3.3.3 Underrepresentation of drought conditions in training data

The growth periods selected for model training may contribute to an underestimation of drought impacts on plant growth, as spring seasons are typically not water-limited. The training dataset includes only a limited number of dry periods in the training data. As a result, the model may not have sufficiently learned the dynamics of grass growth under drought stress, which occurs more frequently in later stages of the growing season. Without a sufficient amount of data reflecting a low-water environment, the model may show reduced sensitivity to drought effects and have difficulty accurately predicting grass growth under such conditions.The sensitivity analysis suggests this potential underestimation, as it reveals relatively low sensitivity to both precipitation and the 4-week precipitation average (Figure 5.11).

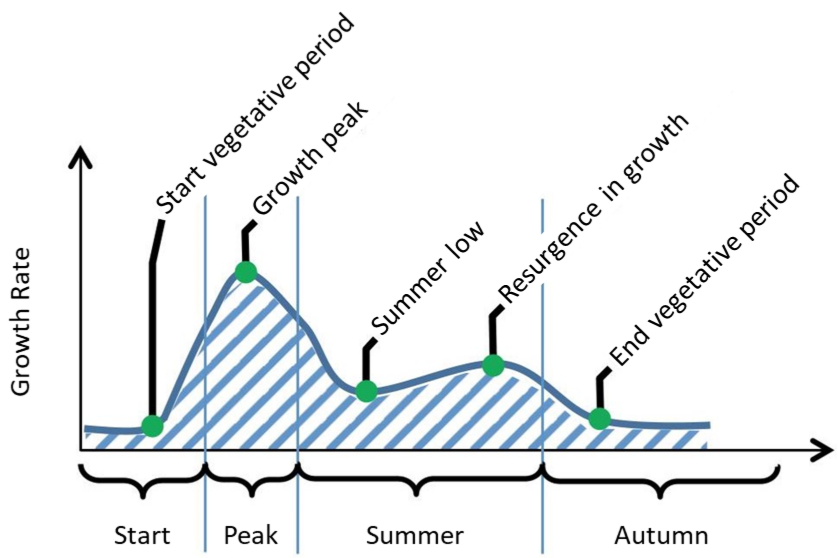

Figure 6.1: The four grass growth phases in the vegetative period (Vuffray et al., 2017)

6.3.3.4 No growth limitations

To train the grass growth model, the training dataset was selectively filtered to include only periods of vegetation growth, excluding any instances of dieback or senescence. Environmental conditions, such as temperature and precipitation, often exhibit a parabolic distribution in relation to plant growth. Optimal growth tends to occur under moderate conditions, while extremes (either too low or too high) can inhibit growth. Given that the dataset predominantly comprised data from the spring season, the model was not exposed to the upper range of environmental stressors, such as extreme temperatures. As a result, the model possibly did not learn to associate growth limitations with adverse conditions. This is also reflected in the sensitivity analysis. The model shows steady increases in daily growth with increasing temperature from 0.11 to 0.23 over the range from 2.5 to 20 degrees Celsius (Figure 5.11). No upper growth limit is visible in the sensitivity analysis. This potentially lead to an additional overestimation of growth under non-optimal conditions.

6.3.3.5 Inherent data dependency due to data collection at the same location over several years

The quality of the input data is influenced by several factors related to environmental and climatological dependencies within the dataset. First, the inclusion of six years of data introduces a yearly cycle pattern, reflecting the seasonal variability inherent to plant growth and weather. While this provides comprehensive temporal coverage, it also means that data points are not fully independent, as patterns may repeat annually due to consistent environmental conditions. Additionally, the data was acquired from the same fields over multiple years, resulting in similarities due to consistent soil composition and management practices. This lack of variability in field conditions could introduce bias, as the underlying biological processes and land management remained relatively stable. Furthermore, the close proximity of the fields means that they were likely exposed to similar weather conditions, potentially limiting the diversity in environmental responses. Thus, while the dataset provides valuable long-term insights, these factors suggest some degree of correlation between observations, reducing the independence of the data and affecting the generalizability of the findings to other locations or conditions. This limitation could possibly explain the higher performance on the training compared to the testing data split (see Section 6.3.1.2).

That the quality of the model is highly dependent on the input data is also visible in the distribution of R^2 values in Figure A.4, where the range from 0.2 to 0.6 illustrates varying levels of model performance in explaining the data. The broad spread of R^2 indicates that the model does not consistently achieve high predictive accuracy, suggesting that the model quality is highly dependent on the training-testing data split.

6.3.3.6 Accuracy of PAR estimation from daily sunshine duration

It needs to be noted that PAR can only be approximated from the measured relative sunshine duration. The relative sunshine duration is not measured in hourly resolution, which would provide crucial information about the angle of incidence of the radiation. Radiation received at a lower sun angle is less effective at providing PAR compared to radiation received at a steeper angle. MeteoSwiss only provides the average daily sunshine duration, which may affect the accuracy of the PAR estimate.

6.3.3.7 4-week precipitation average as a proxy for soil moisture

Soil moisture represents one of the main drivers for vegetation growth (Hopkins, 2000). In this study, soil moisture was very roughly approximated with the 4-week average precipitation. However, besides precipitation it is also very dependent on soil composition, temperature, and evapotranspiration (Hopkins, 2000). A more precise approximation could thus provide more insight into the significance of this variable.

6.3.3.8 Extreme events challenging model predictions in simulating real-world dynamics

It is important to acknowledge that no model prediction can fully capture the complexity of reality. While meteorological conditions such as weather patterns influence grass growth, they also affect farm management decisions. For example, longer periods of precipitation - such as those observed in spring and early summer of 2024 - prevented farmers from mowing their fields for an extended time. Episodes like these, in turn, impact subsequent grass growth and management practices for the remainder of the season. Such interactions between environmental conditions and management responses are inherently difficult to model using meteorological data alone. The increase in extreme weather conditions due to climate change will pose further challenges for modelling in the future.

3. Research Question*: Can a growth model be learned from Earth Observation data?*
Yes, a growth model can be learned from EO data. The ML grass growth model developed in this study demonstrates the capability to accurately predict LAI dynamics, comparable to those derived from Sentinel-2 imagery. This provides a valuable tool for bridging gaps in time series data from optical satellite observations. By including a scale factor, the model can further be used to estimate the growth dynamics of in-situ measured LAI. The ML grass growth model also showed fairly good agreement with the mechanistically modelled grass growth. To improve the accuracy of predictions, it is essential to account for seasonal growth patterns and the full range of meteorological conditions occurring throughout the year. This could be achieved by incorporating data from the entire growing season into the model's training process.

6.4 Model based drought impact analysis

In the last research question it was investigated whether the ML grass growth model was capable of capturing the impact of droughts on grassland growth. The generation of different future scenarios with increased and reduced precipitation explored the sensitivity of the model to different quantities of available water (Section 6.4.1). Finally, the case study examined whether the model would have predicted more growth during a 3-week period of reduced rainfall in spring 2020 if the amount of water had not been limited (Section 6.4.2).

6.4.1 Future water availability: Scenarios

The impact of drought on grassland productivity, as captured by the grass growth model, indicates a linear relationship between precipitation and grass growth. This can be seen in Figure 5.16 and is in line with what Reinermann et al. (2020) have concluded. In their review, they found that precipitation and grassland productivity show positive correlations especially in the early and mid-growing season. When considering the results of the sensitivity analysis of the model however, this relationship is only valid up to 4.5 mm of average daily precipitation (Figure 5.11).
Figure 5.16 shows that the change in daily precipitation affects daily LAI growth much earlier in the year (around DOY 40) compared to the 4-week precipitation average (around DOY 250). The different response between the daily precipitation and the 4-week precipitation average could be due to differences in the computational methods or to a delayed response of soil moisture and a limitation of soil moisture later in the year. However, since water-limited conditions were scarce in the training data (see Section 6.3.3.3), it would require further investigations to fully understand the underlying mechanisms.
Considering the results of the sensitivity analysis and the relatively low responsiveness of the model to both precipitation and the 4-week precipitation average, it was anticipated that the effects of drought would likely be relatively small. While the model reflects an influence of precipitation on productivity, the magnitude of this impact is notably smaller (cumulative total difference of 5 LAI in a year considering the $\pm$ 50% scenario, see Figure 5.16) compared to the influence of management events, such as mowing, which implied a cumulative total difference of 18 LAI in a year between managed and unmanaged scenario (see

Figure 5.10). This is consistent with the sensitivity analysis and the response of the model to precipitation and the 4-week precipitation average compared to current LAI, which is the variable directly affected by mowing events. This suggests that the model captures a much greater influence of management on grassland productivity than drought. Interestingly, Vogel et al. (2012b) have found that the stability of grasslands (resistance and resilience) under drought conditions is highly dependent on management intensity.

Although the model is sensitive to changes in precipitation, it may underestimate the full extent of drought's effects on grass growth. This underestimation is probably due to the limitations in the training dataset, which lacked sufficient data from periods of drought (see Section 6.3.3). Consequently, the model's ability to fully capture the effects of prolonged dry conditions is likely constrained, potentially leading to an incomplete representation of the drought's impact on grassland productivity.

6.4.2 Case study: impact of a dry period on grass growth in Chamau in spring 2020

The National Center for Climate Services states that in Switzerland, dry periods will last up to 3 weeks in the future NCCS (Hrsg.) (2018). Thus as a last analysis, a prolonged dry period of about 3 weeks on the FluxNet field in spring 2020 was analysed. A counterfactual analysis helped to understand, whether the ML grass growth model would have predicted increased grass growth when there would have been precipitation. Figure 5.17 shows grass growth under actual weather conditions as well as growth modelled with increased precipitation levels. The increase of 2 mm of rain for each day with less than 0.1 mm of precipitation resulted in an increased growth of 2%, a 5 mm increase in precipitation for these days resulted in an overall 12% growth increase. These results suggest, that the dry conditions have reduced growth by 2 to 12%. Surprisingly, the differences between the growth curves are most distinct at the beginning of the dry period (around DOY 90) and become more similar towards the end of the period (around DOY 110). This was contrary to expectations, as the compounding effect of reduced water availability intensifies over time, thus an increasing and more distinct reduction in growth was expected towards the end of the dry period.

The previously discussed limitations of the ML grass growth model and the limited data on drought periods in the training database likely contributed to these results. Additional factors require consideration, such as the time scale at which the drought impact is assessed. Almeida-Ñauñay et al. (2022) emphasize the importance of analyzing vegetation-climate relationships across different time scales, as the effects of various climate variables manifest over distinct temporal periods. Similarly, Petrie et al. (2016) demonstrate that the sensitivity of vegetation productivity to precipitation fluctuates across daily, monthly, and even seasonal scales. Further research is required to determine the specific time scales at which Swiss grasslands are most responsive to drought conditions.

Additionally, studies showed that species composition and richness significantly influence both the resistance and resilience of grasslands to drought (Vogel et al., 2012b). Potential previous adaptations at the FluxNet site may have already enhanced drought resistance, possibly attenuating the severity of drought impacts. Such adaptations could have resulted from long-term exposure to variable environmental conditions, leading to an ecosystem that is more resistant to drought. To assess whether the ML grass growth model captured these species-level effects, it would be necessary to analyze data from multiple sites with well-documented species compositions. This approach would allow for evaluating the model's sensitivity to biodiversity-related factors, which are crucial in determining grassland resilience (Vogel et al., 2012b).

Analyzing sites with varying species compositions could provide deeper insights into the model's performance in simulating the complex interactions between drought and grassland productivity.

4. Research Question*: Is the grass growth model trained on Earth Observation data capable of capturing the impact of drought on grassland growth?*

Partly yes, but not in its entirety. The ML grass growth model captures a linear relationship between precipitation and grassland productivity. It shows that changes in precipitation influence grass growth from early in the year, while the 4-week precipitation average impacts growth later. While it reflects the impact of precipitation, its overall sensitivity to both daily and 4-week precipitation averages is relatively low. The model's ability to fully capture the effects of drought is most likely constrained by the lack of sufficient drought data in the training set. As a result, the effects of drought are likely underestimated. The model indicates that the influence of drought on grassland productivity is much smaller compared to management events like mowing.

Chapter 7

Conclusion

The main objective of this study was to develop a robust ML grass growth model based on EO data and environmental variables, with a specific focus on assessing the model's ability to capture the impact of drought on grassland growth in Switzerland.

This study demonstrated that Sentinel-2 can effectively capture changes in grassland biomass across space and time. EVI was related to in-situ measured biomass with an R^2 of 0.22. RTM retrieved LAI were related to in-situ biomass measurements with an R^2 of 0.12 (rising plate meter reference measurements) and to in-situ measured LAI with an R^2 of up to 0.92 (LAI-2000 Plant Canopy Analyzer) depending on the year. The Sentinel-2 LAI time series derived with an RTM were able to detect mowing dates with a 87% accuracy when comparing to a grassland use-intensity map.
The developed ML based grass growth model that predicts LAI growth based on meteorological data, achieved R^2 scores ranging from 0.62 to 0.96, depending on the year, when relating the model predicted LAI to Sentinel-2 derived LAI. By including a scale factor, the model was able to predict in-situ measured LAI with R^2 values ranging from 0.38 to 0.93, again depending on the year. When relating the model predicted LAI growth to a mechanistic model, R^2 scores between 0.76 to 0.92 were achieved.
Assessing the impact of drought on grassland growth using predictions from the ML grass growth model resulted in an estimated growth decrease of 2 - 12% depending on the scenario, but also proved to be challenging due to the limited representation of drought periods in the training data. The model's grass growth predictions were largely influenced by management events and current LAI, making it difficult to isolate the effects of reduced precipitation.

Nevertheless, the ML grass growth model has shown that grass growth can be learned from EO and environmental data and that grass growth can be predicted under varying weather conditions. It has shown that such models have the potential to be a valuable tool to complement missing data where no direct measurements from optical satellites are available.

7.1 Further work

Potential analysis that could be done on the existing model include the investigation on possible overfitting. Although the model performed well on the data from the FluxNet field, the potential overfitting that was indicated during the performance analysis on the training and testing dataset (Section 6.3.1.2) could be further explored. While the inclusion of data from consecutive years provides a comprehensive temporal coverage, it also possibly induced an inherent data dependency (Section 6.3.3.5). This issue could be addressed by training the model on the data of a single year instead of six consecutive years, to reduce data redundancy in the training set. While this approach would reduce the overall dataset size, it would enable a more rigorous assessment of the model's performance by testing its capacity to generalize across temporally distinct data. Two primary limitations of the model are its tendency to overestimate growth during the later stages of the growing season (Section 6.3.3.2) and its weak sensitivity of drought effects on growth (Section 6.3.3.3). Both of these limitations are probably due to the lack of data, and could be addressed by incorporating growth data covering the entire growing season. Such data would capture the reduced growth rates typically observed in the late season and account for more extreme weather conditions, including droughts, which are more prevalent in late summer.

Building on the findings of this study, further research could focus on analysing the impact of the temporal difference of LAI and leaf chlorophyll on biomass estimations with LAI and EVI as a proxy for biomass (Appendix A.9). Additionally, the underlying mechanisms behind the observed effects of current LAI on each meteo variable (Figure 5.12) could be investigated.

Further studies could explore at what time scale grasslands in Switzerland become sensitive to droughts, while also including the spatial aspect and examining potential differences across the country's pronounced elevation gradient. Investigating the role of species richness on this elevation gradient using EO based data models would also provide valuable insights.

Last but not least, further research should focus on the promising approach of training ML models on EO data to not only assess the impacts of droughts on grassland in Switzerland, but possibly train a model with global data such that growth predictions can be made for anywhere on the globe. Additionally, the broader effects of meteorological extreme events could be investigated. This would contribute to a deeper understanding of how future climate scenarios and compound events may affect grassland ecosystems on which we humans are so heavily dependent.

Bibliography

Alexandridis, T. K., Ovakoglou, G., & Clevers, J. G. P. W. (2020). Relationship between modis evi and lai across time and space. *Geocarto International*, *35*(13), 1385–1399. https://doi.org/10.1080/10106049.2019.1573928

Ali, I., Cawkwell, F., Dwyer, E., Barrett, B., & Green, S. (2016). Satellite remote sensing of grasslands: from observation to management. *Journal of Plant Ecology*, *9*(6), 649–671. https://doi.org/10.1093/jpe/rtw005

Almeida-Ñauñay, A. F., Villeta, M., Quemada, M., & Tarquis, A. M. (2022). Assessment of drought indexes on different time scales: A case in semiarid mediterranean grasslands. *Remote Sensing*, *14*(3). https://doi.org/10.3390/rs14030565

Andreatta, D., Gianelle, D., Scotton, M., Vescovo, L., & Dalponte, M. (2022). Detection of grassland mowing frequency using time series of vegetation indices from sentinel-2 imagery. *GIScience & Remote Sensing*, *59*(1), 481–500. https://doi.org/10.1080/15481603.2022.2036055

Asam, S., Klein, D., & Dech, S. (2015). Estimation of grassland use intensities based on high spatial resolution LAI time series. *The International Archives of the Photogrammetry, Remote Sensing and Spatial Information Sciences*, *XL-7/W3*, 285–291. https://doi.org/10.5194/isprsarchives-XL-7-W3-285-2015

Atzberger, C., Darvishzadeh, R., Immitzer, M., Schlerf, M., Skidmore, A., & Le Maire, G. (2015). Comparative analysis of different retrieval methods for mapping grassland leaf area index using airborne imaging spectroscopy. *International Journal of Applied Earth Observation and Geoinformation*, *43*, 19–31. https://doi.org/10.1016/j.jag.2015.01.009

Atzberger, C., & Richter, K. (2012). Spatially constrained inversion of radiative transfer models for improved LAI mapping from future sentinel-2 imagery. *Remote Sensing of Environment*, *120*, 208–218. https://doi.org/10.1016/j.rse.2011.10.035

Bausenwein, U., Millard, P., & Raven, J. A. (2001). Remobilized old-leaf nitrogen predominates for spring growth in two temperate grasses. *New Phytologist*, *152*(2), 283–290. https://doi.org/https://doi.org/10.1046/j.0028-646X.2001.00262.x

Belgiu, M., & Drăguţ, L. (2016). Random forest in remote sensing: A review of applications and future directions. *ISPRS Journal of Photogrammetry and Remote Sensing*, *114*, 24–31. https://doi.org/https://doi.org/10.1016/j.isprsjprs.2016.01.011

Bento, V. A., Trigo, I. F., Gouveia, C. M., & DaCamara, C. C. (2018). Contribution of land surface temperature (tci) to vegetation health index: A comparative study using clear sky and all-weather climate data records. *Remote Sensing*, *10*(9). https://doi.org/10.3390/rs10091324

Bergstra, J., & Bengio, Y. (2012). Random search for hyper-parameter optimization. *J. Mach. Learn. Res.*, *13*(null), 281–305.

Blaney, H. F., & Criddle, W. D. (1962). *Determining consumptive use and irrigation water requirements* (Technical Bulletin No. 1275). USDA Agricultural Research Service.

Breiman, L. (2001). Random forests. *Machine Learning*, *45*(1), 5–32. https://doi.org/10.1023/A:1010933404324

Calanca, P. (2007). Climate change and drought occurrence in the alpine region: How severe are becoming the extremes? *Global and Planetary Change*, *57*(1), 151–160. https://doi.org/https://doi.org/10.1016/j.gloplacha.2006.11.001

Calanca, P., Deléglise, C., Martin, R., Carrère, P., & Mosimann, E. (2016). Testing the ability of a simple grassland model to simulate the seasonal effects of drought on herbage growth. *Field Crops Research*, *187*, 12–23. https://doi.org/https://doi.org/10.1016/j.fcr.2015.12.008

Calanca, P., Wüst-Galley, C., Giuliani, S., & Erdin, D. (2022). Auswirkungen der trockenheit auf die produktivität des schweizer grünlands. *Agrarforschung Schweiz*, *13*, 135–144. https://doi.org/10.34776/afs13-135

Carroll, C. J. W. (2021). Is a drought a drought in grasslands? productivity responses to different types of drought. *Oecologia*.

Chávez, R., Rocco, R., Gutierrez, A., Dörner, M., & Estay, S. (2019). A self-calibrated non-parametric time series analysis approach for assessing insect defoliation of broad-leaved deciduous nothofagus pumilio forests. *Remote Sensing*, *11*, 204. https://doi.org/10.3390/rs11020204

Combal, B., Baret, F., Weiss, M., Trubuil, A., Macé, D., Pragnere, A., Myneni, R., Knyazikhin, Y., & Wang, L. (2003). Retrieval of canopy biophysical variables from bidirectional reflectance: Using prior information to solve the ill-posed inverse problem. *Remote sensing of environment*, *84*(1), 1–15.

Copernicus Open Access Hub. (n.d.). *Sentinel-2 level-2a data documentation* [Accessed: 2024-09-03]. https://documentation.dataspace.copernicus.eu/APIs/SentinelHub/Data/S2L2A.html

Croft, H., Chen, J. M., Froelich, N. J., Chen, B., & Staebler, R. M. (2015). Seasonal controls of canopy chlorophyll content on forest carbon uptake: Implications for gpp modeling. *Journal of Geophysical Research: Biogeosciences*, *120*(8), 1576–1586. https://doi.org/https://doi.org/10.1002/2015JG002980

Cuddington, K., Fortin, M.-J., Gerber, L. R., Hastings, A., Liebhold, A., O'Connor, M., & Ray, C. (2013). Process-based models are required to manage ecological systems in a changing world. *Ecosphere*, *4*(2), art20. https://doi.org/https://doi.org/10.1890/ES12-00178.1

Danner, M., Berger, K., Wocher, M., Mauser, W., & Hank, T. (2021). Efficient RTM-based training of machine learning regression algorithms to quantify biophysical & biochemical traits of agricultural crops. *ISPRS Journal of Photogrammetry and Remote Sensing*, *173*, 278–296. https://doi.org/10.1016/j.isprsjprs.2021.01.017

Darvishzadeh, R., Skidmore, A., Schlerf, M., & Atzberger, C. (2008). Inversion of a radiative transfer model for estimating vegetation LAI and chlorophyll in a heterogeneous grassland. *Remote Sensing of Environment*, *112*(5), 2592–2604. https://doi.org/10.1016/j.rse.2007.12.003

De Rosa, D., Basso, B., Fasiolo, M., Friedl, J., Fulkerson, B., Grace, P. R., & Rowlings, D. W. (2021). Predicting pasture biomass using a statistical model and machine learning algorithm implemented with remotely sensed imagery. *Computers and Electronics in Agriculture*, *180*, 105880. https://doi.org/https://doi.org/10.1016/j.compag.2020.105880

Di Giulio, M., Edwards, P. J., & Meister, E. (2001). Enhancing insect diversity in agricultural grasslands: The roles of management and landscape structure. *Journal of Applied Ecology*, *38*(2), 310–319. https://doi.org/https://doi.org/10.1046/j.1365-2664.2001.00605.x

Dlamini, L., Crespo, O., van Dam, J., & Kooistra, L. (2023). A global systematic review of improving crop model estimations by assimilating remote sensing data: Implications for small-scale agricultural systems. *Remote Sensing*, *15*(16). https://doi.org/10.3390/rs15164066

European Space Agency. (2024). *SentiWiki: Copernicus Sentinel-2 Mission* [Accessed: 2024-09-17]. https://sentiwiki.copernicus.eu/web/s2-mission

FAO. (2009). *The state of food and agriculture: Livestock in the balance*. Food and Agriculture Organization of the United Nations. https://www.fao.org/3/i0680e/i0680e.pdf

Federal Statistical Office. (2023). *Landwirtschaftsflächen* [Accessed: 2024-08-09]. https://www.bfs.admin.ch/bfs/en/home/statistics/territory-environment/land-use-cover/agricultural-areas.html

Finger, R., Gilgen, A. K., Prechsl, U. E., & Buchmann, N. (2013). An economic assessment of drought effects on three grassland systems in switzerland. *Regional Environmental Change*, *13*(2), 365–374. https://doi.org/10.1007/s10113-012-0346-x

Gao, Q., Schwartz, M. W., Zhu, W., Wan, Y., Qin, X., Ma, X., Liu, S., Williamson, M. A., Peters, C. B., & Li, Y. (2016). Changes in global grassland productivity during 1982 to 2011 attributable to climatic factors. *Remote Sensing*, *8*(5). https://doi.org/10.3390/rs8050384

Gaso, D. V., de Wit, A., Berger, A. G., & Kooistra, L. (2021). Predicting within-field soybean yield variability by coupling sentinel-2 leaf area index with a crop growth model. *Agricultural and forest meteorology*, *308*, 108553.

Gibon, A. (2005). Managing grassland for production, the environment and the landscape. challenges at the farm and the landscape level [Livestock Farming Systems and their Environmental Impacts]. *Livestock Production Science*, *96*(1), 11–31. https://doi.org/https://doi.org/10.1016/j.livprodsci.2005.05.009

Gibson, D. J. (2009). Grasses and grassland ecology. *Oxford University Press*.

Gibson, D. J., & Newman, J. A. (2019). *Grasslands and climate change*. Cambridge University Press.

Gilgen, A. K., & Buchmann, N. (2009). Response of temperate grasslands at different altitudes to simulated summer drought differed but scaled with annual precipitation. *Biogeosciences*, *6*(11), 2525–2539. https://doi.org/10.5194/bg-6-2525-2009

Graf, L. V., Perich, G., & Aasen, H. (2022). Eodal: An open-source python package for large-scale agroecological research using earth observation and gridded environmental data. *Computers and Electronics in Agriculture*, *203*, 107487. https://doi.org/https://doi.org/10.1016/j.compag.2022.107487

Griffiths, P., Nendel, C., Pickert, J., & Hostert, P. (2020). Towards national-scale characterization of grassland use intensity from integrated sentinel-2 and landsat time series. *Remote Sensing of Environment*, *238*, 111124. https://doi.org/10.1016/j.rse.2019.03.017

Guerini Filho, M., Kuplich, T. M., & Quadros, F. L. F. D. (2020). Estimating natural grassland biomass by vegetation indices using sentinel 2 remote sensing data. *International Journal of Remote Sensing*, *41*(8), 2861–2876. https://doi.org/10.1080/01431161.2019.1697004

Guo, L. B., & Gifford, R. M. (2002). Soil carbon stocks and land use change: A meta analysis. *Global Change Biology*, *8*(4), 345–360. https://doi.org/https://doi.org/10.1046/j.1354-1013.2002.00486.x

Habel, J. C., Dengler, J., Janišová, M., Török, P., Wellstein, C., & Wiezik, M. (2013). European grassland ecosystems: Threatened hotspots of biodiversity. *Biodiversity and Conservation*, *22*, 2131–2138.

Hatfield, J. L., & Prueger, J. H. (2015). Temperature extremes: Effect on plant growth and development [USDA Research and Programs on Extreme Events]. *Weather and Climate Extremes*, *10*, 4–10. https://doi.org/https://doi.org/10.1016/j.wace.2015.08.001

Hoover, D. L., Knapp, A. K., & Smith, M. D. (2014). Resistance and resilience of a grassland ecosystem to climate extremes. *Ecology*, *95*(9), 2646–2656. https://doi.org/https://doi.org/10.1890/13-2186.1

Hopkins, A. (2000). Chapter 4: Herbage production. In A. Hopkins (Ed.), *Grass: Its production and utilization* (3rd ed., pp. 90–110). Blackwell Science, Published for the British Grassland Society.

Huete, A. R., Didan, K., Miura, T., Rodriguez, E., Gao, X., & Ferreira, L. (2002). Overview of the radiometric and biophysical performance of the modis vegetation indices [The Moderate Resolution Imaging Spectroradiometer (MODIS): a new generation of Land Surface Monitoring]. *Remote Sensing of Environment*, *83*(1), 195–213. https://doi.org/https://doi.org/10.1016/S0034-4257(02)00096-2

Huete, A. R., Huemmrich, K. F., Miura, T., Xiao, X., Didan, K., Leeuwen, W., Hall, F., & Tucker, C. J. (2006). Vegetation index greenness global data set. *NASA ESDR/CDR*.

Imran, H. A., Gianelle, D., Rocchini, D., Dalponte, M., Martín, M. P., Sakowska, K., Wohlfahrt, G., & Vescovo, L. (2020). VIS-NIR, red-edge and NIR-shoulder based normalized vegetation indices response to co-varying leaf and canopy structural traits in heterogeneous grasslands. *Remote Sensing*, *12*(14), 2254. https://doi.org/10.3390/rs12142254

IPCC. (2023). Weather and climate extreme events in a changing climate. In T. F. Stocker, D. Qin, G.-K. Plattner, M. Tignor, S. K. Allen, J. Boschung, A. Nauels, Y. Xia, V. Bex, & P. M. Midgley (Eds.), *Climate change 2021 – the physical science basis: Working group i contribution to the sixth assessment report of the intergovernmental panel on climate change* (pp. 1513–1766). Cambridge University Press. https://doi.org/10.1017/9781009157896.013

Jacquemoud, S., & Baret, F. (1990). Prospect: A model of leaf optical properties spectra. *Remote Sensing of Environment*, *34*(2), 75–91. https://doi.org/https://doi.org/10.1016/0034-4257(90)90100-Z

Jacquemoud, S., Verhoef, W., Baret, F., Bacour, C., Zarco-Tejada, P. J., Asner, G. P., François, C., & Ustin, S. L. (2009). Prospect+sail models: A review of use for vegetation characterization [Imaging Spectroscopy Special Issue]. *Remote Sensing of Environment*, *113*, S56–S66. https://doi.org/https://doi.org/10.1016/j.rse.2008.01.026

Jouven, M., Carrère, P., & Baumont, R. (2006). Model predicting dynamics of biomass, structure and digestibility of herbage in managed permanent pastures. 1. model description. *Grass and Forage Science*, *61*(2), 112–124. https://doi.org/https://doi.org/10.1111/j.1365-2494.2006.00515.x

Kenny, E. M., Ruelle, E., Keane, M. T., & Shalloo, L. (2024). A hybrid model that combines machine learning and mechanistic models for useful grass growth prediction. *Computers and Electronics in Agriculture*, *219*, 108805. https://doi.org/https://doi.org/10.1016/j.compag.2024.108805

Kooistra, L., Berger, K., Brede, B., Graf, L. V., Aasen, H., Roujean, J.-L., Machwitz, M., Schlerf, M., Atzberger, C., Prikaziuk, E., Ganeva, D., Tomelleri, E., Croft, H., Reyes Muñoz, P., Garcia Millan, V., Darvishzadeh, R., Koren, G., Herrmann, I., Rozenstein, O., … Verrelst, J. (2024). Reviews and syntheses: Remotely sensed optical time series for monitoring vegetation productivity. *Biogeosciences*, *21*(2), 473–511. https://doi.org/10.5194/bg-21-473-2024

Kramer, K. P., & Calanca, P. (2024). Growr: R implementation of the vegetation model modvege. *Journal of Open Source Software*, *9*(94), 6260. https://doi.org/10.21105/joss.06260

Kuusk, A. (1991). The hot spot effect in plant canopy reflectance. In R. B. Myneni & J. Ross (Eds.), *Photon-vegetation interactions: Applications in optical remote sensing and plant ecology* (pp. 139–159). Springer Berlin Heidelberg. https://doi.org/10.1007/978-3-642-75389-3_5

Lange, M., Feilhauer, H., Kühn, I., & Doktor, D. (2022). Mapping land-use intensity of grasslands in germany with machine learning and sentinel-2 time series. *Remote Sensing of Environment*, *277*, 112888. https://doi.org/https://doi.org/10.1016/j.rse.2022.112888

Lantinga, E. A., Nassiri, M., & Kropff, M. J. (1999). Modelling and measuring vertical light absorption within grass–clover mixtures. *Agricultural and Forest Meteorology*, *96*(1), 71–83. https://doi.org/https://doi.org/10.1016/S0168-1923(99)00040-4

Lary, D. J., Alavi, A. H., Gandomi, A. H., & Walker, A. L. (2016). Machine learning in geosciences and remote sensing [Special Issue: Progress of Machine Learning in Geosciences]. *Geoscience Frontiers*, *7*(1), 3–10. https://doi.org/https://doi.org/10.1016/j.gsf.2015.07.003

Leafe, E., Stiles, W., & Dickinson, S. (1974). Physiological processes influencing the pattern of productivity of the intensively managed grass sward. In V. Iglovikov & A. Movsissyants (Eds.), *Proceedings of the 12th international grassland congress, moscow, vol. 1* (pp. 442–457). State Committee of Science; Technology.

Lei, T. (2020). Net primary productivity loss under different drought levels in different grassland ecosystems. *Journal of Environmental Management*.

Lei, T., Wu, J., Li, X., Geng, G., Shao, C., Zhou, H., Wang, Q., & Liu, L. (2015). A new framework for evaluating the impacts of drought on net primary productivity of grassland. *Science of The Total Environment*, *536*, 161–172. https://doi.org/https://doi.org/10.1016/j.scitotenv.2015.06.138

Li, T., Cui, L., Scotton, M., Dong, J., Xu, Z., Che, R., Tang, L., Cai, S., Wu, W., Andreatta, D., Wang, Y., Song, X., Hao, Y., & Cui, X. (2022). Characteristics and trends of grassland degradation research. *Journal of Soils and Sediments*, *22*(7), 1901–1912. https://doi.org/10.1007/s11368-022-03209-9

Lin, S., Li, J., Liu, Q., Li, L., Zhao, J., & Yu, W. (2019). Evaluating the effectiveness of using vegetation indices based on red-edge reflectance from Sentinel-2 to estimate gross primary productivity. *Remote Sensing*, (11). https://doi.org/10.3390/rs11111303

McCree, K. (1971). The action spectrum, absorptance and quantum yield of photosynthesis in crop plants. *Agricultural Meteorology*, *9*, 191–216. https://doi.org/https://doi.org/10.1016/0002-1571(71)90022-7

Merz, Q. N., Walter, A., Maier, R., Hörtnagl, L., Buchmann, N., Kirchgessner, N., & Aasen, H. (2022). Relationship of leaf elongation rate of young wheat leaves, gross primary productivity and environmental variables in the field with hourly and daily temporal resolution. *Agricultural and Forest Meteorology*, *320*, 108902. https://doi.org/https://doi.org/10.1016/j.agrformet.2022.108902

MeteoSwiss. (2024). *Meteoswiss spatial climate dataset*. https://www.meteoschweiz.admin.ch/klima/klima-der-schweiz/raeumliche-klimaanalysen.html

Mishra, A. K., & Singh, V. P. (2010). A review of drought concepts. *Journal of Hydrology*, *391*(1), 202–216. https://doi.org/https://doi.org/10.1016/j.jhydrol.2010.07.012

Muro, J., Linstädter, A., Magdon, P., Wöllauer, S., Männer, F. A., Schwarz, L.-M., Ghazaryan, G., Schultz, J., Malenovský, Z., & Dubovyk, O. (2022). Predicting plant biomass and species richness in temperate grasslands across regions, time, and land management with remote sensing and deep learning. *Remote Sensing of Environment*, *282*, 113262. https://doi.org/https://doi.org/10.1016/j.rse.2022.113262

Nagamani, K., & Nethaji Mariappan, V. E. (2017). Remote sensing, gis and crop simulation models – a review. *International Journal of Current Research in Biosciences and Plant Biology*, *4*, 80–92. https://doi.org/10.20546/ijcrbp.2017.408.011

NCCS (Hrsg.) (2018). *CH2018 - Klimaszenarien für die Schweiz*. National Centre for Climate Services.

NCCS (Hrsg.) (2021). *Klimawandel im Kanton Luzern – Was geschah bisher und was erwartet uns in Zukunft?* (Version 1.0). National Centre for Climate Services.

Olden, J. D., Lawler, J. J., & Poff, N. L. (2008). Machine learning methods without tears: A primer for ecologists. *The Quarterly Review of Biology*, *83*(2), 171–193. https://doi.org/10.1086/587826

Parker, G. G. (2020). Tamm review: Leaf area index (lai) is both a determinant and a consequence of important processes in vegetation canopies. *Forest Ecology and Management*, *477*, 118496. https://doi.org/https://doi.org/10.1016/j.foreco.2020.118496

Pedregosa, F., Varoquaux, G., Gramfort, A., Michel, V., Thirion, B., Grisel, O., Blondel, M., Prettenhofer, P., Weiss, R., Dubourg, V., Vanderplas, J., Passos, A., Cournapeau, D., Brucher, M., Perrot, M., & Duchesnay, E. (2011). Scikit-learn: Machine learning in python. *Journal of Machine Learning Research*, *12*, 2825–2830.

Pedregosa, F., Varoquaux, G., Gramfort, A., Michel, V., Thirion, B., Grisel, O., Blondel, M., Prettenhofer, P., Weiss, R., Dubourg, V., Vanderplas, J., Passos, A., Cournapeau, D., Brucher, M., Perrot, M., & Duchesnay, E. (2023). *Cross-validation: Evaluating estimator performance* [Accessed: 2024-09-12]. https://scikit-learn.org/stable/modules/cross_validation.html

Petrie, M. D., Brunsell, N. A., Vargas, R., Collins, S. L., Flanagan, L. B., Hanan, N. P., Litvak, M. E., & Suyker, A. E. (2016). The sensitivity of carbon exchanges in great plains grasslands to precipitation variability. *Journal of Geophysical Research: Biogeosciences*, *121*(2), 280–294. https://doi.org/https://doi.org/10.1002/2015JG003205

Planet Labs PBC. (2024). *Planet application program interface: In space for life on earth* [Accessed: 2024-02-20]. Planet Labs Inc. https://api.planet.com

Pogačar, T., Žnidaršič, Z., Vlahović, Ž., Črepinšek, Z., & Sušnik, A. (2022). Grassland model based evaluation of drought indices: A case study from the slovenian alpine region. *Agronomy*, *12*(4). https://www.mdpi.com/2073-4395/12/4/936

Punalekar, S., Verhoef, A., Quaife, T., Humphries, D., Bermingham, L., & Reynolds, C. (2018). Application of sentinel-2a data for pasture biomass monitoring using a physically based radiative transfer model. *Remote Sensing of Environment*, *218*, 207–220. https://doi.org/10.1016/j.rse.2018.09.028

Quan, X., He, B., Yebra, M., Yin, C., Liao, Z., Zhang, X., & Li, X. (2017). A radiative transfer model-based method for the estimation of grassland aboveground biomass. *International Journal of Applied Earth Observation and Geoinformation*, *54*, 159–168. https://doi.org/10.1016/j.jag.2016.10.002

Reinermann, S., Asam, S., & Kuenzer, C. (2020). Remote sensing of grassland production and management—a review. *Remote Sensing*, *12*(12), 1949. https://doi.org/10.3390/rs12121949

Reinermann, S., Gessner, U., Asam, S., Kuenzer, C., & Dech, S. (2019). The effect of droughts on vegetation condition in germany: An analysis based on two decades of satellite earth observation time series and crop yield statistics. *Remote Sensing*, *11*(15). https://doi.org/10.3390/rs11151783

Reynolds, S. (Ed.). (2005). *Grasslands: Developments, opportunities, perspectives* (1st). CRC Press. https://doi.org/10.1201/9780429187872

Rose, L., Coners, H., & Leuschner, C. (2011). Effects of fertilization and cutting frequency on the water balance of a temperate grassland. *Ecohydrology*, *22*(3), 482–493. https://doi.org/10.1111/j.1654-1103.2011.01259.x

Ryu, Y., Berry, J. A., & Baldocchi, D. D. (2019). What is global photosynthesis? history, uncertainties and opportunities. *Remote Sensing of Environment*, *223*, 95–114. https://doi.org/https://doi.org/10.1016/j.rse.2019.01.016

Schils, R. L., Bufe, C., Rhymer, C. M., Francksen, R. M., Klaus, V. H., Abdalla, M., Milazzo, F., Lellei-Kovács, E., ten Berge, H., Bertora, C., Chodkiewicz, A., Dămătîrcă, C., Feigenwinter, I., Fernández-Rebollo, P., Ghiasi, S., Hejduk, S., Hiron, M., Janicka, M., Pellaton, R., ... Price, J. P. N. (2022). Permanent grasslands in europe: Land use change and intensification decrease their multifunctionality. *Agriculture, Ecosystems & Environment*, *330*, 107891. https://doi.org/https://doi.org/10.1016/j.agee.2022.107891

Schläpfer, F. (2021). Landwirtschaft und Umwelt in den Kantonen. *Vision Landwirtschaft*.

Schrödter, H. (1985). *Verdunstung – anwendungsorientierte messverfahren und bestimmungsmethoden*. Springer Verlag.

Street, L. E., Shaver, G. R., Williams, M., & Van Wijk, M. T. (2007). What is the relationship between changes in canopy leaf area and changes in photosynthetic co2 flux in arctic ecosystems? *Journal of Ecology*, *95*(1), 139–150. https://doi.org/https://doi.org/10.1111/j.1365-2745.2006.01187.x

Stumpf, F., Schneider, M. K., Keller, A., Mayr, A., Rentschler, T., Meuli, R. G., Schaepman, M., & Liebisch, F. (2020). Spatial monitoring of grassland management using multi-temporal satellite imagery. *Ecological Indicators*, *113*, 106201. https://doi.org/10.1016/j.ecolind.2020.106201

Swiss FluxNet. (2024). *Ch-cha site information* [Accessed: 2024-08-05]. https://www.swissfluxnet.ethz.ch/index.php/sites/site-info-ch-cha/

Tanaka, S., Kawamura, K., Maki, M., Muramoto, Y., Yoshida, K., & Akiyama, T. (2015). Spectral index for quantifying leaf area index of winter wheat by field hyperspectral measurements: A case study in gifu prefecture, central japan. *Remote Sensing*, *7*, 5329–5346. https://doi.org/10.3390/rs70505329

Temperton, V. M., Buchmann, N., Buisson, E., Durigan, G., Kazmierczak, Ł., Perring, M. P., de Sá Dechoum, M., Veldman, J. W., & Overbeck, G. E. (2019). Step back from the forest and step up to the bonn challenge: How a broad ecological perspective can promote successful landscape restoration. *Restoration Ecology*, *27*(4), 705–719. https://doi.org/https://doi.org/10.1111/rec.12989

Thornthwaite, C. W. (1948). An approach toward a rational classification of climate. *Geographical Review*, *38*(1), 55–94.

Török, P., Brudvig, L. A., Kollmann, J., N. Price, J., & Tóthmérész, B. (2021). The present and future of grassland restoration. *Restoration Ecology*, *29*(S1), e13378. https://doi.org/https://doi.org/10.1111/rec.13378

Van Sundert, K., Arfin Khan, M. A. S., Bharath, S., Buckley, Y. M., Caldeira, M. C., Donohue, I., Dubbert, M., Ebeling, A., Eisenhauer, N., Eskelinen, A., Finn, A., Gebauer, T., Haider, S., Hansart, A., Jentsch, A., Kübert, A., Nijs, I., Nock, C. A., Nogueira, C., ... Vicca, S. (2021). Fertilized graminoids intensify negative drought effects on grassland productivity. *Global Change Biology*, *27*(11), 2441–2457. https://doi.org/https://doi.org/10.1111/gcb.15583

Veen, P., Jefferson, R., De Smidt, J., & Van der Straaten, J. (2014). *Grasslands in europe: Of high nature value*. BRILL.

Verhoef, W. (1984). Light scattering by leaf layers with application to canopy reflectance modeling: The sail model. *Remote Sensing of Environment*, *16*(2), 125–141. https://doi.org/https://doi.org/10.1016/0034-4257(84)90057-9

Verrelst, J., Malenovský, Z., Van der Tol, C., Camps-Valls, G., Gastellu-Etchegorry, J.-P., Lewis, P., North, P., & Moreno, J. (2019). Quantifying vegetation biophysical variables from imaging spectroscopy data: A review on retrieval methods. *Surveys in Geophysics*, *40*(3), 589–629. https://doi.org/10.1007/s10712-018-9478-y

Verrelst, J., Rivera, J. P., Veroustraete, F., Muñoz-Marí, J., Clevers, J. G., Camps-Valls, G., & Moreno, J. (2015). Experimental sentinel-2 lai estimation using parametric, non-parametric and physical retrieval methods – a comparison. *ISPRS Journal of Photogrammetry and Remote Sensing*, *108*, 260–272. https://doi.org/https://doi.org/10.1016/j.isprsjprs.2015.04.013

Vicente-Serrano, S. M., Beguería, S., & López-Moreno, J. I. (2010). A multiscalar drought index sensitive to global warming: The standardized precipitation evapotranspiration index. *Journal of Climate*, *23*(7), 1696–1718. https://doi.org/10.1175/2009JCLI2909.1

Vogel, A., Scherer-Lorenzen, M., & Weigelt, A. (2012a). Grassland resistance and resilience after drought depends on management intensity and species richness. *PLOS ONE*, *7*(5), 1–10. https://doi.org/10.1371/journal.pone.0036992

Vogel, A., Scherer-Lorenzen, M., & Weigelt, A. (2012b). Grassland resistance and resilience after drought depends on management intensity and species richness. *PLOS ONE*, *7*(5), 1–10. https://doi.org/10.1371/journal.pone.0036992

Vuffray, Z., Deléglise, C., Schori, F., Glauser, W., Calanca, P., Meisser, M., Frund, D., Stévenin, L., Bittar, A., & Mosimann, E. (2017). Typologie der Produktion von Weiden. *Agrarforschung Schweiz*, *8*(11-12), 428–437. https://www.agrarforschungschweiz.ch/wp-content/uploads/2019/12/2017_1112_2340.pdf

Wang, Z., Ma, Y., Zhang, Y., & Shang, J. (2022). Review of remote sensing applications in grassland monitoring. *Remote Sensing*, *14*(12), 2903. https://doi.org/10.3390/rs14122903

Watson, D. J. (1947). Comparative physiological studies on the growth of field crops: I. variation in net assimilation rate and leaf area between species and varieties, and within and between years. *Annals of botany*, *11*(41), 41–76.

Weber, D., Schwieder, M., Ritter, L., Koch, T., Psomas, A., Huber, N., Ginzler, C., & Boch, S. (2023). Grassland-use intensity maps for switzerland based on satellite time series: Challenges and opportunities for ecological applications. *Remote Sensing in Ecology and Conservation*, rse2.372. https://doi.org/10.1002/rse2.372

Wu, C., Niu, Z., Jindi, W., Gao, S., & Huang, W. (2010). Predicting leaf area index in wheat using angular vegetation indices derived from in situ canopy measurements. *Canadian Journal of Remote Sensing*, *36*, 301–312. https://doi.org/10.5589/m10-050

Xue, J., & Su, B. (2017). Significant remote sensing vegetation indices: A review of developments and applications. *Journal of Sensors*, *2017*(1), 1353691. https://doi.org/https://doi.org/10.1155/2017/1353691

Zhang, L., Hickel, K., Dawes, W. R., Chiew, F. H. S., Western, A. W., & Briggs, P. R. (2004). A rational function approach for estimating mean annual evapotranspiration. *Water Resources Research*, *40*(W02502). https://doi.org/10.1029/2003WR002710

Zhang, Y., Lu, W., Zhang, H., Zhou, J., & Shen, Y. (2018). Grassland management practices in chinese steppes impact productivity, diversity and the relationship. *Frontiers Agricult Sci Eng*, *5*(1), 57–63.

Zhou, G., Zhou, X., He, Y., & Shao, J. (2016). Grazing intensity significantly affects belowground carbon and nitrogen cycling in grassland ecosystems: A meta-analysis. *Global Change Biology*.

Zhou, Y., Zhang, L., Xiao, J., Chen, S., Kato, T., & Zhou, G. (2014). A comparison of satellite-derived vegetation indices for approximating gross primary productivity of grasslands. *Rangeland Ecology & Management*, *67*(1), 9–18. https://doi.org/https://doi.org/10.2111/REM-D-13-00059.1

Appendix A

Appendix

A.1 Field EVI and time series

The image on the left shows a VSLU field parcel and the EVI that was retrieved from the Sentinel-2 image. Each 10 x 10 m pixel represents one EVI value. The right graph is the time series created from the median EVI of every image in 2021.

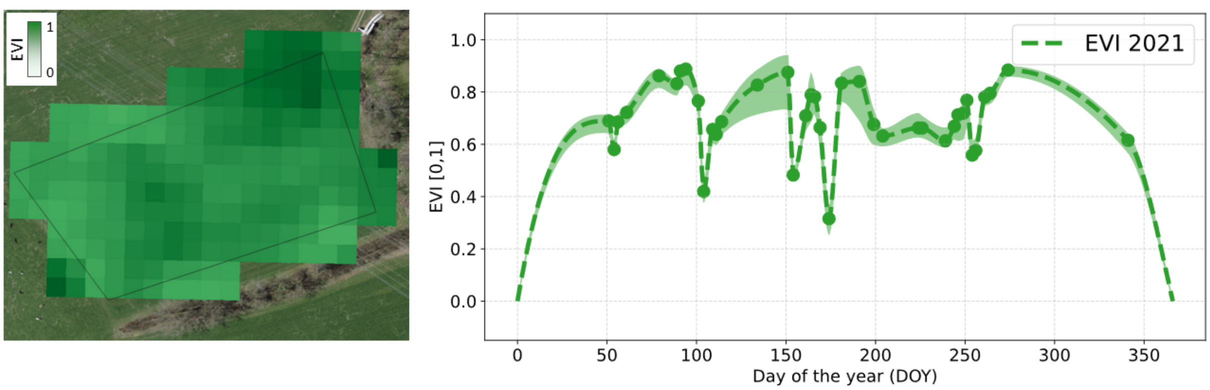

Figure A.1: Left: Retrieved EVI on a field parcel. Each pixel represents the EVI of a 10x10 m area. Right: EVI time series from 2021 calculated from Sentinel-2 images. Each point in the time series is the median of scene.

A.2 Preliminary analysis to parametrize LAI in PROSAIL

Time series of in-situ LAI measurements at the FluxNet site and the RTM retrieved LAI with the three different maximum values.

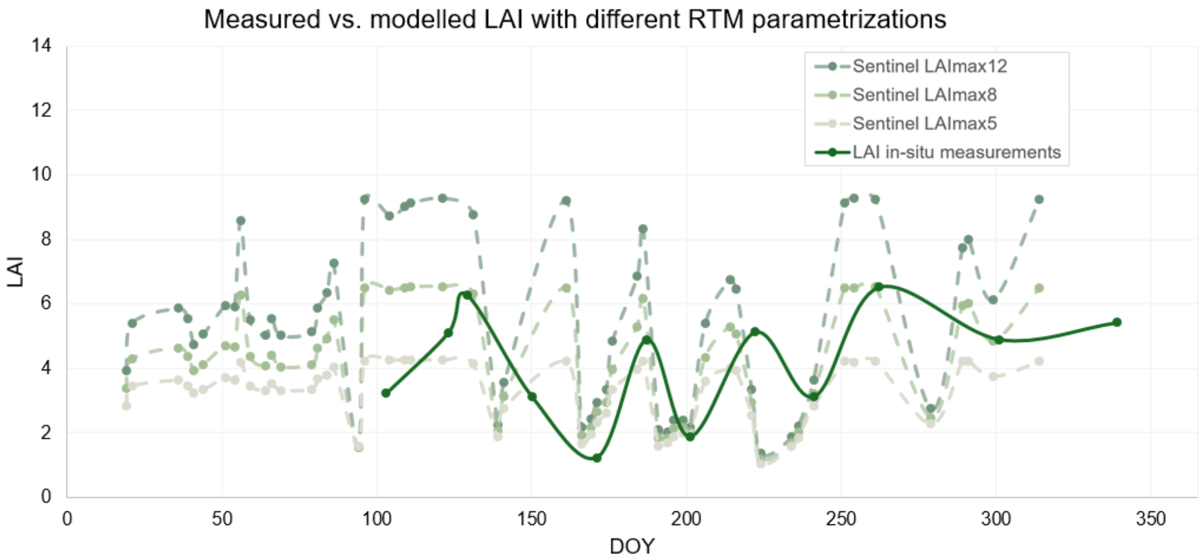

Figure A.2: Time series comparison of in-situ LAI measurements with different maximum LAI as initialization parameters for the RTM.

A.3 ModVege initialization parameters

Detailed initialization parameters for ModVege at the FluxNet and VSLU sites:

Parameter	**VSLU**	**FluxNet**
Nitrogen Index (NI)	1.0	1.05
Water Holding Capacity (WHC)	100	140
w_FunctionalGroupA	0.5	1.0
w_FunctionalGroupB	0.5	0.0
w_FunctionalGroupC	0.0	0.0
w_FunctionalGroupD	0.0	0.0
Longitude	site dependent	8.41
Latitude	site dependent	47.21
Elevation	site dependent	392

Table A.1: ModVege init. parameters for the VSLU and the FluxNet fields.

A.4 PAR estimation from relative sunshine duration

The code below was provided by Kevin Kramer (Agroscope) and implemented in the script to extract the meteorological data from MeteoSwiss.

```
# Constants
solar_constant = 1361.  # Solar constant in W/m^2
angular_velocity = 2 * np.pi / 365.25  # Angular velocity of Earth's orbit around the sun
    (radian/day)
radian = np.pi / 180  # Conversion from degree to radians


# Functions to estimate PAR
def get_number_of_days_in_year(year):
    if (year % 4 == 0 and year % 100 != 0) or (year % 400 == 0):
        return 366
    else:
        return 365

def swiss_coords_to_wgs84(x, y):
    # Define the projection for Swiss coordinates (LV03) and WGS84
    lv95 = pyproj.Proj(init='epsg:2056')  # Swiss coordinates (LV95)
    wgs84 = pyproj.Proj(init='epsg:4326')  # WGS84
    # Transform Swiss coordinates to WGS84
    lon, lat = pyproj.transform(lv95, wgs84, x, y)
    return lat, lon

def inverse_relative_distance(DOY):
    return 1. + 0.033 * np.cos(angular_velocity * DOY)

def solar_declination(DOY):
    return 0.408 * np.sin(angular_velocity * (DOY - 79))

def sunset_hourangle(DOY, latitude):
    declination = solar_declination(DOY)
    return acos(-np.tan(latitude * radian) * np.tan(declination))

def extraterrestrial_radiation(DOY, lat): # MJ m2 day
    d = solar_declination(DOY)
    hourangle = sunset_hourangle(DOY, lat)
    term1 = 1 / np.pi * solar_constant * inverse_relative_distance(DOY) # Kevins code:
    why 1? and not 24(60)
    term2 = (hourangle * np.sin(lat * radian) * np.sin(d) + cos(lat * radian) * cos(d) *
    sin(hourangle))
    return term1 * term2

def terrestrial_radiation(r_extraterrestrial, relative_sunshine_duration):
    rssd = relative_sunshine_duration
    a = 0.10 + 0.24 * rssd
    b = 0.78 - 0.44 * rssd
    return 1.07 * (a + b * rssd) * r_extraterrestrial

def srad_to_PAR(srad, fraction=0.47):
    return srad * fraction * 86400 * 1e-6
```

```python

# Actual estimation of PAR (extraction from the full code)
for year in years:
    n_days = get_number_of_days_in_year(year)

    if variable == "sunshine":
        lat_ch = site_data.loc[site_data['Site'] == site, 'yCH']
        lon_ch = site_data.loc[site_data['Site'] == site, 'xCH']
        lat, lon = swiss_coords_to_wgs84(lon_ch, lat_ch)

        # extraterrestrial radiation
        extraterr_rad = []
        for i in range(1, n_days+1):
            DOY = i
            rad_extraterr = extraterrestrial_radiation(DOY, lat)
            extraterr_rad.append(rad_extraterr[0])

        # terrestrial radiation
        terr_rad = terrestrial_radiation(extraterr_rad, (extracted_data['sunshine']/100))

        # terrestrial radiation to PAR
        PAR = srad_to_PAR(terr_rad)
```

A.5 Full list of variables in the growth-meteo database

- **Location**: Describes the specific location of the observation.
- **Year**: The year in which the observations was collected.
- **DOY_start**: Day of the year when the observation period starts.
- **DOY_end**: Day of the year when the observation period ends.
- **LAI_DOY_start**: LAI at the start of the observation period.
- **LAI_DOY_start_sd**: Standard deviation of the LAI at the start.
- **LAI_DOY_end**: LAI at the end of the observation period.
- **LAI_DOY_end_sd**: Standard deviation of the LAI at the end.
- **LAI_abs_diff**: Absolute difference in LAI between the start and end of the observation period.
- **Slope_per_DOY**: LAI growth with respect to DOY.
- **Slope_per_T**: LAI growth with respect to temperature.
- **sum_Ta_between_DOY**: Temperature sum between DOY_start and DOY_end.
- **sum_precip_between_DOY**: Precipitation sum between DOY_start and DOY_end.
- **sum_sunshine_between_DOY**: Sum of sunshine hours between DOY_start and DOY_end.
- **sum_PAR_between_DOY**: Sum of PAR between DOY_start and DOY_end.
- **cumsum_Ta**: Cumulative air temperature on DOY_end of the respective year.
- **cumsum_precip**: Cumulative precipitation on DOY_end of the respective year.
- **cumsum_sunshine**: Cumulative sunshine hours on DOY_end of the respective year.
- **cumsum_PAR**: Cumulative PAR on DOY_end of the respective year.
- **avg_precip_1w**: Average daily precipitation over the past 1 week.
- **avg_precip_2w**: Average daily precipitation over the past 2 weeks.
- **avg_precip_4w**: Average daily precipitation over the past 4 weeks.
- **sum_precip_4w**: Total precipitation over the past 4 weeks.
- **dry_days_1w**: Number of dry days over the past 1 week.
- **dry_days_2w**: Number of dry days over the past 2 weeks.
- **dry_days_4w**: Number of dry days over the past 4 weeks.
- **EVI_start**: EVI at the start of the observation period.
- **EVI_end**: EVI at the end of the observation period.

A.6 Growth periods included in the grass growth model training data set

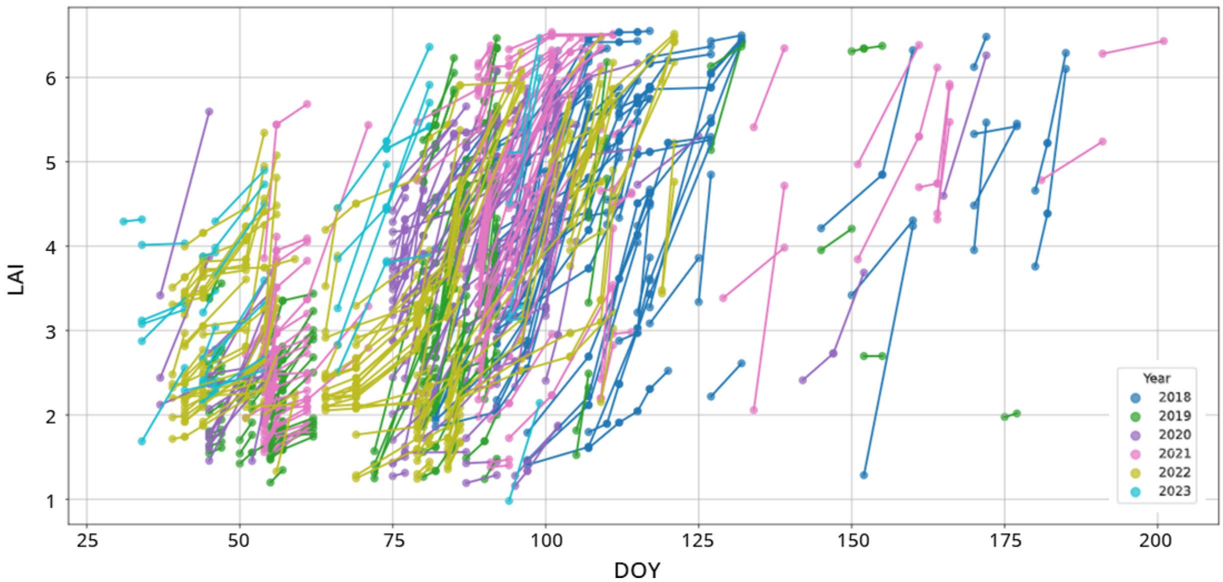

Figure A.3: Growth periods used to train the growth model colored by year.

A.7 Histogram of R^2 of the 100 generated models with the best feature set and the tuned hyperparameters

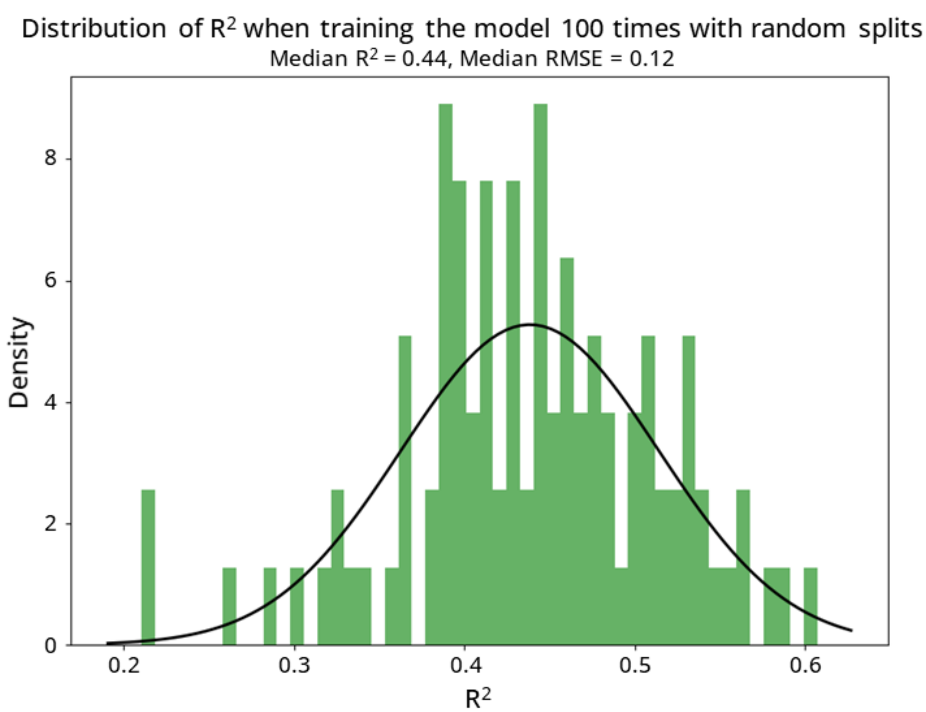

Figure A.4: Distribution of the resulting R^2 of 100 randomly generated models. The model with the highest R^2 was chosen as the final ML grass growth model.

A.8 Calculation of ETrel

ET_{rel} scales between 0 and 1 and estimates drought severity, with 0 indicating extremely dry and 1 extremely wet conditions. Daily relative evaporation (ET_{rel}) is calculated by first estimating potential evaporation with the formula developed by Blaney and Criddle (1962) and approximated for Central European climate conditions by Schrödter (1985):

$$\mathrm{ET}_p = -1.55 + 0.96 \left[p \left(0.457T + 8.128\right)\right] \tag{A.1}$$

where:

T = daily average temperature in [°C],

p = number of day light hours in percent of the sum of yearly day light hours

Relative evaporation is further calculated by (L. Zhang et al., 2004):

$$ET_{rel} = \frac{ET_a}{ET_p} = 1 + \frac{N}{ET_p} - \left(1 + \left(\frac{N}{ET_p}\right)^w\right)^{\frac{1}{w}} \tag{A.2}$$

where:

ET_a = daily average actual evaporation [mm],

N = daily average precipitation [mm],

w = 5 (constant to compensate for soil composition and vegetation)

For temperatures below zero, ET_p was assumed to be zero (Thornthwaite, 1948). However, since equation A.2 contains a fraction with ET_p as the denominator, which would produce a non-valid output, zero ET_p was approximated by 0.00001.

A.9 LAI and leaf chlorophyll content across a growing season

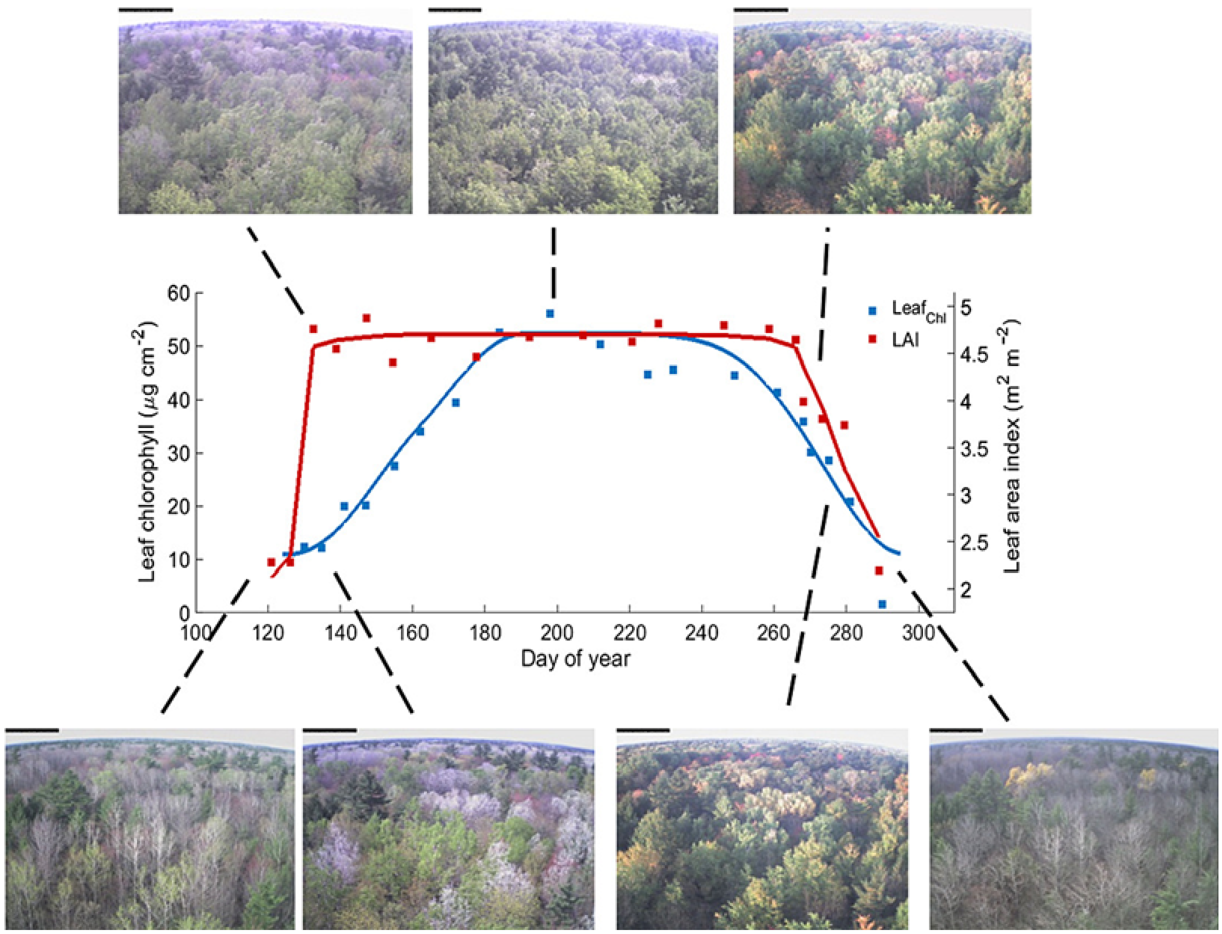

Figure A.5: Variations in leaf chlorophyll content and LAI across a growing season. Individual measurements are shown with a fitted asymmetric Gaussian function. Top of canopy photographs are given alongside ground measurement dates (Croft et al., 2015).

Personal Declaration

I hereby declare that the submitted thesis is the result of my own, independent work. All external sources are explicitly acknowledged in the thesis.

September 30, 2024

Daria Larcher

D. Larcher